Program Overview

Room /Time	Agassiz/Fremont	Humphreys
MoM		MIOMD1-MoM: Thz Quantum Cascade Lasers MIOMD2-MoM: Quantum Cascade Lasers
MoA		MIOMD3-MoA: Interband Cascade Lasers MIOMD4-MoA: Nanostructured MIR Optoelectronics/Detector and TPV Devices
MoP	Poster Sessions	
TuM		MIOMD6-TuM: QCLs for Sensing MIOMD7-TuM: Emerging MIR Materials and Devices
TuA		MIOMD8-TuA: Antimonide-Based Detectors MIOMD9-TuA: IV-VI and II-VI Detectors
WeM		MIOMD10-WeM: MIR Lasers MIOMD11-WeM: Integrated MIR Photonics
WeA		MIOMD12-WeA: Group IV Alloys and Devices MIOMD13-WeA: Devices on Mismatched Substrates

Monday Morning, October 8, 2018

	Room Humphreys	
8:15am		**MIOMD Session MIOMD1-MoM Thz Quantum Cascade Lasers**
8:30am	**INVITED: MIOMD1-MoM2** High Power Quantum Cascade Lasers: New Frontiers of Frequency Combs and THz Communications, ***Federico Capasso***, Harvard University	
8:45am	Invited talk continues.	
9:00am		
9:15am	**INVITED: MIOMD1-MoM5** Terahertz Quantum Cascade Laser Frequency Combs, ***David Burghoff***, University of Notre Dame	
9:30am	Invited talk continues.	
9:45am	**INVITED: MIOMD1-MoM7** High-power and Tunable Terahertz Quantum-Cascade VECSELs, *C. Curwen, L. Xu,* University of California at Los Angeles; *J. Reno,* Sandia National Laboratories; ***Benjamin Williams***, University of California at Los Angeles	
10:00am	Invited talk continues.	
10:15am	**MIOMD1-MoM9** Temperature Driven Enhancement of the Stimulated Emission Rate in Terahertz Quantum Cascade Lasers, ***Asaf Albo***, Bar-Ilan University, Israel; *Y. Flores,* MIT	
10:30am	**Coffee Break**	
10:45am	**Coffee Break**	
11:00am	**MIOMD2-MoM12** Interband and Quantum Cascade Lasers Integrated on Silicon, *C. Merritt,* Naval Research Laboratory; *A. Spott, E. Stanton,* University of California Santa Barbara; *I. Vurgaftman, C. Canedy,* Naval Research Laboratory; *A. Torres,* University of California Santa Barbara; *M. Kim,* KeyW; *M. Davenport,* University of California Santa Barbara; *C.S. Kim,* Naval Research Laboratory; *N. Volet,* University of California Santa Barbara; *W. Bewley,* Naval Research Laboratory; *A. Malik, J. Liu,* University of California Santa Barbara; ***Jerry Meyer***, Naval Research Laboratory; *J. Bowers,* University of California Santa Barbara	**MIOMD Session MIOMD2-MoM Quantum Cascade Lasers**
11:15am	**MIOMD2-MoM13** Entrainment of Chaotic Optical Power Dropouts Driven by Weak Modulation in a Quantum Cascade Laser with Optical Feedback, ***Olivier Spitz***, Télécom ParisTech, France; *J. Wu,* Southwest University, China; *M. Carras,* mirSense; *C.W. Wong,* University of California at Los Angeles; *F. Grillot,* Télécom ParisTech, France	
11:30am	**MIOMD2-MoM14** Optimization of Laser Cavity Designs of Tapered Quantum Cascade Lasers Emitting in 4.5 µm Range, ***Kamil Pierściński***, *M. Sakowicz, A. Kuźmicz, G. Sobczak, K. Janus, K. Michalak, E. Pruszyńska-Karbownik, D. Pierścińska, P. Gutowski, M. Bugajski,* Institute of Electron Technology, Poland	
11:45am	**MIOMD2-MoM15** Efficient Mid-infrared Electroluminescence from Sb based QW LEDs Grown on GaAs substrates, ***Tony Krier***, Lancaster University	

Monday Afternoon, October 8, 2018

	Room Humphreys	
1:30pm	**INVITED: MIOMD3-MoA1** Mid Infrared DFB Interband Cascade Lasers with low threshold power for gas sensing applications*, R. Weih, J. Scheuermann,* Nanoplus GmbH, Germany*; S. Höfling,* Universität Würzburg, Germany*; **Johannes Koeth**,* Nanoplus GmbH, Germany	**MIOMD** **Session MIOMD3-MoA** **Interband Cascade Lasers**
1:45pm	Invited talk continues.	
2:00pm	**INVITED: MIOMD3-MoA3** Interband Cascade Devices: From Lasers to LEDs and Detectors*, A. Schade,* Universität Würzburg, Germany*; F. Rothmayr,* nanoplus Nanosystems and Technologies GmbH, Germany*; A. Pfenning,* Universität Würzburg, Germany*; N. Schaefer, J. Scheuermann, C. Kistner, R. Weih, M. Fischer,* nanoplus Nanosystems and Technologies GmbH, Germany*; J. Koeth,* nanoplus GmbH, Germany*; M. Kamp, F. Hartmann, **Sven Hoefling**,* Universität Würzburg, Germany	
2:15pm	Invited talk continues.	
2:30pm	**MIOMD3-MoA5** Low-threshold InAs-based Interband Cascade Lasers near 6.3 um*, **Yiyun Li**, L. Li, W. Huang, R.Q. Yang,* University of Oklahoma*; J.A. Gupta, X. Wu, G. Aers,* National Research Council of Canada	
2:45pm	**Break and Poster Viewing**	
3:00pm	**Break and Poster Viewing**	
3:15pm	**MIOMD4-MoA8** Selective-Area Nanowires for Short-Wavelength and Mid-Wavelength Infrared Optoelectronics*, **Diana L. Huffaker**,* Cardiff University/University of California, Los Angeles*; D. Ren,* University of California, Los Angeles*; K.M. Azizur-Rahman,* Cardiff University, UK*; Z. Rong,* University of California, Los Angeles	**MIOMD** **Session MIOMD4-MoA** **Nanostructured MIR Optoelectronics/Detector and TPV Devices**
3:30pm	**MIOMD4-MoA9** InAs NWs on Si(111) Substrate for Infrared Light-emitting Diodes*, **Xinxin Li**, K. Zhang,* University of Iowa*; J. Treu, L. Stampfer, G. Koblmueller,* Technical University Munich, Germany*; F. Toor, J.P. Prineas,* University of Iowa	
3:45pm		
4:00pm	**MIOMD4-MoA11** Plasma-Enhanced Atomic Layer Deposition of SiO_2 for Channel Isolation of Colloidal Quantum Dots Infrared Phototransistors*, L. Zheng, **Yuhui Yu**,* Shanghai Institute of Microsystem and Information Technology, Chinese Academy of Sciences, China	
4:15pm	**MIOMD4-MoA12** Semimetal/Semiconductor Nanocomposites for Ultrafast Photoconductors*, **Hong Lu**,* Nanjing University, China	
4:30pm	**MIOMD4-MoA13** High Quantum Efficiency GaInAsSb Thermophotovoltaic Cells Integrated on GaAs Substrates*, **Qi Lu**,* Lancaster University, UK*; R. Beanland,* University of Warwick, UK*; D. Cardenes, A. Marshall, A. Krier,* Lancaster University, UK	
4:45pm	**MIOMD4-MoA14** Collection Efficiency and Device Performance in Narrow Bandgap Thermophotovoltaic Cells Based on Interband Cascade Structures*, **Wenxiang Huang**, L. Lin, L. Li, J. Massengale, R.Q. Yang, T. Mishima, M. Santos,* University of Oklahoma	

MIOMD
Room Agassiz/Fremont - Session MIOMD5-MoP
MIOMD Poster Session
5:00pm

MIOMD5-MoP1 Thermal Conductivity Properties of Graphene Using Non-Equilibrium Molecular Dynamics Simulations*, X.Q. Wei,* Research Institute of Xi'an Jiaotong University, China*; S. Yang, **Lin Zhu**, Y.L. Fu, Z.L. Li, Y.F. Liao, L.X. Shi, Z.G. Huang,* Huaihai Institute of Technology, China

MIOMD5-MoP3 Study of Interband Cascade Lasers for MIR-VCSELs*, D.A. Diaz-Thomas, M. Bahriz, A. Meguekam-Sado, A. Baranov, E. Tournié, **Laurent Cerutti**,* Université de Montpellier, France

MIOMD5-MoP4 Suppressing High Order Transverse Modes in Broad Area QCLs*, **Ron Kaspi**, S. Luong, C. Lu, T. Newell, C. Yang, D. Gianardi,* Air Force Research Laboratory

MIOMD5-MoP5 Methods to Enhance Sensitivity to the Surface-normal Dielectric Functions of Anisotropic Layers using Infrared Ellipsometry*, **Thomas Tiwald**, N. Hong,* J.A. Woollam Co., Inc.

MIOMD5-MoP6 Carrier Concentration Verification in Plasmonic Waveguide of the Semiconductor Cascade Lasers by using FTIR Spectroscopy*, **Marcin Motyka**, M. Dyksik, M. Rygala, G. Sęk, K. Ryczko, J. Misiewicz,* Wroclaw University of Science and Technology, Poland*; K. Pierściński, P. Gutowski, M. Bugajski,* Institute of Electron Technology, Poland

MIOMD5-MoP7 Lateral and Vertical Transport in *n*- and *p-type* InAsSb and InAs/InAsSb Type-II Strained Layer Superlattices for Infrared Detector Applications*, **Lilian Casias**,* University of New Mexico*; C.P. Morath, E. Steenbergen, P. Webster,* Air Force Research Laboratory*; J. Kim,* Sandia National Laboratories*; G. Umana-Membreno,* The University of Western Australia*; V. Cowan,* Air Force Research Laboratory*; G. Balakrishnan,* University of New Mexico*; S. Krishna,* Ohio State University

MIOMD5-MoP8 GeSn for Mid-Infrared Applications Grown by Remote Plasma Enhanced Chemical Vapor Deposition*, **Gordon Grzybowski**, S. Chastang,* KBRwyle*; A. Kiefer, B. Claflin,* Air Force Research Laboratory

MIOMD5-MoP9 Advanced Glass Compositions for Mid-IR Laser Applications*, M. Klopfer,* University of New Mexico*; L.J. Henry,* Air Force Research Laboratory*; **Ravi Jain**,* University of New Mexico

MIOMD5-MoP10 High Performance Superlattice Light Emitting Diodes Grown Epitaxially on Silicon*, **Aaron J. Muhowski**, C.L. Bogh, R.L. Heise, T.F. Bogges, J.P. Prineas,* University of Iowa

MIOMD5-MoP11 Graphene-Metamaterial Mid-Infrared Thermal Emitters*, **Cheng Shi**, N.H. Mahlmeister, P. Gowda, I.J. Luxmoore,* University of Exeter, United Kingdom*; G.R. Nash,* University of Exter, United Kingdom

Tuesday Morning, October 9, 2018

	Room Humphreys	
8:30am	**INVITED: MIOMD6-TuM1** Recent Advances in QCL Based Sensing of Gases and Liquids, ***Bernhard Lendl***, TU Wien, Austria	**MIOMD** **Session MIOMD6-TuM** **QCLs for Sensing**
8:45am	Invited talk continues.	
9:00am		
9:15am	**INVITED: MIOMD6-TuM4** Mid-Wave and Long-Wave Infrared Broad-Area Quantum Cascade Lasers, *M. Suttinger, R. Go, H. Shu, A. Azim,* ***Arkadiy Lyakh***, University of Central Florida	
9:30am	Invited talk continues.	
9:45am	**MIOMD6-TuM6** Rapidly Tunable External-cavity Quantum Cascade Lasers for Applications in Real Time MIR Sensing, ***Ralf Ostendorf***, *S. Hugger, L. Butschek, M. Haertelt,* Fraunhofer Institute for Applied Solid State Physics, Germany; *A. Dreyhaupt, J. Grahmann,* Fraunhofer Institute for Photonic Microsystems, Germany; *M. Rattunde, J. Wagner,* Fraunhofer Institute for Applied Solid State Physics, Germany	
10:00am	**Coffee Break**	
10:15am	**Coffee Break**	
10:30am	**INVITED: MIOMD7-TuM9** Development of GaSbBi for the Fabrication of Mid-IR Laser Diodes, ***Jean-Baptiste Rodriguez***, *O. Delorme, L. Cerutti,* Université de Montpellier, France; *R. Kudrawiec,* Paul-Drude-Institut für Festkörperelektronik, Germany; *E. Luna,* Wrocław University of Science and Technology, Poland; *J. Kopaczek, M.P. Polak, M. Gladysiewicz,* Paul-Drude-Institut für Festkörperelektronik, Germany; *M. Trampert,* Wrocław University of Science and Technology, Poland; *E. Tournie,* University Montpellier II, France	**MIOMD** **Session MIOMD7-TuM** **Emerging MIR Materials and Devices**
10:45am	Invited talk continues.	
11:00am	**MIOMD7-TuM11** Mid-infrared 2.7-µm GaSbBi/GaSb Quantum Well Lasers Studied under High Hydrostatic Pressure, *I. Marko,* University of Surrey, UK; *O. Delorme, L. Cerutti, E. Tournié, J.-B. Rodriguez,* Université de Montpellier, France; ***Stephen Sweeney***, University of Surrey, UK	
11:15am	**MIOMD7-TuM12** Growth and Optical Properties of III-V-bismide Alloys for mid-IR Device Applications, ***Stephen Schaefer***, *R. Kosireddy, A. Shalindar, S. Johnson,* Arizona State University	
11:30am	**MIOMD7-TuM13** Influence of Substrate Orientation on Structural Properties of InAsSbBi Alloys for mid IR Applications, ***Rajeev Kosireddy***, *S. Schaefer, A. Shalindar, S. Johnson,* Arizona State University	
11:45am	**MIOMD7-TuM14** Mid-IR and UV-VIS-NIR Mueller Matrix Ellipsometry Characterization of the Hyperbolic Dielectric Tensor of Crystallized Films of Carbon Nanotubes, ***Stefan Schoeche***, J.A. Woollam Co., Inc.; *J. Fan, J. Roberts,* Stanford University; *P.-H. Ho, A. Falk,* IBM T.J. Watson Research Center	
12:00pm		

Tuesday Afternoon, October 9, 2018

Time	Room Humphreys	
1:15pm	**INVITED: MIOMD8-TuA1** Antimonide Unipolar Barrier Infrared Detectors and Focal Plane Arrays, ***David Ting**, A. Soibel, A. Khoshakhlagh, S. Keo, S. Rafol, A. Fisher, E. Luong, C. Hill, B. Pepper, S. Gunapala,* NASA Jet Propulsion Laboratory, California Institute of Technology	**MIOMD Session MIOMD8-TuA Antimonide-Based Detectors**
1:30pm	Invited talk continues.	
1:45pm	**MIOMD8-TuA3** Mid-Infrared Resonant Cavity Detectors, ***Gary Wicks**,* University of Rochester; *G. Savich,* Amethyst Research, Inc.; *T. Golding,* Amethyst Research Inc.; *K. Jamison, L. Fredin,* Amethyst Research, Inc.; *M. Jain,* Amethyst Research, Ltd., UK; *A. Craig, A. Marshall,* Lancaster University, UK; *T. O'Loughlin, B. Marozas,* University of Rochester	
2:00pm	**MIOMD8-TuA4** Minority Carrier Lifetime and Recombination Dynamics in Strain-Balanced InGaAs/InAsSb Superlattices, ***Preston Webster**, E. Steenbergen, G. Ariyawansa, C. Reyner,* Air Force Research Laboratory; *J. Kim,* Sandia National Laboratories	
2:15pm	**MIOMD8-TuA5** Large Photocurrent Amplification in n-GaSb/InAs/p-GaSb Heterostructure with a Single Quantum Well, *P. Mikhailova,* Ioffe Institute, Russian Federation; ***Hafiz Salikhov**,* Institute of Applied Research, Tatarstan Academy of Sciences, Russian Federation; *G. Konovalov, L. Danilov, R. Levin, B. Pushny, I. Andreev, Y. Yakovlev,* Ioffe Institute, Russian Federation	
2:30pm	**MIOMD8-TuA6** A Unified Figure of Merit for Interband and Intersubband Cascade Devices, *W. Huang, S. Rassel, L. Li, J. Massengale, **Rui Q. Yang**, T. Mishima, M. Santos,* University of Oklahoma	
2:45pm	**MIOMD8-TuA7** Epitaxial Lift-Off Technology Based on Water-Soluble MgTe for Multi-Color Photodetector and Solar Cell Applications, ***Cheng-Ying Tsai**, C. Campbell, Y.-H. Zhang,* Arizona State University	
3:00pm	**Break**	
3:15pm	**Break**	
3:30pm	**INVITED: MIOMD9-TuA10** Development of Low-Cost Uncooled/TE-cooled PbSe MWIR Detector For Sensing and Imaging Applications, ***Zhisheng Shi**,* University of Oklahoma	**MIOMD Session MIOMD9-TuA IV-VI and II-VI Detectors**
3:45pm	Invited talk continues.	
4:00pm	**MIOMD9-TuA12** MBE Growth of Monocrystalline PbTe/CdTe/InSb Heterovalent Heterostructures for MWIR Device Applications, ***Maxwell Lassise**, T. McCarthy, B. Tracy, D. Smith, Y.-H. Zhang,* Arizona State University	
4:15pm	**MIOMD9-TuA13** Mid-wave Infrared Imaging with HgTe Colloidal Quantum Dots Photovoltaic Devices, ***Xin Tang**, M. Ackerman, P. Guyot-Sionnest,* University of Chicago	
4:30pm	**MIOMD9-TuA14** Scanning Tunneling Microscopy with Atomic Resolution on HgCdTe, ***Fangxing Zha**,* Shanghai University, China	

	Room Humphreys	
8:30am	**INVITED: MIOMD10-WeM1** Spectroscopic Chemical Sensing and Hyperspectral Imaging with Quantum Cascade Laser Frequency Combs, ***Gerard Wysocki***, Princeton University	**MIOMD Session MIOMD10-WeM MIR Lasers**
8:45am	Invited talk continues.	
9:00am	**INVITED: MIOMD10-WeM3** GaSb-based Lasers for Trace Gas Sensing, ***James A. Gupta***, National Research Council of Canada	
9:15am	Invited talk continues.	
9:30am	**MIOMD10-WeM5** Determination of the Auger Coefficient and its Wavelength Dependence in Type-I Mid-Infrared Laser Diodes, *T. Eales, I. Marko, B. Ikyo,* ***Alf Adams***, University of Surrey, UK; *A. Andrejew, K. Vizbaras, M. Amann,* University of Munich, Germany; *L. Shterengas, G. Belenky,* Stony Brook; *I. Vurgaftman, J. Meyer,* Naval Research Laboratory; *S. Sweeney,* University of Surrey, UK	
9:45am	**MIOMD10-WeM6** Efficiency Limiting Mechanisms in Interband Type-II 'W' Lasers Operating in the Mid-IR, *T. Eales, I. Marko,* University of Surrey, UK; *S. Sprengel, A. Andrejew, K. Vizbaras, M. Amann,* University of Munich, Germany; ***Stephen Sweeney***, University of Surrey, UK	
10:00am	**Coffee Break**	
10:15am	**Coffee Break**	
10:30am	**MIOMD10-WeM9** Dynamic Stabilization of Efficient Mid-Infrared III-V Semiconductor Frequency Combs Using Two-Color Pumping, *R. Weiblen,* ***Igor Vurgaftman***, Naval Research Laboratory	
10:45am	**MIOMD10-WeM10** Quantum Dot Cascade Laser: From Concept to Practice, ***Feng-Qi Liu***, Institute of Semiconductors, Chinese Academy of Sciences, China	
11:00am	**MIOMD10-WeM11** Glass-based MIR Optoelectronic Devices: State-of-the-art and Future Outlook of Mid-Infrared Fiber Lasers, Microresonators and Molecular Sensors, ***Ravi Jain***, University of New Mexico	
11:15am	**MIOMD10-WeM12** Materials Issues Related to the Fabrication of High-Q Mid-Infrared Glass Optical Microresonators, ***Mani Hossein-Zadeh***, *R. Jain,* University of New Mexico	
11:30am	**MIOMD11-WeM13** Recent Progress on GaSb-based Photonic Integrated Circuits, ***Shamsul Arafin***, *A. McFadden, M. Pendharkar, C.J. Palmstrøm, L. Coldren,* University of California Santa Barbara	**MIOMD Session MIOMD11-WeM Integrated MIR Photonics**
11:45am	**MIOMD11-WeM14** Chip-Integrated Plasmonic Flat Optics for Mid-Infrared Polarization Detection, ***Jing Bai***, *C. Wang, X. Chen, A. Basiri, C. Wang, Y. Yao,* Arizona State University	
12:00pm	**MIOMD11-WeM15** Mid-Infrared Modulation in Silicon, *W. Cao, M. Nedeljkovic,* University of Southampton, UK; *D. Hagan,* McMaster University, Canada; *C. Littlejohns, Z. Qu, A. Khokhar, F. Gardes,* University of Southampton, UK; *A. Knights,* McMaster University, Canada; *D. Thomson,* ***Goran Mashanovich***, University of Southampton, UK	

Wednesday Afternoon, October 10, 2018

	Room Humphreys	
1:30pm	**INVITED: MIOMD12-WeA1** Extreme Nonlinearities in the Compositional Dependence of Band Gaps in the Si – Ge–Sn System, *P. Wallace, C. Xu, J.G. Kouvetakis,* ***Jose Menendez,*** Arizona State University	**MIOMD** **Session MIOMD12-WeA** **Group IV Alloys and Devices**
1:45pm	Invited talk continues.	
2:00pm	**INVITED: MIOMD12-WeA3** The Rise of the GeSn/SiGeSn Multiple Quantum Well Laser, ***Detlev Grützmacher****, D. Buca, N. von den Driesch, D. Stange, D. Rainko,* Forschungszentrum Jülich, Germany*; Z. Ikonic,* University of Leeds, UK*; J.M. Hartmann,* CEA-LETI, France*; H. Sigg,* Paul Scherrer Institute, Switzerland	
2:15pm	Invited talk continues.	
2:30pm	**MIOMD12-WeA5** GeSn Lasers and Photodetectors: Key Components for Mid-IRIntegrated Microwave Photonics on the SOI Platform, *W. Du,* Wilkes University*; SA. Ghetmiri,* University of Arkansas at Pine Bluff*; Y. Zhang, S. El-Ghazaly,* University of Arkansas*; J. Margetis, J. Tolle,* ASM*; G. Sun, R. Soref,* University of Massachusetts Boston*; B. Li,* Arktonics*; G. Salamo,* University of Arkansas*; M. Mortazavi,* University of Arkansas at Pine Bluff*;* ***Shui-Qing Yu****,* University of Arkansas	
2:45pm	**MIOMD12-WeA6** Growth and Characterization of GeSn using UHV-CVD System, ***Perry Grant****,* Arktonics LLC*; J. Grant, W. Dou, B. Alharthi, H. Tran,* University of Arkansas*; A. Mosleh,* University of Arkansas at Pine Bluff*; W. Du,* Wilkes University*; B. Li,* Arktonics LLC*; M. Mortizavi,* University of Arkansas at Pine Bluff*; H. Naseem, S.-Q. Yu,* University of Arkansas	
3:00pm	**Break**	
3:15pm	**Break**	
3:30pm	**MIOMD12-WeA9** Buffer-free GeSn on Si Substrate by Plasma Enhanced Chemical Vapor Deposition, *W. Dou, P. Grant, J. Grant, H. Tran,* University of Arkansas*; W. Du,* Wilkes University*; M. Mortazavi,* University of Arkansas at Pine Bluff*; B. Li,* Arktonics LLC*; H. Naseem, S.-Q. Yu,* ***Bader Alharthi****,* University of Arkansas	
3:45pm	**MIOMD12-WeA10** GePb Alloys for Mid-IR Optoelectronics Applications, ***Aboozar Mosleh****,* University of Arkansas at Pine Bluff*; H. Alahmad,* University of Arkansas*; M. Alher,* University of Kerbala, Iraq*; S.F. Banihashemian,* University of Arkansas*; SA. Ghetmiri,* University of Arkansas at Pine Bluff*; S. Al-Kabi,* University of Arkansas*; W. Du,* Wilkes University*; B. Li,* Arktonics LLC*; S.-Q. Yu, H. Naseem,* University of Arkansas	
4:00pm	**MIOMD13-WeA11** Reduction of Twin formation in GaAs/Sapphire Grown by MBE, ***Rahul Kumar****, S.K. Saha, A. Kuchuk, T. Morgan, P.K. Ghosh, M.Z. Alavijeh, S.-Q. Yu, G. Salamo,* University of Arkansas	**MIOMD** **Session MIOMD13-WeA** **Devices on Mismatched Substrates**
4:15pm	**MIOMD13-WeA12** III-As Growth on c-plane Sapphire by MBE, ***Samir Kumar Saha****, R. Kumar, A. Kuchuk, T. Morgan, P.K. Ghosh, M.Z. Alavijeh, S.-Q. Yu, G. Salamo,* University of Arkansas	
4:30pm	**MIOMD13-WeA13** InGaAs Photodetector Grown on InP Substrate with $InAs_xP_{1-x}$ Metamorphic Buffer Layers, *H.K.. Hsieh,* ***Chieh Chou****,* National Taiwan University, Republic of China*; J.J.. Luo, S,Y. Li,* National Chung-Shan Institute of Science & Technology*; H.H. Lin,* National Taiwan University, Republic of China	
4:45pm		

Author Index

Bold page numbers indicate presenter

Author Index

High Power Quantum Cascade Lasers: New Frontiers of Frequency Combs and THz Communications

Federico Capasso

Harvard University

Cambridge, MA 02138

Parametric effects and ultrafast gain dynamics in high power QCLs lead to single mode instability and to a new regime, the "harmonic" state, whereby the lasing longitudinal modes are spaced by many free spectral ranges.[1,2] In this regime the laser acts as self-pumped parametric oscillator generating a highly stable self-starting frequency comb.[3] The comb teeth beat coherently forming a time dependent population grating (transient spatial-hole-burning), which generates a microwave signal that we have utilized to demonstrate quadrature amplitude modulation, a staple of modern communications.[4] This effect has potential for a new class of integrated transmitters, potentially extending from the microwave to the low terahertz band. By integrating an antenna on the device a quantum cascade laser has been transformed into an FM radio transmitter operating at 5.5 GHz — a carrier frequency that is potentially scalable to the sub-terahertz range.

1. T. S. Mansuripur *et al*. *Phys. Rev.* **A 94**, 063807 (2016)
2. M. Piccardo *et al*. *Optics Express* **26**, 9464 (2018)
3. D. Kazakov *et al*. *Nature Photonics* **11**, 789 (2017)
4. M. Piccardo *et al*. *Optica* **5**, 475 (2018)

Terahertz quantum cascade laser frequency combs

David Burghoff
Department of Electrical Engineering, University of Notre Dame, 226B Cushing Hall, Notre Dame, IN 46556

Optical frequency combs—light sources whose lines are evenly spaced—have proven to be remarkable tools for spectroscopy and for metrology. Traditionally, these combs were generated using mode-locked solid-state lasers, which can provide very stable combs with hundreds of thousands of comb lines, but at the cost of being relatively large (~10 cm). However, in the last few years there has been interest in new chip-scale frequency combs, such as microresonator combs and semiconductor mode-locked sources. At long wavelengths, it has been shown that quantum cascade lasers (QCLs) are capable of forming a comb state that does not possess the properties of conventional mode-locking, wherein the dispersed cavity modes of a Fabry-Perot cavity synchronize by four-wave mixing [1].

By incorporating proper dispersion engineering, we have shown that it is possible to create QCL frequency combs at terahertz (THz) wavelengths, which enable offer broad bandwidths in a compact package [1]. These combs are particularly attractive as sources for compact spectroscopy: by using a dual-comb technique, it is possible to perform high-sensitivity spectroscopy without moving parts [2]. In addition, due to the semi-continuous nature of the temporal output of these lasers, it is possible to continuously track the instantaneous phase and timing signals of a dual-comb waveform, enabling computational self-correction of the dual-comb signal even without a reference. Provided the signal-to-noise ratio of the acquired dual-comb signal is high enough to enable self-correction, one does not require stability for many spectroscopic measurements [3].

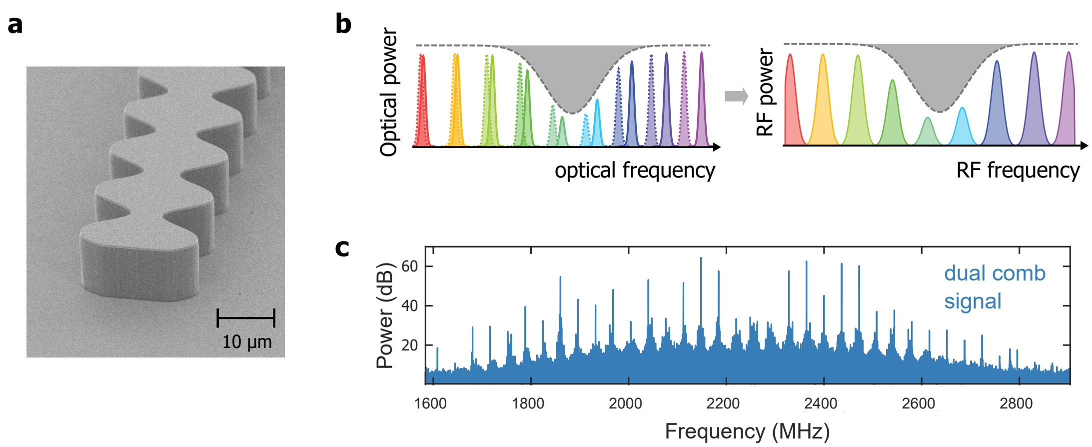

Figure 1. (a) SEM of a THz double-chirped mirror. (b) Schematic version of dual comb spectroscopy. (c) THz QCL dual comb spectroscopy, measured on a hot electron bolometer (HEB).

[1] A. Hugi et al., Nature **492**, 229 (2012).
[2] D. Burghoff et al., Nat. Photonics **8**, 462 (2014).
[3] Y. Yang et al., Optica **3**, 499 (2016).
[4] D. Burghoff et al., Sci. Adv. **2**, e1601227 (2016).

+ Author for correspondence: dburghoff@nd.edu

High-power and tunable terahertz quantum-cascade VECSELs

Christopher A. Curwen[1], Luyao Xu[1], John L. Reno[2], Benjamin S. Williams[1]
[1] *Dept. of Electrical and Computer Engineering, University of California Los Angeles (UCLA), Los Angeles, CA 90095*
[2] *Sandia National Laboratories, Center of Integrated Nanotechnologies (CINT), Albuquerque, NM*

The terahertz quantum-cascade vertical-external-cavity surface-emitting laser (THz QC-VECSEL) is a recently demonstrated architecture for terahertz lasers with excellent beam qualities and scalable power [1, 2]. The enabling component of the THz QC-VECSEL is an active metasurface loaded with QC-gain material that reflects and amplifies normally incident THz waves. The metasurface is made up of a reflectarray of surface radiating antenna elements spaced with a sub-wavelength periodicity to avoid effects of higher-order diffraction, as shown in Figure 1(a). The QC-VECSEL architecture offers a solution to many problems that have plagued THz QC-lasers – namely their low emission powers and efficiencies (especially above 77 K), their limited beam quality (especially at high powers), and their limited range of continuous single-mode tunability.

We report recent results in which the emitted power from THz QC-VECSELs is scaled up to greater than 1 W. A new metasurface design is presented based upon 3rd-order laterally resonant stripe antennas fabricated in metal-metal waveguide. This metasurface increases the areal density of gain material, which allows one to increase the output power without increasing the area of the metasurface itself. Figure 1(b) shows a power-voltage-current characteristic in pulsed mode for such a device which exhibits watt-level peak powers. Figure 1(c) shows the tuning of the output spectrum as the cavity length is varied, and the output beam remains nearly unchanged.

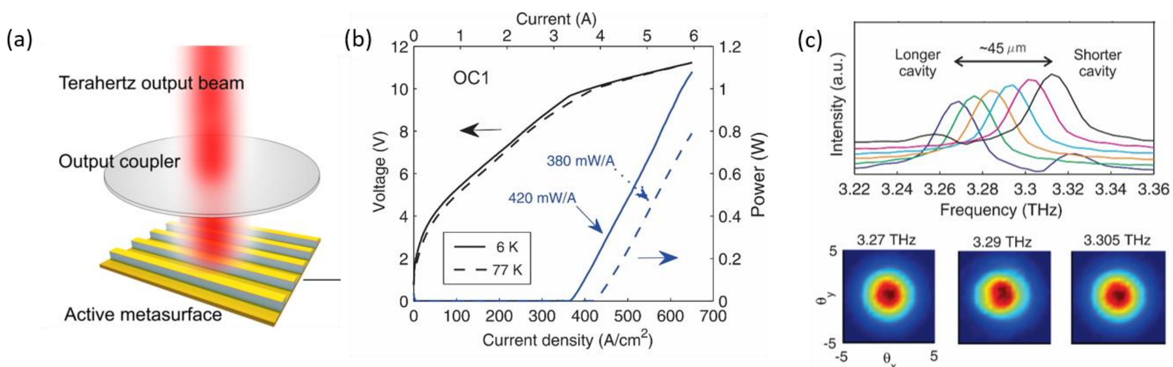

Figure 1. (a) Schematic for metasurface QC-VECSEL. (b) Pulsed-mode power-voltage-current characteristic at 77 K and 6 K. (c) Tuning of output spectrum as length of cavity changes. Far-field beam pattern remains unchanged.

[1] L. Xu, C. A. Curwen, P. W. C. Hon, Q.-S. Chen, T. Itoh, and B. S. Williams, "Metasurface external cavity laser," Appl. Phys. Lett. **107**, 221105 (2015).
[2] L. Xu, C. A. Curwen, D. Chen, J. L. Reno, T. Itoh, and B. S. Williams, "Terahertz metasurface quantum-cascade VECSELs: theory and performance," IEEE J. Sel. Topics Quantum Electron. **23**, 1200512 (2017).

+ Author for correspondence: bswilliams@ucla.edu

Temperature driven enhancement of the stimulated emission rate in terahertz quantum cascade lasers

Asaf Albo[1,*] **and Yuri V. Flores**[2]

[1] *Faculty of Engineering, Bar-Ilan University, Ramat Gan 5290002, Israel.*

[2] *Department of Electrical Engineering and Computer Science and Research Laboratory of Electronics, Massachusetts Institute of Technology, Cambridge, Massachusetts 02139, USA.*

**Contact Email: asafalbo@gmail.com*

The terahertz spectral region is subject to intensive research in view of its potential in a number of application domains such as medical diagnostics, trace molecule sensing, astronomical detection, non-invasive quality control and more. However, maximum operating temperature achieved with terahertz quantum cascade lasers (T_{max}~ 200 K) imposes cryogenic techniques.

In general, the ideal operation mode of a terahertz quantum cascade laser assumes that an electron injected externally into the device will generate multiple photons – one in each "energy cascade"– while transporting through the heterostructure. However, alternative scattering leakage paths deviate electron transport from the ideal picture and present a considerable effect on devices' performance. In that context, temperature-driven leakage of charge carriers out of the laser's active region states is considered as an unwanted effect that limit its temperature performance [1-2]. However, as we showed in our latest works [2-3], contrary to common sense expectations, carrier leakage under some conditions can be beneficial for the device and enhance lasing.

In our works we demonstrated that that thermally activated leakage of electrons from the lower laser level into the continuum can be fast enough to effectively counteract the population inversion decrease as the temperature increases. This effect leads to a higher output power by means of an enhancement of the stimulated emission rate with temperature increase and contributes significantly to the performance of state of the art devices. This finding opens the question if new design approaches for terahertz quantum cascade lasers that exploit this effect can be developed in order to demonstrate devices with higher T_{max}. This work is the first demonstration of a thermophotonic mechanism in semiconductor lasers, which utilizes generated heat in order to increase the number of coherent photons. A similar effect has been recently reported for infrared light emitting diodes [3].

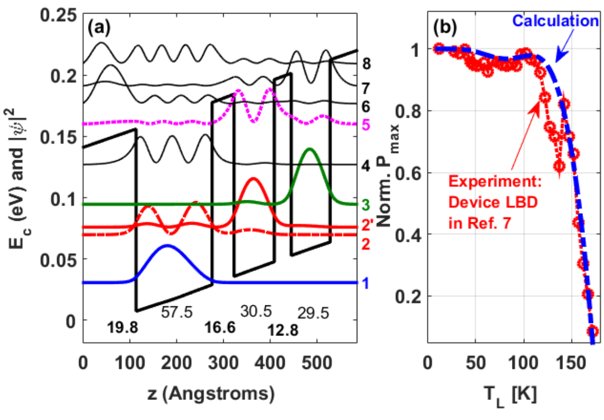

Fig. 1. (a) Conduction band profile of the device investigated in this work (LBD of Ref. [1]) under 13.4 kV/cm design electric field. Layer thicknesses in monolayers are indicated. Calculated design parameters are $E_3 - E_{2'} = h\nu =$ 16 meV (photon energy), $f_{32'} = 0.17$ (oscillator strength) and $L_{mod} = 470$ Å (module length). (b) Measured (red circles) and calculated (dashed-dotted blue line) normalized light output power as a function of temperature.

1. Carrier leakage into the continuum in diagonal GaAs/Al0.15GaAs terahertz quantum cascade lasers", Asaf Albo and Qing Hu, Appl. Phys. Lett. **107**, 241101, 2015.

2. "Room temperature negative differential resistance in terahertz quantum cascade laser structures", Asaf Albo, Qing Hu and John L. Reno, Appl. Phys. Lett. **109**, 081102, 2016.

3. "Temperature driven enhancement of the stimulated emission rate in terahertz quantum cascade lasers", Asaf Albo and Yuri V. Flores, Journal of Quantum Electronics **53**(1), 1-5, 2017.

4. "Carrier Leakage Dynamics in Terahertz Quantum Cascade Lasers", Asaf Albo and Yuri V. Flores, IEEE Journal of Quantum Electronics **53**(1), 2300105, 2017.

5. P. Santhanam, D. J. Gray Jr., and R. J. Ram, "Thermoelectrically pumped light-emitting diodes operating above unity efficiency," *Phys. Rev. Lett.*, vol. **103**, p. 097403, 2012.

Interband and Quantum Cascade Lasers Integrated on Silicon

C. D. Merritt,[1] A. Spott,[2] E. J. Stanton,[2] I. Vurgaftman,[1] C. L. Canedy,[1] A. Torres,[2] M. Kim,[3] M. L. Davenport,[2] C. S. Kim,[1] N. Volet,[2] W. W. Bewley,[1] A. Malik,[2] J. Liu,[2] J. R. Meyer,[1] and J. E. Bowers[2]

[1]*Code 5613, Naval Research Laboratory, Washington DC 20375*
[2]*Dept. of Electrical & Computer Engr., University of California, Santa Barbara CA 93106*
[3]*KeyW Corporation, 7740 Milestone Parkway, Suite 150, Hanover MD 21076*

We have heterogeneously integrated interband and quantum cascade lasers on silicon by bonding the active III-V layers above silicon waveguides. We previously demonstrated Fabry-Perot [1] and distributed feedback (DFB) [2] QCLs integrated on a silicon-on-nitride-on-insulator (SONOI) platform. The DFB lasers emitted > 200 mW in pulsed mode at room temperature, and operated up to 100 ºC.

Here we report the first GaSb-based ICLs to be heterogeneously integrated on a silicon chip. Figure 1 is a cross-sectional schematic of the hybrid III-V/Si active region. The 3-mm-long hybrid mesa is bounded on both ends by tapers that transfer the light to passive silicon waveguides. The ICLs with 7 active stages were bonded to silicon-on-insulator (SOI) with a 1.5 µm-thick silicon device layer and 1-µm-thick buried oxide layer above a silicon substrate.

Figure 2 shows the light output (in arbitrary units) vs. injection current for an 11-µm-wide III-V mesa on top of a 1-µm-wide silicon waveguide. When driven by 250 ns pulses at 1 kHz repetition rate, the device operated to 40 °C. The plot of threshold current density vs. temperature in Fig. 3 indicates a characteristic temperature of T_0 = 39 K. The observed thresholds are much higher than those of ICLs fabricated on the native GaSb substrate, and increase rapidly with decreasing ridge width. This implies most of the injected current was lost to sidewall leakage. A consistent longitudinal mode spacing of ~5 nm, measured for all the lasers at all temperatures, indicates coupling to a ~320–350 µm-long Fabry-Perot cavity formed between the tapered ends of the III-V mesa and the silicon waveguide end facets.

We also report arrayed waveguide gratings (AWGs) that couple up to three QCL inputs into a single output silicon waveguide[3,4].

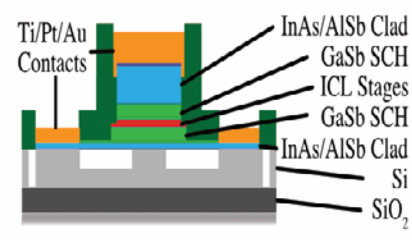

Figure 1 - Cross section of the hybrid III-V/Si active region for the ICL integrated on silicon.

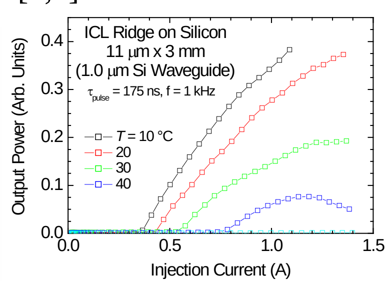

Figure 2 - Pulsed light-current characteristics of the integrated ICL at a series of temperatures.

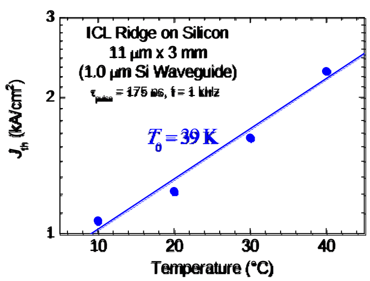

Figure 3 - Threshold current density vs. temperature for the integrated ICL.

[1] A. Spott et al., "Quantum Cascade Laser on Silicon." *Optica* 3, 545 (2016).
[2] A. Spott et al., "Heterogeneously Integrated DFB Quantum Cascade Lasers on Silicon," *Photonics* 3, 35 (2016).
[3] Eric J. Stanton et al., "Quantum cascade multi-spectral laser with integrated beam combiner on silicon", CLEO (2018);
[4] E. J. Stanton et al., "Multi-spectral QCLs on silicon with integrated multiplexers" submitted to *APL Photonics*.

+ Author for correspondence (Jerry Meyer): mwir_laser@nrl.navy.mil

Entrainment of chaotic optical power dropouts driven by weak modulation in a quantum cascade laser with optical feedback

O. Spitz,[1,2,3,+] **J. Wu,**[3,4] **M. Carras,**[2] **C. W. Wong,**[3] **F. Grillot**[1,3,5]
[1]*LTCI Télécom ParisTech, Université Paris-Saclay, 46 rue Barrault, Paris, 75013, France*
[2]*mirSense, Centre d'intégration NanoInnov, 8 avenue de la Vauve, Palaiseau, France*
[3]*Fang Lu Mesoscopic Optics & Quantum Electronics Laboratory, UCLA, CA 90095, USA*
[4]*College of Electronic & Information engineering, Southwest University, Chongqing, China*
[5]*Center for High Technology Materials, University of New-Mexico, NM 87106, USA*

Quantum cascade lasers (QCLs) are optical sources exploiting radiative intersubband transitions within the conduction band of semiconductor heterostructures [1]. The QCL dynamics has become nowadays a field of growing interests with plethora of applications [2]. Prior work found that the dynamics of a QCL operating with time-delayed optical feedback exhibits sudden power dropouts in the laser output. These power dropouts result from low frequency fluctuations (LFF) hence a manifestation of deterministic chaos [2]. In this paper, we investigate a way of controlling these irregular dropouts by using an external periodic forcing [3,4]. When no modulation is applied, the laser under optical feedback displays a chaotic behavior with LFF dynamics (Fig. 1(a)). However when the external forcing is applied, the chaotic pattern exhibits a repetition rate of 5 MHz when a 2.5 MHz modulation is applied (Fig. 1(b)) and 6.6 MHz when a 3.3 MHz modulation (Fig. 1(c)). The results show that optimal entrainment to external modulation takes place when the time period of this modulation is close to one of the multiple of the system. Further work will discuss how to control the rareness of the dropouts with respect to the modulation characteristics. These initial results are meaningful for novel mid infrared sensing solutions.

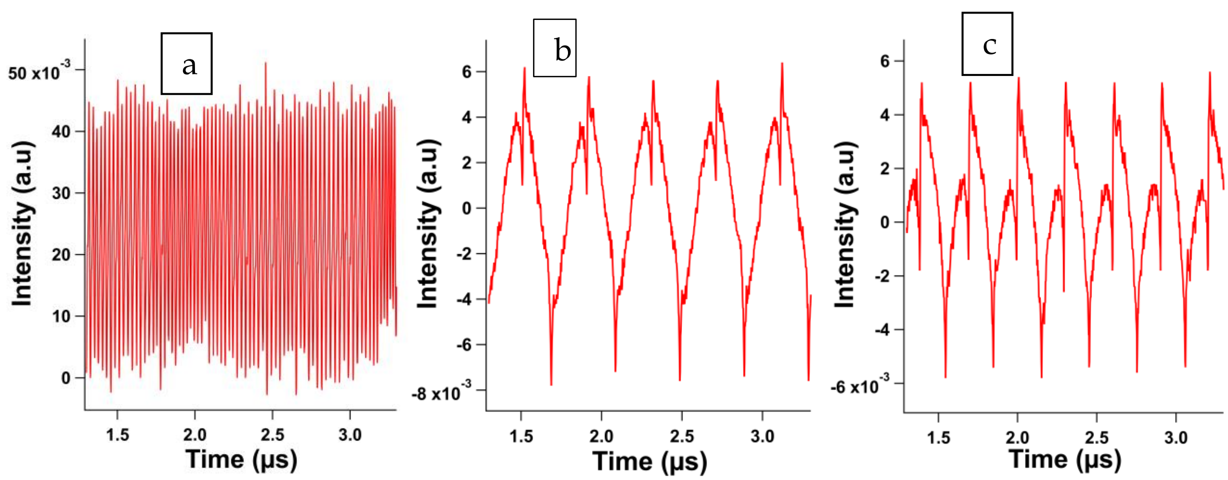

Figure **1** Experimental chaotic time traces of the QCL under external optical feedback when no electric modulation is applied (a), when a low electric sine modulation at 2.5 MHz is applied (b) and when a low electric sine modulation at 3.3 MHz is applied (c) to the QCL

[1] Faist, J. et al., *Science, 264* (5158), 553-556. (1994)
[2] Jumpertz, L, Nonlinear Photonics in Mid-infrared Quantum Cascade Laser, Springer (2017)
[3] Buldù, J. M. et al., *Physical Review E* **66**, 021106. (2002)
[4] Tiana-Alsina, J. et al., *Optics Express* 26, 7. (2018)

[+] Author for correspondence: olivier.spitz@telecom-paristech.fr

Optimization of laser cavity designs of tapered quantum cascade lasers emitting in 4.5 µm range.

K. Pierściński, M. Sakowicz, A. Kuźmicz, G. Sobczak, K. Janus, K. Michalak, E. Pruszyńska–Karbownik, D. Pierścińska, P. Gutowski, M. Bugajski

[1] *Institute of Electron Technology, Al. Lotników 32/46, 02-668 Warsaw, Poland*

Quantum cascade lasers have a well-established position as mid-infrared sources with a large number of applications such as free space communication, absorption spectroscopy-based molecular sensing, breath analysis for medical diagnostics.

In most of the applications, lasing on the fundamental transverse mode with high output power is desirable. However, increasing the output power by increasing the ridge width results in deterioration of beam quality, as the QC laser operates on operates on high order transverse mode. Tapered designs allow increasing the output power while maintaining TEM00 operation.

In this work, we demonstrate experimental investigation of optimisation of tapered laser cavity designs. Various shapes and section length ratios of tapered QCLs were investigated. Devices were designed for emission wavelength in the range of 4.5 um and grown by molecular beam epitaxy. Experimental works were preceded by systematic numerical simulations of optical mode propagation in different geometrical variants of the cavity.

Figure 1. presents the comparison of LIV characteristics for typical Fabry-Perot and tapered QC lasers. Schematic top view of the waveguide design is shown in the inset of Fig. 1. The comparison of far-field profiles (in the slow axis plane) is shown in Fig. 2.

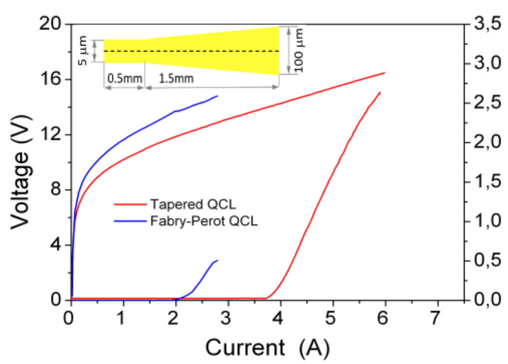

Figure 1 LIV characteristics for FP and tapered QCLs.

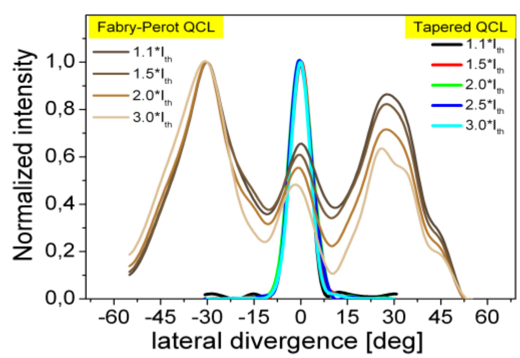

Figure 2 Far Field profiles for FP and tapered QCLs.

A significant increase of emitted power was achieved while TEM00 operation was maintained. Several aspects of concerning thermal, spectral and degradation properties of tapered QC lasers will be discussed. Spatial patterns of emitted radiation will be presented for various cavity designs.

This work was financially supported by National Center for Research and Development (Poland) grant no. LIDER/019/317/L-5/13/NCBR/2014.

+ Author for correspondence: kamil.pierscinski@ite.waw.pl

Efficient Mid-infrared Electroluminescence from Sb based QW LEDs grown on GaAs substrates

A. Krier[1*], E. Repiso[1], P.J. Carrington[1], K. J. Lulla[1], A.R. Marshall[1], L.Qi[1]
M. Steer[2], C. MacGregor[2]
R. Arkani[3] , C.A. Broderick,[3] E.O'Reilly[3] M. Sorel[4],
S. I. Molina[5], M. De La Mata[5]

[1]Department of Physics, Lancaster University, Lancaster, LA1 4YB, UK
[2]Gas Sensing Solutions, Cumbernauld, G68 9HQ, UK
[3]Tyndall National Institute, Lee Maltings, Dyke Parade, Cork, Ireland
[4]Department of Physics, Glasgow University, Glasgow, G12 8LP, UK
[5]Facultad de Ciencias, IMEYMAT, Universidad de Cadiz, Cadiz, Spain

Mid-infrared LEDs operating in the 2-5 μm spectral range are potentially of major importance for a wide variety of applications, including; chemical process control, atmospheric pollution monitoring, non-invasive medical diagnosis and free space optical communications. However, the advantages of the mid-infrared have not been fully exploited due to the lack of suitable room temperature sources and photodetectors. One attractive route to create such LEDs is the $Al_xIn_{1-x}Sb$ alloy system, with varying Al compositions which has already produced effective room temperature devices based on bulk active regions. In this work we investigate the use of In(As)Sb/InAlSb quantum wells (QWs) which have the advantages of strong quantum confinement with a type I band alignment and which can be easily tailored for the mid-infrared spectral range. We report on the MBE growth, structural and optical properties of these structures and observed bright mid-infrared electroluminescence up to room temperature.

Samples were grown on (001) undoped GaAs substrates, which offers potential advantages in terms of maturity and cost compared to GaSb or InAs. To overcome the high lattice mismatch between GaAs and $Al_{0.2}In_{0.8}Sb$ a metamorphic buffer layer was developed, using a dislocation filter consisting of 3 periods of superlattices, in which two strained materials alternate. High resolution X-ray diffraction (XRD) measurements reveal that the resulting $In_{0.8}Al_{0.2}Sb$ virtual substrate is fully relaxed -see Figure 1. The LED structure was grown on top of the $In_{0.8}Al_{0.2}Sb$ with an active region containing three compressively strained 5 nm InSb/ $In_{0.8}Al_{0.2}Sb$ QWs, followed by an electron blocking barrier. The wafers were processed into mesa-etched p-i-n devices with top-top metallic contacts using conventional photolithographic techniques and a dry etching process as shown in Figure 2. The LED emission spectrum was studied over the range 5-300 K as shown in Figure 3. These LEDs exhibit bright electroluminescence at room temperature where the peak emission at 3.4 µm originates from e1-hh1 recombination within the QW and is well-suited to hydrocarbon detection. An output power of 41 µW was measured under quasi-continuous drive conditions using 100 mA injection current and the internal quantum efficiency was 9.8%.

Acknowledgements: This work was supported by the EU M*arie Skłodowska-Curie Initial Training network (ITN) PROMIS - Grant agreement No 641899, EPSRC (EP/N018605/1), the Royal Academy of Engineering.*

*Corresponding author: a.krier@lancaster.ac.uk

Mid Infrared DFB Interband Cascade Lasers with low threshold power for gas sensing applications

R. Weih[1], J. Scheuermann[1], S. Höfling[2,3], J. Koeth[1]
[1] Nanoplus GmbH, Oberer Kirschberg 4, Gerbrunn D-97218, Germany
[2] Technische Physik, Physikalisches Institut and Wilhelm Conrad Röntgen-Research Center for Complex Material Systems, Universität Würzburg, Am Hubland, Würzburg D-97074, Germany
[3] SUPA, School of Physics and Astronomy, University of St Andrews, St Andrews, KY16 9SS, United Kingdom

After DFB ICLs have already shown to be able to cover a wide window (2.8µm [1] - 5.2µm [2]) of the mid infrared spectral region they are suitable light sources for applications where smallest concentrations of several gases have to be traced via absorption spectroscopy. The broken gap alignment of the two binaries GaSb and InAs enables carriers to re-enter the conduction band after making a radiative recombination in a quantum well. Thus cascading of multiple stages as in a QCL is possible. Due to the interband nature of the transition the gain per stage is larger and fewer stages are required in order to reach threshold at moderate current levels. In addition this comes with the advantage of significantly lower operation voltages. In Figure 1 the I-V as well as the I-P characteristics are shown for a loss coupled ICL DFB device in the 5.2µm spectral region with several improvements compared to the last generation of devices. Typical threshold currents are in the range of 20 to 60 mA depending on the heat sink temperature. The device emits a few mW which is sufficient for most spectroscopic applications. Figure 2 shows the corresponding tuning diagram in the temperature range from 0°C to 30°C. The tuning rates are 0.16 nm/mA with current and 0.52 nm/°C with temperature which enables an overall tuning range of more than 20 nm.

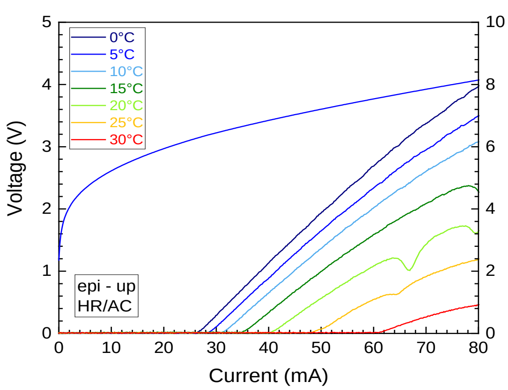

Figure 1: Electro-optical characteristics of a 5.2µm DFB-ICL.

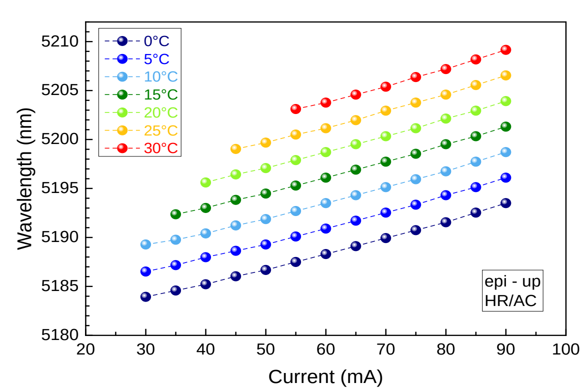

Figure 2: Temperature and current tuning diagram of a 5.2µm DFB-ICL.

[1] J.Scheuermann et al., Appl. Phys. Lett. **106**, 161103 (2015).
[2] M.V.Edlinger et al., IEEE Photon. Technol. Lett. 26, 5 (2014).

+ Author for correspondence: r.weih@nanoplus.com

Interband cascade devices: from lasers to LEDs and detectors

A. Schade,[1] F. Rothmayr,[2] A. Pfenning,[1] N. Schäfer,[2] J. Scheuermann[2], C. Kistner,[2] R. Weih,[2] M. Fischer,[2] J. Koeth,[2] M. Kamp,[1] F. Hartmann,[1] S. Höfling,[1,3]

[1] *Technische Physik, Physikalisches Institut and Wilhelm Conrad Röntgen-Center for Complex Material Systems, Universität Würzburg, D-97074 Würzburg, Germany*

[2] *nanoplus Nanosystems and Technologies GmbH, Oberer Kirschberg 4, Gerbrunn D-97218, Germany*

[3] *SUPA, School of Physics and Astronomy, University of St Andrews, St Andrews, KY16 9SS, United Kingdom*

Light sources and detectors covering the mid-infrared (MIR) spectral wavelength region are building blocks on the forefront of technological innovations tackling safety, environmental and health related applications. Very promising technological candidates of MIR light sources and detectors are based on the interband cascade scheme, which combine the cascading of active stages known from quantum cascade lasers (QCLs) and radiative interband transitions known from diode lasers. By exploiting the type-II transitions between InAs and GaInSb layers, the transition energy can be widely tuned by structural dimensions of the semiconductor layers. Thus, it is not limited by the semiconductor bandgap energy. Currently, three device types are actively researched for their optoelectronic properties, and will be discussed here: interband cascade laser (ICLs), light emitting diodes (IC-LEDs) and detectors (ICDs).

As key-element in tunable diode laser absorption spectroscopy to selectively detect and identify concentrations of gases and molecules, ICLs have shown remarkable progress within the past 10 years [1-3]. ICLs cover a broad spectral wavelength range from ~2.7 µm to 6 µm. Currently, its sweet spot emission wavelength with lowest threshold currents, largest output powers, and cw single mode operation, is at ~3.5 µm. We discuss critical parameters, from the electron injector quantum wells and improving doping in the active region, increasing thicknesses of the separate confinement layer and cladding layer and describe how these affect the emission properties.

IC-LEDs have sparked considerable interest due to their desirable characteristics such as considerable high yield at low cost, a wide spectral emission, and high spatial uniformity, which allows for large arrays of surface emitting diodes [4].

ICDs make use of a type-II superlattice absorber region that is sandwiched in-between charge carrier selective extraction regions. The type-II superlattice allows for normal incident detection and the low-energy detection limit can be designed by the superlattice period, whereas the selective electron and hole extraction regions guarantee extraordinarily low dark currents and high-speed operation [5, 6].

[1] I. Vurgaftman, et al., *Journal of Physics D: Applied Physics* **48**.12, 123001, (2015).
[2] J. R. Meyer, et al., *Electronics Letters* **32**.1, 45-46, (1996).
[3] R. Weih, et al., *Applied Physics Letters* **102**.23, 231123, (2013).
[4] N. Das, et al., *Applied Physics Letters* **87**.4, 041105, (2005).
[5] R. Yang, et al., *Journal of Applied Physics* **107**.5, 054514, (2010).
[6] S. Höfling, et al., *Infrared Remote Sensing and Instrumentation XXIV*. Vol. 9973, (2016).

[+] Author for correspondence: sven.hoefling@physik.uni-wuerzburg.de

Low-threshold InAs-based interband cascade lasers near 6.3 μm

Yiyun Li,[1,+] Lu Li,[1] Wenxiang Huang,[1] Rui Q. Yang,[1,+] James A. Gupta,[2] Xiaohua Wu,[2] and Geof C. Aers[2]

[1] *University of Oklahoma, School of Electrical and Computer Engineering, Norman, Oklahoma, 73019, United States*

[2] *National Research Council of Canada, Ottawa, Ontario K1A 0R6 Canada*

Interband cascade lasers (ICLs) [1-3] can be regarded as a hybrid of conventional diode lasers that employ electron-hole recombination, and a cascade structure that reuses the injected carriers. With these features, ICLs are capable of covering a wide range of the mid-infrared spectrum while maintaining a relatively low threshold current density.

Excellent device performance has been achieved in the wavelength region of 3~6 μm, especially in the range from 3- 4 μm [3-5]. Recently, progress has been made to extend the room temperature continuous wave (cw) operation of ICLs with lasing wavelengths beyond 6 μm [6]. As the wavelength becomes longer, free-carrier absorption loss and Auger recombination increase and it is more challenging to achieve room temperature operation with low threshold current density.

In this work, we report a study of InAs-based interband cascade lasers with lasing wavelengths near 6.3 μm. The ICL structure was grown by MBE on an InAs substrate and has 15 cascade stages. Broad-area laser devices were fabricated from this ICL wafer. A 1.5-mm-long broad-area device lased in pulsed mode at 300 K at a lasing wavelength of 6.26 μm with a threshold current density of 395 A/cm^2 (Figures 1 and 2), which is the lowest ever reported among semiconductor lasers at similar wavelengths. In pulsed mode, a 100 μm ×1.5 mm ICL was operated in pulsed at temperatures up to 335 K near 6.5 μm (Fig. 2), possibly limited by joule heating with 1 μs pulses (5 kHz) at a large current (>4 A). More results will be reported at the conference.

Acknowledgments: This work was partially supported by the National Science Foundation (IIP-1640576).

1. R. Q. Yang, "Infrared laser based on intersubband transitions in quantum wells," at *7th Inter. Conf. on Superlatt., Microstruc. & Microdevices*, Banff, Canada, Aug. 1994; Superlatt. Microstruc., **17**, 77 (1995).
2. J. R. Meyer, I. Vurgaftman, R. Q. Yang, and L. R. Ram-Mohan, "Type-II and type-I interband cascade lasers", Electronics Letters, **32**, 45 (1996).
3. R. Q. Yang, "Interband Cascade (IC) Lasers", Chap. 12, in *Semiconductor lasers: fundamentals and applications*, edited by A. Baranov & E. Tournie (Woodhead Publishing Limited, Cambridge, UK, 2013).
4. I. Vurgaftman, R. Weih, M. Kamp, J R Meyer, C. L. Canedy, C. S. Kim, M. Kim, W. W. Bewley, C. D. Merritt, J. Abell and S. Höfling, "Interband cascade lasers", *J. Phys. D: Appl. Phys.* **48** 123001 (2015).
5. L. Li, Y. Jiang H. Ye, R. Q. Yang, T. D. Mishima, M.B. Santos, and M. B. Johnson, "Low-threshold InAs-based interband cascade lasers operating at high temperatures," Appl. Phys. Lett. **106**, 251102 (2015).
6. S M S. Rassel, L. Li, Y. Li, R. Q. Yang, J. A. Gupta, X. Wu, and G. C. Aers, "High-temperature and low-threshold interband cascade lasers at wavelengths longer than 6 μm", Optical Engineering, **57**, 011021 (2018).

[+] Author for correspondence: Yiyun.li-1@ou.edu; Rui.q.Yang@ou.edu

Selective-Area Nanowires for Short-Wavelength and Mid-Wavelength Infrared Optoelectronics

Diana L. Huffaker,[1,2,3] Dingkun Ren,[2] Khalifa M. Azizur-Rahman,[1] Zixuan Rong[2]
[1] *School of Physics and Astronomy, Cardiff University, Cardiff, Wales CF24 3AA, UK*
[2] *Department of Electrical and Computer Engineering, University of California at Los Angeles, Los Angeles, California 90095, USA*
[3] *California NanoSystems Institute, University of California at Los Angeles, Los Angeles, California 90095, USA*

Semiconductor nanowires are frequently highlighted as promising building blocks for next-generation photodetectors. Their unique properties, namely small junction area and heteroepitaxy of different bandgap materials, are advantageous for significantly suppressing dark current from generation-recombination and minority carriers. This capability can lead to a higher signal-to-noise ratio (SNR) and pave the way to accomplish room-temperature operation of small bandgap detectors with higher detectivities. In this study, we explore short-wavelength infrared (SWIR) and mid-wavelength infrared (MWIR) selective-area nanowire photodetectors on InP substrates, which are composed of nanoscale photoabsorbers and 3D plasmonic gratings. We observe a remarkable reduction of dark current with high optical absorption in nanowires through excitation of surface plasmonic waves at metal-nanowire interfaces. Our work shows that, through sophisticated optical and electrical designs, nanowire-based photodetectors can demonstrate equivalent or better performance compared to their planar device counterparts for SWIR and MWIR.

Figure 1(a) shows current-voltage (I-V) characteristics of n-InAs nanowires grown on p-InP. A rectification ratio > 300 is measured at room temperature, which indicates a desirable diode performance. Figure 2(b) shows room-temperature photoluminescence of InAsSb nanowires, spanning from 2.5 μm to 3.5 μm, and optical absorption tuning by modulating surface plasmon resonance enhanced by metallic gratings.

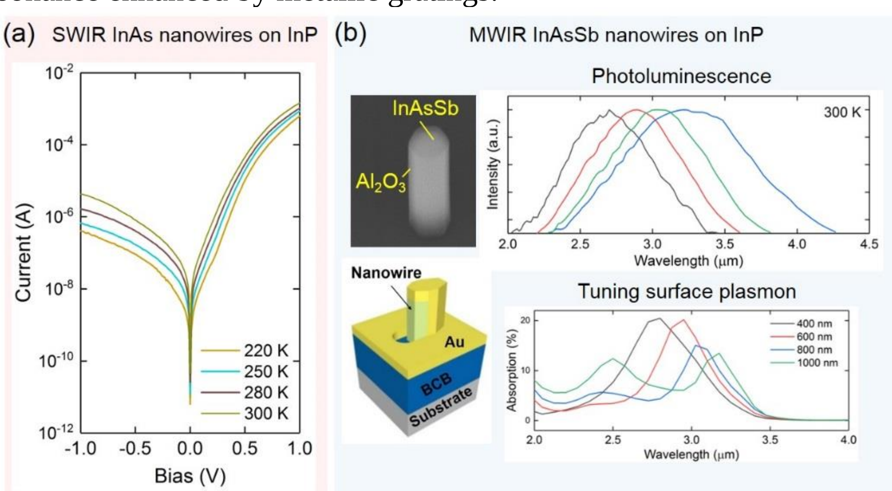

Figure 1 (a) I-V characteristics of InAs-InP (nanowire-substrate) diodes. (b) Optical properties of InAsSb nanowires. grown on InP substrates.

+ Author for correspondence: huffakerdl@cardiff.ac.uk or huffaker@ee.ucla.edu

InAs NWs on Si(111) Substrate for Infrared Light-emitting Diodes

X. Li[1,3,+], K. Zhang[1,3], J. Treu[4], L. Stampfer[4], G. Koblmueller[4], F. Toor[1,2,3], J.P. Prineas[1,2,3]

[1] Department of Physics and Astronomy, [2] Department of Electrical and Computer Engineering, [3]Optical Science and Technology Center, University of Iowa, Iowa City, IA 52242, USA
[4]Walter Schottky Institut and Physics Dept., Technical Univ. Munich, Garching, 85748, Germany

Silicon (Si) has been widely utilized in electronic devices due to its natural abundance and high crystal quality. There has been great interest in integrating the optical benefits that the III-V materials provide with Si. However, it is challenging to design III-V planar heterostructures due to the large lattice mismatch between III-Vs and Si. This lattice mismatch introduces misfit dislocations which degrade the crystal quality[1]. In the case of III-V nanowires (NWs) on Si, strain has been found to be coherently accommodated in the interface[2] through lateral expansion of the NW. Dislocation-free III-V NWs grown on a lattice-mismatched Si substrate by epitaxy has been demonstrated, opening the door to new possibilities of heterostructure design[3]. In this work we present characterization of recombination mechanisms in selective-area-grown InAs-based NWs on a Si (111) substrate by molecular beam epitaxy. These (wurzite) NWs were measured to have a nonradiative Auger recombination rate as much as one order of magnitude smaller[4] than comparable (zinc-blende) planar materials, making InAs/InAsSb NWs promising for devices like infrared light-emitting diodes, which operate at high carrier density[5]. Challenges remain, such as short Shockley-Read-Hall recombination rates (more important in low carrier density devices such as photodiode detectors), and a tendency of the nanowires to heat.

We applied an ultrafast laser differential transmission measurement on both InAs and InAs/InAlAs core-shell NWs shown in Fig. 1 to investigate the total carrier recombination rate (R) illustrated in Fig. 2. Ultrafast measurements were also used to determine Shockley-Read-Hall, and Auger recombination rates, as illustrated in Fig. 2, while radiative rates were determined by a separate continuous wave quantum efficiency measurement.

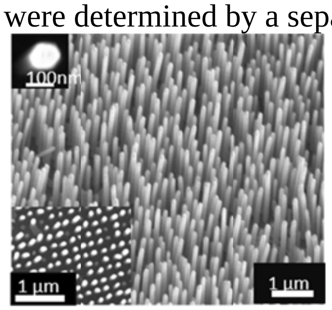

Figure 1. Scanning electron microscope image of the core-shell NWs

Figure 2. Recombination rate of both the core-shell and core-only NWs at 293K.

Plasma-enhanced atomic layer deposition of SiO_2 for channel isolation of colloidal quantum dots infrared phototransistors

L. Zheng,[1,+] Y. Yu[1]

[1] *State Key Laboratory of Functional Materials for Informatics, Shanghai Institute of Microsystem and Information Technology, Chinese Academy of Sciences, Changning Road 865, Shanghai 200050, P. R. China*

The solution-processed infrared optoelectronic materials, CQDs, provide quantum size effect tuning with low cost and substrate compatibility.[1-3] Three main classes of photodetectors have attracted much attention. The first, photodiodes, generally provide low dark currents with no gain. Another widely explored photodetectors are photoconductors, which produce a large number of electrons of photocurrent collected for each absorbed photon and offer photoconductive gain with a relatively high dark current. A different class of photo detectors, phototransistors, combines gain and a transistor effect. But for CQDs phototransistors, a reliable and thin dielectric film with preventive withstanding voltage and smooth surface morphology is required for the channel regulation.[2,3] Thermal oxidation is a commonly used method of SiO_2 deposition on Si. But it is difficult for thermal oxidation to control the thickness when the required SiO_2 thickness is down to nanoscale (e. g. 10 nm). Plasma enhanced chemical vapor deposition (PECVD) is another method of SiO_2 deposition but it also meet the ultrathin thickness control problem and the surface morphology is not quite good. In this work, PEALD is performed to grow SiO_2 on Si at a low temperature of 150C°. The breakdown electric field of SiO_2 is as high as 7 MV/cm when the thickness of is down to 10 nm. In addition, the surface RMS roughness of SiO_2 is only 0.3 nm, indicating the obtained SiO_2 can be a reliable dielectric for CQDs infrared phototransistors.

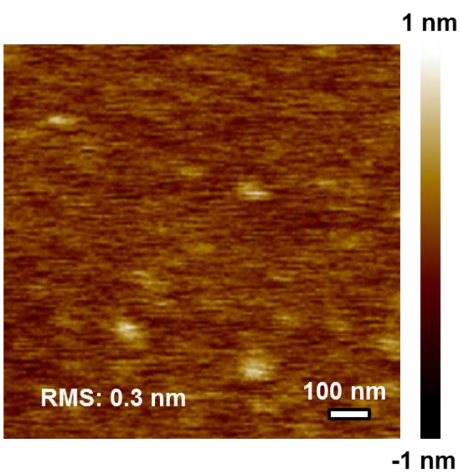

Figure 1 The AFM image of SiO_2 on Si deposited by PEALD.

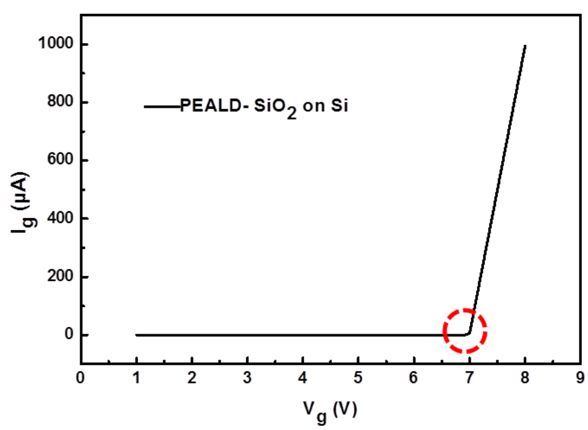

Figure 2: I-V characterization of PEALD-SiO_2.

[1] O. Voznyy et al., Nat. Rev. Mater. 2 (2017), 16100-2053
[2] A. P. Litvin et al., J. Mater. Chem. A 86 (2017), 13252-13275.
[3] V. Adinolfi et al., ACS Nano 9 (2015), 356-362.
.

+ Author for correspondence: zhengli@mail.sim.ac.cn

Semimetal/Semiconductor Nanocomposites for Ultrafast Photoconductors

Hong Lu

College of Engineering and Applied Sciences, Nanjing University, Nanjing, China

Using MBE, we are able to incorporate rare earth elements, such as Er, into a III-V matrix to form a nanocomposite material. The rare earth element forms semimatallic nanostructures that are embedded in the III-V coherently to form a high crystalline quality material, and behave as trap states for the carriers to achieve an ultrafast photocarrier lifetime. Short carrier lifetimes increase the speed of the photoconducting device. We will discuss the growth, nanostructure formation, electrical properties, photocarrier dynamics and device performance of these semimetal/semiconductor nanocomposites, especially for 1.55 μm applications.

High quantum efficiency GaInAsSb thermophotovoltaic cells integrated on GaAs substrates

Q. Lu,[1+] **R. Beanland,**[2] **D.M. Cardenes,**[1] **A.R.J. Marshall,**[1] **A. Krier**[1]

[1] *Physics department, Lancaster University, Lancaster, LA1 4YB, United Kingdom*

[2] *Department of physics, University of Warwick, Coventry, CV4 7AL, United Kingdom*

Thermophotovoltaic (TPV) cells can absorb the mid-infrared photons emitted from thermal sources to produce current flow and voltage bias, providing a direct and convenient energy conversion method from heat to electricity [1]. TPVs based on narrow bandgap GaInAsSb are promising candidates for waste heat recovery applications at relatively low temperatures ~1000 °C [2]. However, a cost-effective material platform is needed to enable large area TPV panel fabrication. In this work, we integrated GaInAsSb TPVs on GaAs substrates by using an advanced metamorphic technique. The buffer region consisted of GaSb/GaAs interfacial misfit (IMF) arrays and GaInSb/GaSb strained layer superlattices, which serve as dislocation filtering layers (DFLs). The resulting TPV on GaAs was compared with the TPV lattice matched on GaSb. They were characterized using an 800 ˚C thermal emitter and a solar simulator (1 sun AM 1.5 condition). In both cases, the J_{sc} from TPV on GaAs was very close to the reference cell, whereas the V_{oc} was about 40 meV lower, as shown in Fig. 1. The peak EQE of the TPV on GaAs exceeded 60%, which is the highest reported for any GaInAsSb TPV on GaAs (Fig. 2). It gives a clear indication that the dislocations in the cell were sufficiently reduced to have a very small impact on the quantum efficiency. This metamorphic buffer layer technique can enable high quality GaInAsSb TPVs to be grown on GaAs, which will help to significantly reduce the cost of large area TPVs for waste heat recovery.

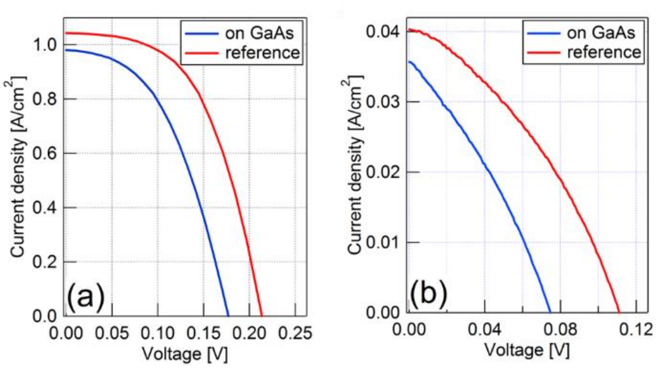

Figure 1. J-V curves from the TPV on GaAs and the reference cell when illuminated using (a) an 800 ˚C blackbody emitter, and (b) a solar simulator; 1 sun AM 1.5 condition

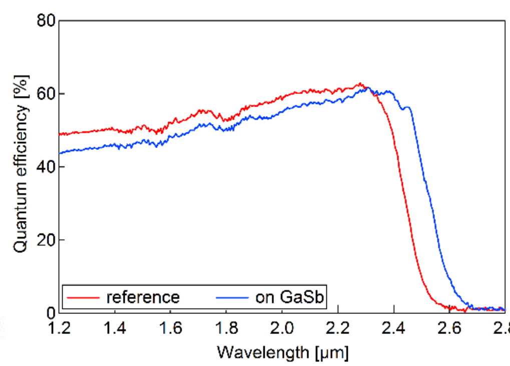

Figure 2. EQE curves of the GaInAsSb TPV on GaAs and the reference cell.

[1] Ferrari C, Melino F, Pinelli M, Spina PR, Venturini M. Overview and status of thermophotovoltaic systems. *Energy Procedia*. 2014;45:160-169.

[2] Dashiell MW, Beausang JF, Ehsani H, et al. Quaternary InGaAsSb thermophotovoltaic diodes. *IEEE Trans Electron Devices*. 2006;53(12):2879-2888.

[+] Author for correspondence: q.lu3@lancaster.ac.uk

Collection Efficiency and Device Performance in Narrow Bandgap Thermophotovoltaic Cells Based on Interband Cascade Structures

Wenxiang Huang,[1,2,+] **Lin Lei,**[1,2] **Lu Li,**[1] **Jeremy A. Massengale,**[1,2] **Rui Q. Yang,**[1,+] **Tetsuya D. Mishima,**[2] **Michael B. Santos**[2]

[1] *School of Electrical and Computer Engineering, University of Oklahoma, Norman, Oklahoma 73019, USA*

[2] *Homer L. Dodge Department of Physics and Astronomy, University of Oklahoma, Norman, Oklahoma 73019, USA*

Thermophotovoltaic (TPV) systems are an attractive technology to convert otherwise-wasted radiant energy from a heat source into useful electrical energy. TPV cells are critical components that absorb incident radiation to produce electrical current. Most previous research on TPV cells concentrated on diode structures made of bulk semiconductors with bandgaps (E_g) above 0.5 eV. However, theoretical projections of the ultimate efficiency for the photovoltaic conversion of energy, based on the model of Shockley and Queisser in the detailed balance limit, reveal that the optimum bandgap of TPV cells for heat sources of 500-2,000°C is in the range of 0.12 to 0.41 eV. Artificial quantum-engineered superlattice (SL) structures are capable of covering this range of bandgaps. In this work, we present a comparative study of three narrow-bandgap (~0.2 eV at 300 K) TPV cells with InAs/GaSb type-II superlattice absorbers. One of the three cells has a single absorber, while the other two are constructed with three and five cascade stages with relatively shorter individual absorbers.

By comparing the characteristics of these three narrow bandgap TPV structures [1-2], it is clear that the device performance of a conventional single-absorber TPV cell is limited mainly by the small collection efficiency (η_c) associated with a relatively short diffusion length (1.5 μm at 300 K). Furthermore, this study revealed that multi-stage interband cascade (IC) TPV structures with thin individual absorbers can circumvent the diffusion length limitation and are capable of achieving a collection efficiency approaching 100% for photo-generated carriers. Additionally, the open-circuit voltage, the fill factor, the output power, and the power conversion efficiency can be significantly increased in IC TPV devices compared to the conventional single-absorber TPV structure. The collection efficiencies and the conversion efficiencies (η) for the three representative TPV cells at 300 K are shown in Figures 1 and 2, respectively. More detailed results will be reported at the conference. These results have further validated the potential and advantages of narrow bandgap IC structures for TPV cells.

Acknowledgements: This work was supported in part by the National Science Foundation (NSF) under Grant DMR-1608224.

1. R.Q. Yang, Z. Tian, J. Klem, T.D. Mishima, M.B. Santos, and M.B. Johnson, "Interband cascade photovoltaic devices", Appl. Phys. Lett. **96**, 063504 (2010).
2. H. Lotfi, L. Li, L. Lei, R.Q. Yang, J.F. Klem, and M.B. Johnson. "Narrow-bandgap interband cascade thermophotovoltaic cells", IEEE. J. Photovoltaics. **7**, 1462 (2017).

[+] Corresponding authors: wxhuang@ou.edu; rui.q.yang@ou.edu

Thermal Conductivity Properties of Graphene Using Non-Equilibrium Molecular Dynamics Simulations

X. Q. Wei,[1,2+] S. Yang,[1] L. Zhu,[3] Y. L. Fu,[1] Z. L. L,[1] Y. F. L,[1] L. X. Shi,[1] Z. G. Huang[1]

[1] *Science School , Huaihai Institute of Technology, Lianyungang, Jiangsu, China, 222005*

[2] *Research Institute of Xi'an Jiaotong University, No. 328 Wenming Road, Xiaoshan District, Hangzhou City, Zhejiang Province, 311215*

[3] *Art of Huaihai Institute of Technology, Lianyungang, Jiangsu, China, 222005*

Recent years, we have seen a rapid growth of interest by the scientific and engineering application in the thermal management of materials. Heat dissipation has become a crucial issue for continuing progress in the sate-of-the-art electronic industry. Carbon-based materials occupy a unique place in the terms of the heat transport ability and revealed truly intriguing features, especially for graphene. Here, I investigate the thermal properties of graphene focusing on armchair graphene and zigzag graphene with different size, using non-equilibrium molecular dynamics simulations (NEMDS). The simulation shows that the thermal conductivity of zigzag graphene is higher than that of the armchair, which is because of the better dispersion curves displaying on zigzag graphene. The results also indicate the thermal conductivities increase with the increasing length of graphene.

This study highlights the importance of structure-thermal conductivity property relationship and provides simulation results of thermal transport property for practical applications, which is valuable insight into thermal management of thermoelectric devices.

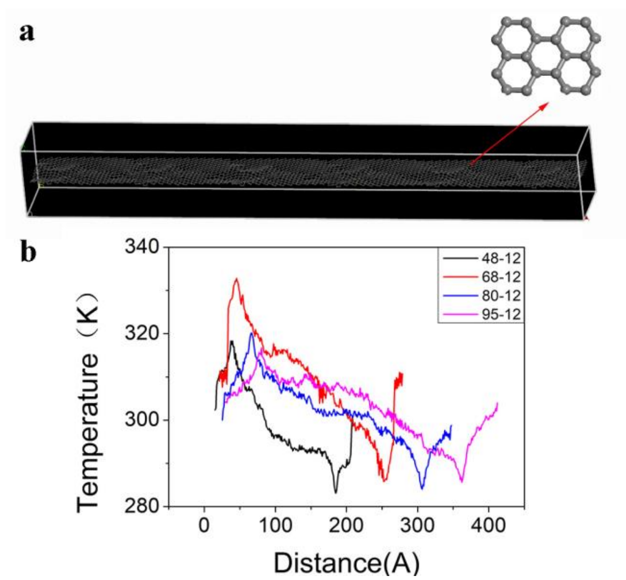

Figure 1 (a) Armchair graphene model for NEMDS. (b) Temperature distribution of graphene with different length.

+ Author for correspondence: wei.wxq@163.com

Study of interband cascade lasers for MIR-VCSELs

D. A. Diaz-Thomas, M. Bahriz, A. Meguekam-Sado, E. Tournié, A.N. Baranov, and L. Cerutti+

IES, Université de Montpellier, CNRS, F-34000, Montpellier, FRANCE

Over the last decade, significant progress has been achieved in mid-infrared Interband Cascade Lasers (ICLs). Indeed, low threshold continuous wave (cw) operation of ICLs at room temperature (RT) has been reported for the whole 3-5µm wavelength range. Vertical cavity surface emitting lasers (VCSELs) are particularly well suited to TDLAS due to their intrinsic characteristics. The low threshold current, single frequency emission with a circular low divergent output beam are beneficial for the development of compact systems for molecular spectroscopy. However, only one report on ICL-based VCSELs has been published so far [1]. These devices operated near 3.4 µm only in pulsed mode.

We studied a series of ICLs with a waveguide employing $Al_{0.85}Ga_{0.15}As_{0.07}Sb_{0.93}$ cladding layers. We studied the effect of growth temperature of the top cladding layer on the laser performances. It was previously shown that annealing of the active region of GaSb-based quantum wells laser diodes during growth of the upper cladding layer affected both the laser emission wavelength and its efficiency [2]. In this work, we demonstrate a direct correlation between the growth temperature of the upper cladding layer and the ICL performances. For broad area lasers (100 µm x 2 mm) characterized in the pulsed regime at RT, the threshold current density dropped from 700 to 220 A/cm^2 and the wavelength emission shifted from 2.98 to 3.3 µm when the growth temperature decreased from 490 to 435°C (fig 1). CW operation of 19-µm-wide ridge lasers fabricated from the best wafer was obtained up to 55°C. The output measured power of these devices reached 8 mW/facet at 27°C. The emission wavelength around 3.33 µm is of great interest for sensing of hydrocarbons and other organic molecules (fig.2).The obtained results will be used for the development of IC VCSELs.

This work was partially supported by the French "Investment for the Future" program (EquipEx EXTRA, ANR-11-EQPX-0016) and by the French ANR (MIMIC-SEL, ANR-16-CE24-0011)

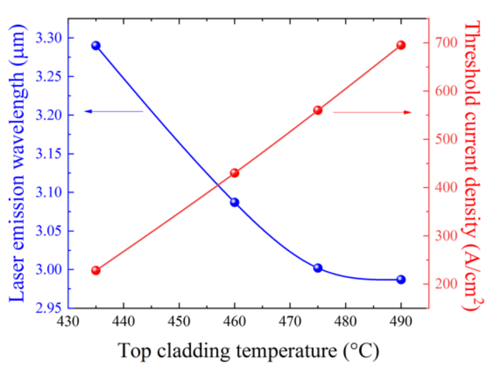

Figure 1 Evolution of current density threshold and wavelength emission for ICL with the top cladding growth temperature.

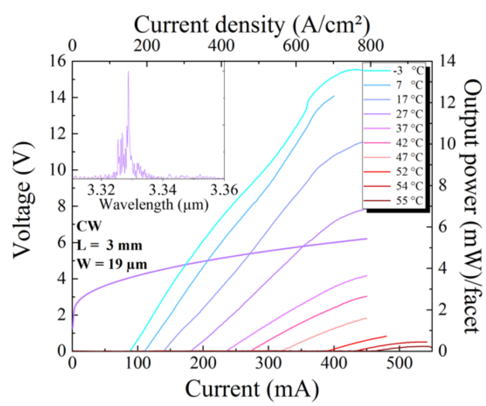

Figure **2:** I-P-V characteristics of narrow ridge device operating in cw-mode. *Inset*: laser spectrum at 27°C under 200 mA CW current injection.

[1] W.W. Bewley, APL **109**, 151108 (2016).
[2] K. Vizbaras, JCG **323**, 446-449 (2011)

+ Author for correspondence: laurent.cerutti@umontpellier.fr

Suppressing high order transverse modes in broad area QCLs

<u>R. Kaspi</u>, S. Luong, C. Lu, T.C. Newell, C. Yang and D. Gianardi
Air Force Research Laboratory, AFRL/RDLTD Albuquerque, NM 87117 USA

Fabricating a broad-area device is the most straight-forward method to achieve power scaling in a QCL. Instead of the fundamental mode, however, high-order transverse optical modes will be preferred, resulting in a two-lobed beam and degradation of beam quality [1].

We have recently described a method to provide preferential losses to the high-order transverse modes with the presence of metallic layers that are in contact with the sidewalls of the optical cavity [2]. The standard "dual channel" fabrication procedure is modified to remove the top portion of the dielectric layer that is normally deposited at the sidewalls. This method allows the deposition of gold in direct contact with the sidewalls along the top clad, and provide coarse adjustment of the contact area. Examination of far field spectra in broad-area QCLS emitting at ~4.7µm shows that transverse mode selection is altered in favor of the fundamental mode as a result of the metal layer. When metal coverage of the sidewall is greater than ~3µm, the device emits a single lobed peak, centered with the optical axis that is primarily composed of fundamental mode emission which results in increased brightness. The optically lossy metal layer provides preferential losses to the high order transverse modes, presumably because more of their electric fields penetrate the semiconductor-metal interface. The loss is provided in a distributive manner along the entire length of the cavity length. Only a small (<10%) increase in threshold current density and a small (<10%) reduction in slope efficiency is observed.

To accompany these experimental results, we have conducted COMSOL modeling of mode selection as a function of cavity width, as well as the extent of sidewall metal coverage. We calculate a figure-of-merit that is inversely proportional to the threshold current density for each higher order mode to determine its likelihood of selection. We find that the modeling results are consistent with experimental observations; i.e. high order transverse modes are preferentially suppressed with additional metal coverage, and for a large range of broad-area device geometry, fundamental transverse mode operation is preferred.

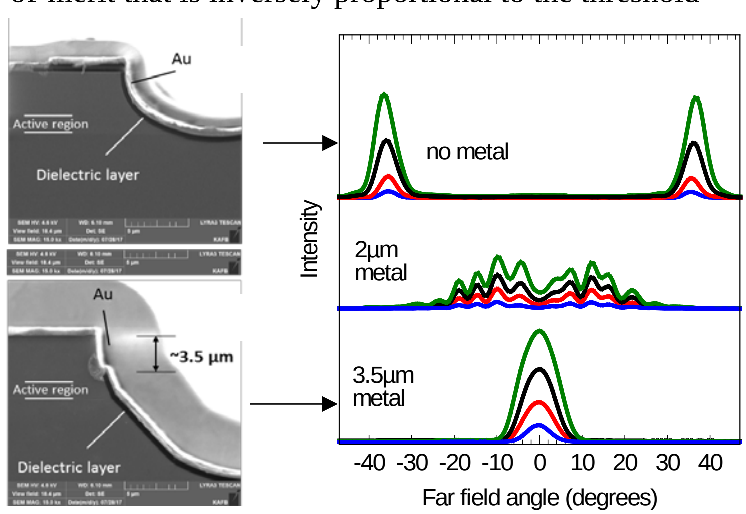

[1] Y. Bai, S. Slivken, S.R. Darvish, A. Haddadi, B. Gokden, and M. Razeghi, APL **95**, 221104 (2009).
[2] R. Kaspi, S. Luong, T. Bate, C. Lu, T.C. Newell, and C. Yang, APL **111**, 201109 (2017).

Methods to Enhance sensitivity to the surface-normal dielectric functions of anisotropic layers using Infrared Ellipsometry

Thomas E. Tiwald[1], Nina Hong[1]
[1] *J.A. Woollam Co., Inc., 645 M St., Suite 102, Lincoln, NE 68508 USA*

For anisotropic films – this includes many metamaterial layers – it is often difficult to determine the surface-normal dielectric function in spectral regions where the anisotropic layer is absorbing. It can be demonstrated that reflection measurements at non-normal incidence angles (including reflection ellipsometry) have low sensitivity to optical properties out of the surface plane. The primary reason: when light enters a material from a low index medium like air, refraction at the ambient-film interface tends to direct the beam towards surface normal. This causes both the p- (TM) and s- (TE) components of the electric field to be oriented mostly parallel to the film surface, and the optical response in spectral regions are dominated by projection of the dielectric tensor on the sample surface [1][2]. This is a particular problem in spectral regions where the layer is absorbing, since much of the light that is collected by the detector is reflected from the ambient/film interface and not from the film/substrate interface. We demonstrate two methods that can enhance the sensitivity to the surface-normal dielectric function of an anisotropic layer at infrared wavelengths: grazing angle of incidence infrared ellipsometry [3], and infrared Total Internal Reflection ellipsometry – which has already been applied to hyperbolic metamaterial layers at UV-visible wavelengths [4]. Both of these methods enhance the out-of-plane electric fields within the layer, which increase the contribution of the surface-normal absorptions to p-polarized Fresnel reflection coefficient. As a demonstration, both of these techniques are applied at infrared wavelengths to a polyimide film (CP1), which is a uniaxially anisotropic film that has both film surface-normal and surface-parallel modes that are IR-active.

[1] D.E. Aspnes. *J. Opt. Soc. Am.*, **70**, 10, 1275 (1980).
[2] G. E. Jellison Jr. and J. S. Baba, *J. Opt. Soc. Am. A* **23**, 2 468 (2006).
[3] A. Naqavi, S. P. Loke, M. D. Kelzenberg, D. M. Callahan, T. Tiwald, E. C. Warmann, P. Espinet-González, N. Vaidya, T. A. Roy, J-S. Huang, T. G. Vinogradova, and H. A. Atwater, accepted for publication in *Optics Express*.
[4] C. Zhang, N. Hong, C. Ji, W. Zhu, X. Chen, A. Agrawal, Z. Zhang, T. E. Tiwald, S. Schoeche, J. N. Hilfiker, L. J. Guo, and H. J. Lezec, *ACS Photonics*, accepted for publication and current in press.

[+] Author for correspondence: ttiwald@jawoollam.com

Carrier concentration verification in plasmonic waveguide of the semiconductor cascade lasers by using FTIR spectroscopy

Marcin Motyka,[1] Mateusz Dyksik, [1] Michał Rygała,[1] Grzegorz Sęk,[1] Krzysztof Ryczko,[1] Jan Misiewicz,[1] Kamil Pierściński,[2] Piotr Gutowski,[2] Maciej Bugajski.[2]

[1] *Department of Experimental Physics, Wrocław University of Science and Technology, Wybrzeże Wyspiańskiego 27, 50-370 Wrocław, Poland*
[2] *Institute of Electron Technology, Al. Lotników 32/46,02-668 Warsaw, Poland*

One of the most important issues in the long process of the quantum cascade lasers (QCLs) growth is obtaining the proper concentration of electrons in different parts of the multilayer structure. It especially concerns the injector part, where electrons tunnel between the respective quantum wells but also the plasmonic waveguides responsible for proper light propagation along the whole structure. For doped plasmonic waveguides, one can use a direct correlation between the resonant plasmonic frequency and concentration of electrons in the given layer or material. Determining the latter, even post-growth, is crucial from several reasons. First, the carrier concentration has to be significantly high to get a good refractive index contrast between the resonator material and the waveguides. Second, depending on the emitted wavelength it has to fit to the proper plasmon frequency to allow efficient internal reflection for the given wavelengths. Finally, the concentration has to be high enough to satisfy the two mentioned points, but at the same time, the free carrier related losses should be minimized.

There exist several methods to determine the carrier concentration in semiconductors e.g. Hall and capacitance-voltage measurements. They are very useful from the point of view setup calibration, however require quite precise contacts preparation (which makes them destructive) and, or application of the external magnetic field.

In this communication, we present a different concept, namely fast differential reflectance technique (FDR)[1] based on Fourier transformed infrared (FTIR) spectroscopy, which is an non-destructive optical method, which allows to learn about the carriers' density, also in the buried waveguide layers of a QCL. Depending on the semiconductor, the effective mass of the electrons changes, and for high concentrations (~10^{18}) allows to get significant electron - phonon interaction and further absorption minimum related to the plasmonic frequency, which can be observed in mid, and long wavelength infrared range [2]. The measurement sensitivity might be improved being realized in function of light polarization, which allows emphasizing such absorption in respect to polarization selection rules (Berreman effect). We present such measurements applied to differently doped semiconductors layers, e.g. InAs, InGaAs, InAlAs and InP, which can be considered for plasmonic waveguides of the quantum cascade lasers emitting in the mid and long wavelength infrared range.

[1] M. Motyka, J. Misiewicz, Appl. Phys. Express 3 (2010) 112401
[2] M. Dyksik, M. Motyka, G. Sęk, J. Misiewicz, M. Dallner, S. Höfling, and M. Kamp, J. App. Phys. 120 (2016) 043104

Lateral and Vertical Transport in *n*- and *p-type* InAsSb and InAs/InAsSb Type-II Strained Layer Superlattices for Infrared Detector Applications

Lilian K. Casias[1], Christian P. Morath[2], Elizabeth H. Steenbergen[2], Preston T. Webster[2], Jin Kim[3], Gilberto Umana-Membreno[4], Vincent Cowan[2], Ganesh Balakrishnan[1] and Sanjay Krishna[5]

[1]*Center for High Technology Materials, University of New Mexico, Albuquerque, NM USA;*
[2] *Air Force Research Laboratory, Space Vehicles Directorate, Kirtland AFB, NM, USA;*
[3]*Sandia National Laboratory, Albuquerque, NM USA;*
[4]*School of Electrical, Electronic and Computer Engineering, The University of Western Australia, Crawley WA, Australia;*
[5]*Department of Electrical and Computer Engineering, The Ohio State University, Columbus, OH USA;*

The InAs/InAsSb type-II strained layer superlattice (T2SLS) material system has significant potential for infrared (IR) detector applications, including space-based detection, when utilized in a unipolar barrier detector architecture (nBn). However, recent studies revealed the quantum efficiency in nBn detectors degrades significantly faster from proton-irradiation induced displacement damage as compared to HgCdTe photodiodes [1]. Improving the quantum efficiency radiation-tolerance is theoretically possible by enhancing vertical hole mobility and thereby the vertical hole diffusion length. The vertical hole mobility of T2SLS materials differs significantly from the lateral mobility and measuring it is much less straightforward.

Here, an investigation of the transport properties of *n*- and *p*-type InAs/InAsSb T2SLS materials was performed in an effort to establish a relatively direct and effective methodology to measure vertical hole mobility and thereby set the stage for future studies to enhance it. The vertical transport properties of *n*-doped $(n^+n^-n^+)$ and *p*-doped $(p^+p^-p^+)$ lattice-matched InAsSb and strain-balanced InAs/InAsSb MWIR superlattices grown on GaSb substrates using molecular beam epitaxy were determined using temperature-dependent magneto-resistivity measurements in conjunction with lateral transport measurements. Substrate-removed, metal-semiconductor-metal (MSM) devices were fabricated for vertical measurements, while standard van der Pauw structures were used for lateral measurements. AlAsSb layers served as an etch-stop layer (vertical structures) and as an insulating layer (in-plane structures). To accurately determine the electronic transport properties in the presence of multiple carrier species, High Resolution Mobility Spectrum Analysis (HR-MSA) was employed.

[1] Morath, Christian P., et al. "Proton irradiation effects on the performance of III-V-based, unipolar barrier infrared detectors." *IEEE Transactions on Nuclear Science* 62.2 (2015): 512-519.

+ Author for correspondence: lkacosta@unm.edu

GeSn for Mid-Infrared Applications Grown by Remote Plasma Enhanced Chemical Vapor Deposition.

Gordon Grzybowski[1], Stephanie Chastang[1], Arnold Kiefer[2], Bruce Claflin[2]

1) KBRwyle 2601 Mission Point Blvd., Suite 300, Dayton, OH 45431
2) Air Force Research Laboratory, Sensors Directorate, Wright-Patterson AFB, Dayton, OH 45433

We report the growth and electronic, structural, and optical characterization of Ge and GeSn thin films on Sapphire, Si (001), Ge (001), and Ge-Virtual Substrates (VS) on silicon produced by Remote Plasma Enhanced Chemical Vapor Deposition (RPECVD) at temperatures ranging from 300-410 C. Film compositions varied from 0-10% Sn with thicknesses from 5-1100 nm showing different surface morphologies based on substrate and composition. The effect of growth parameters and rapid thermal annealing of Ge-VS on GeSn film quality is also detailed.

Advanced Glass Compositions for Mid-IR Laser Applications

M. Klopfer,[1] L. J. Henry[2], R. K. Jain[1]
[1] *University of New Mexico, Center for High Tech Materials, Albuquerque, NM 87131*
[2] *Air Force Research Laboratory, AFRL/RDLTD, Kirtland AFB, NM 87117*

There is significant interest in high-power mid-IR lasers -- and key enabling "gain materials" -- for numerous defense applications including IRCMs. Rare-earth-doped and transition-metal-ion-doped mid-IR transparent glasses, ceramics, and crystals have shown great potential as MIR gain media [1, 2], particularly if these media can be drawn into high quality double-clad fibers to obtain highly efficient high-beam quality high power Watt-level MIR lasers [1] pumped with relatively "low beam quality" high power laser diodes.

We will discuss our work on developing advanced mid-IR transparent oxide laser glasses (including germanosilicates and tellurites such as TZNL) and the use of appropriate rare earth (including Er, Tm, Ho) and transition metal (notably Fe, Bi, and Cr) ion dopants embedded in the glass, either as network modifiers, free ions, or *in nanocrystalline "cages" that keep the ions (eg, Fe) in "benign" local environments for tetrahedral co-ordination [2] and inhibit clustering and self-quenching.* In particular, we will discuss key challenges and our results associated with the development of the host glasses for mid-IR fiber fabrication, including: (1) the use of heavy ions to enable low-phonon energies to "push the multi-phonon absorption edge to longer wavelengths; (2) the use of appropriate index modifiers for creating index steps between the core and cladding, as well as to match the refractive indices of host glasses to high-index nanocrystallites and minimize losses due to Rayleigh scattering; (3) the maintenance of dopant ions in the correct reduction states (as is critical for Bi); and (4) careful removal of absorbing impurities such as water [3] (see absorption in the 2.5 to 4.5 μm region in Fig. 1 below) by careful dehydration and addition of appropriate matrix modifiers such as lead (Fig. 1). Figure 2 shows a strong nonlinear increase in the MIR emission in Er-doped tellurite due to the strong onset of cross-relaxation processes [1], *an important effect, reported for the first time in oxide glasses.*

[1] X.S. Zhu and R. K. Jain, Opt. Lett, vol 32, p.26 (2007)
[2] S,B. Mirov et al, IEEE Journ. of Sel. Topics in Quant. Electr., vol 21, 160179 (2015).
[3] H. Ebendorff-Heidepriem st al, Opt. Matl. Expr., vol 2, p. 432 (2015)

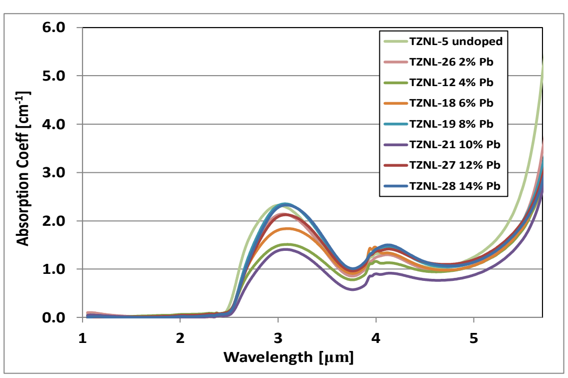

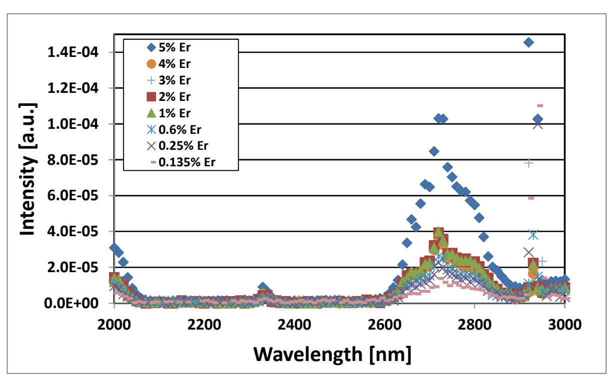

Figure 1: MIR absorption spectra of TZNL tellurite glasses as a function of Pb content

Figure 2: MIR luminescence spectra of Er-doped TZNL. Note nonlinear increase after 4% doping.

High Performance Superlattice Light Emitting Diodes Grown Epitaxially on Silicon

A.J. Muhowski,[1,2,+] **C.L. Bogh,**[1,2] **R.L. Heise,**[1,2] **T.F. Boggess,**[1,2,3] **and J.P. Prineas**[1,2,3]
[1] *Department of Physics and Astronomy, University of Iowa, Iowa City, IA 52242 USA*
[2] *Optical Science and Technology Center, University of Iowa, Iowa City, IA 52242 USA*
[3] *Department of Electrical and Computer Engineering, University of Iowa, Iowa City, IA 52242 USA*

InAs/GaSb superlattice light emitting diodes were epitaxially grown and fabricated on highly mismatched, heterovalent Si substrates and lattice-matched GaSb substrates. Structural analyses of the epitaxial layers showed degraded material quality on Si, with a concomitant decrease in the photoluminescence and Shockley-Read-Hall lifetime as resolved by ultrafast differential transmission. However, LED performance improved in the Auger-limited recombination regime, yielding enhanced performance due to improved thermal conductivity and transparency of the Si substrate over the GaSb substrate.[1] This effect was especially pronounced for large LEDs, while smaller LEDs tended to fail earlier on Si substrates than GaSb substrates.

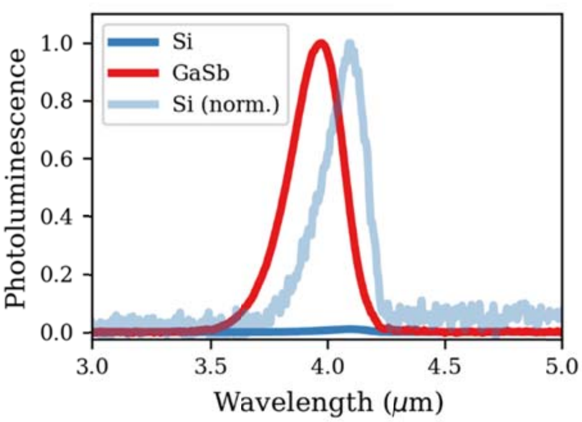

Figure 1: Spectrally resolved photoluminescence at 77K of a superlattice grown on Si (blue) and GaSb (red). The normalized output is also shown for the superlattice on Si.

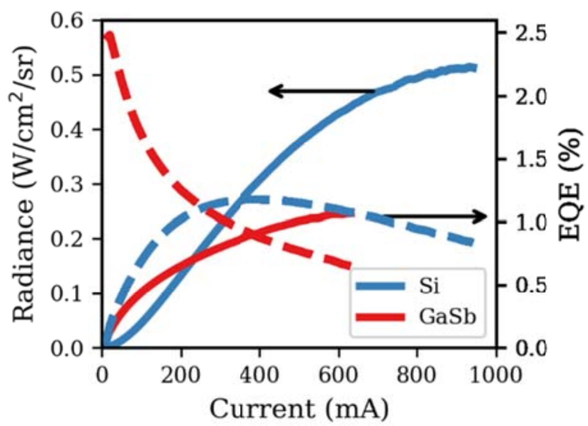

Figure 2: Radiance (solid) and external quantum efficiency (dashed) for 400μm x 400μm LED mesas on Si (blue) and GaSb (red).

[1] A.J. Muhowski, C.L. Bogh, R.L. Heise, T.F. Boggess, J.P. Prineas, "Superlattice Light Emitting Diodes Grown Epitaxially on Silicon," submitted to Appl. Phys. Lett. July 2018.

[+] Author for correspondence: aaron-muhowski@uiowa.edu

Graphene-metamaterial mid-infrared thermal emitters

C. Shi, [1+] N. H. Mahlmeister, [1] P. Gowda, [1] I. J. Luxmoore, [1] and G. R. Nash[1]
College of Engineering, Mathematics and Physical Sciences, University of Exeter, EX4 4QF, Exeter, United Kingdom.

There is a continuing need for the development of cost-effective and sustainable mid-infrared emitters for applications such as gas sensing. Over the last few years, there has been much recent interest [1] in the use of graphene as an incandescent source emitting in the visible, an effect which exploits the ability of graphene to sustain extremely large current densities. We have recently assessed the potential of using graphene based thermal emitters as an alternative, less complicated, approach to mid-infrared semiconductor LEDs [2], where the low thermal mass of graphene offers the potential for high frequency modulation [3]. Encapsulation of the emitting layer with hexagonal boron nitride allowed devices to run continuously in air for over 1000 hours [4], with the emission spectrum covering the absorption bands of many important gases. The h-BN encapsulation also allows the integration of structures to tailor the emission properties of the device. In this work, we demonstrate that the broadband thermal emission can engineered into two main spectral bands integration of a frequency selective surface metamaterial, consisting of ring resonators Measurements of both reflection and emission spectra agreeing well with simulations. We will also discuss how the addition of a conductive layer beneath the emitting layer, separated from it by a thin dielectric layer, could potentially enhance the quality factor of the resonances [5].

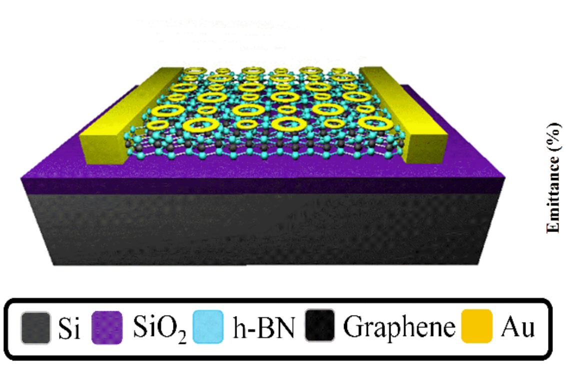

Figure 1 Schematic of the proposed metamaterial graphene mid-infrared emitter

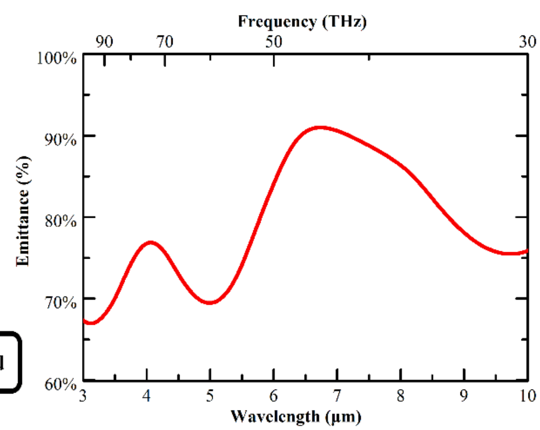

Figure 2 Measured emission spectrum of the device

[1] Young Duck Kim, Hakseong Kim, Yujin Cho *et al*, Nature Nanotechnology **10**, 676 (2015).

[2] L. M. Lawton, N. H. Mahlmeister, I. J. Luxmoore, and G. R. Nash, AIP Adv. **4**, 087139 (2014).

[3] N. H. Mahlmeister, L. M. Lawton, I. J. Luxmoore, and G. R. Nash, Appl. Phys. Express **9**, 012105 (2016).

[4] H. R. Barnard, E. Zossimova, N. H. Mahlmeister, L. M Lawton, I. J. Luxmoore, and G. R. Nash, Appl. Phys. Lett. **108**, 131110 (2016).

[5] C. Shi, N. H. Mahlmeister, I. J. Luxmoore, and G. R. Nash, Nano Res. **11**,3567 (2018)

[+] Author for correspondence: cs595@exeter.ac.uk

Recent Advances in QCL Based Sensing of Gases and Liquids

B. Lendl[1], J. Hayden[1], S. Lindner[1], A. Schwaighofer[1], M. Montemurro[2], J.P. Waclawek[1], A. Genner[1], H. Moser[1]

[1] *Institute of Chemical Technologies and Analytics, Technische Universität Wien, Getreidemarkt 9-164, A-1060 Vienna, Austria*

[2] *Laboratorio de Desarrollo Analítico y Quimiometría (LADAQ), Universidad Nacional del Litoral-CONICET, Ciudad Universitaria, 3000 Santa Fe, Argentina.*

Advances in Analytical Chemistry are often linked to technological developments in neighboring disciplines. This also concerns the recent development of quantum cascade lasers, which allows realization of sensing approaches in the mid-IR range that are different and potentially more powerful compared to classical absorption measurements based on Lambert-Beer law. In this presentation, new approaches for gas and liquid sensing as well as different applications using quantum cascade lasers will be discussed.

In the field of trace gas sensing indirect methods such as photothermal and photoacoustic techniques are very promising as their analytical signal is directly proportional to the analyte concentration and the employed laser power. This presentation will focus on recent advances in Photothermal Interferometry (PTI) employing distributed feedback Quantum Cascade Lasers. LODs in the single digit ppb range for SO_2 have been recently achieved when working in a balanced detection mode.

For liquid sensing external cavity Quantum Cascade Lasers are used. The latest generation of these lasers finally allows to outperform state-of-the-art FTIR spectrometers in terms of signal to noise in the recorded absorbance spectra. In this presentation special focus will be given to the qualitative and quantitative analysis of proteins in aqueous media in the spectral region from 1530-1700 cm^{-1}. On the example of milk analysis it will be shown how different milk proteins (casein, β-lactoglobulin,..) can be distinguished and simultaneously quantified. Finally, a Mach Zehnder interferometer for performing dispersion and absorption spectroscopy of liquid samples will be introduced. The operation principle will be outlined and examples for sugar analysis in aqueous solution presented. Using refractive index spectra in the spectral range from 1000-1200 cm^{-1} quantitative analysis of ternary sugar samples will be shown.

Mid-Wave and Long-Wave Infrared Broad-Area Quantum Cascade Lasers

Matthew Suttinger[1,2], Rowel Go[1,1], Hong Shu[1], Ahmad Azim[1,2], Arkadiy Lyakh[1,2,3,+]
[1]*UCF NanoSicence Technology Center, 12424 Research Pkwy #400, Orlando, FL USA 32826;*
[2]*UCF CREOL, The College of Optics and Photonics, 4304 Scorpius St, Orlando, FL USA 32816;*
[3]*UCF Physics Department, 4111 Libra Drive, Orlando, FL USA 32816*

While most prior works in high power QCLs focus on increasing the efficiency of the laser core, fundamental physical properties limit the potential gains of this design direction. Standard designs feature a 10μm ("narrow-ridge") wide laser core featuring 30-40 active region stages taking up approximately 2μm of depth. The number of layers in the laser core gives an anisotropic heat conductivity due to waves of heat being reflected off the multiple interfaces. Thus, heat extraction from the laser core is made more difficult in the vertical direction than the horizontal direction. This leads to a buildup of temperature in the laser core that destroys continuous wave (CW) performance.

To avoid thermal problems impacting very high power QCLs, a broad-area configuration can be used. A broad-area configuration of the QCL waveguide features a much wider laser core width with a reduced number of stages (reduced thickness) and an optimized active region configuration. The reduced thickness eases heat extraction from the laser core, while the increased width expands the gain volume to allow more overall CW laser power to be generated for a given optical power density. This simultaneously avoids laser core overheating and optical damage while allowing for much greater CW optical powers to be obtained from a single emitter.

This approach was proven experimentally [1] when the UCF group's QCL design with record efficiency [2] was grown with a reduced number of stages in broad-area configurations. Other parameters being equal, the doubling of the nominal ridge width from 10μm to 20μm showed a marked increase of CW optical power out for a single device. Critically, our simulation results indicate that power level of 20W can be achieved from a single emitter if the fundamental active region design is carefully tailored to the broad-area configuration.

In this talk we will discuss main aspects of broad-area laser design and present the latest experimental data, including data demonstrating that a high beam quality can be achieved for 20μm-wide devices. The data suggest that broad-area QCLs soon transition to practical applications and they will be the cornerstone of the next generation infrared laser systems.

References:

1. M. Suttinger, R. Go, P. Figueiredo, A. Todi, J. Leshin, and A. Lyakh, Optical Engineering 57 (2017)
2. A. Lyakh, M. Suttinger, R. Go, P. Figueiredo, and A. Todi, Applied Physics Letters 109, 121109 (2016)

[+] Author for correspondence: Arkadiy.lyakh@ucf.edu

Rapidly tunable external-cavity Quantum Cascade Lasers for applications in real time MIR sensing

R. Ostendorf[1*], S. Hugger[1], L. Butschek[1], M. Härtelt[1], A. Dreyhaupt[2], J. Grahmann[2], M. Rattunde[1], J. Wagner[1]

[1] *Fraunhofer Institute for Applied Solid State Physics, Tullastrasse 72, 79108 Freiburg, Germany*

[2] *Fraunhofer Institute for Photonic Microsystems, Maria-Reiche-Strasse 2, 01109 Dresden, Germany*

The combination of spectral broadly tunable quantum cascade laser chips in an external cavity (EC-QCL) with a rapid scanning MOEMS grating as wavelength selective element has attracted a lot of attention in recent years. Spectral tuning ranges of more than 350 cm^{-1} in the mid-infrared fingerprint region combined with scan frequencies of up to 1 kHz for a complete wavelength scan have enabled new approaches for sensing applications such as contactless real time identification of chemical substances via backscattering spectroscopy. Moreover, the technological approach of a MOEMS EC-QCL allows for a dense integration of the electro optical components resulting in a footprint size for the laser source comparable to that of a matchbox. This makes the MOEMS EC-QCL especially attractive for portable and even handheld sensing systems.

In this talk we present the recent advances on the MOEMS EC-QCL technology made at Fraunhofer IAF and IPMS within the European projects MIRPHAB, AQUARIUS and CHEQUERS. A detailed analysis of spectral reproducibility of consecutive scans, amplitude noise, and spectral resolution in pulsed and cw operation of the laser source is shown and several showcase applications are discussed, focusing on online process control for chemical and pharmaceutical industry employing backscattering spectroscopy on solids as well as transmission measurements on liquids and gases.

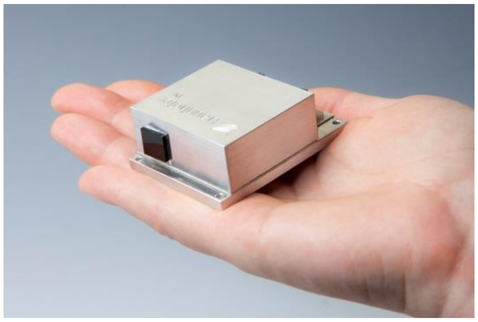

Figure 1: Photograph of the MOEMS EC-QCL.

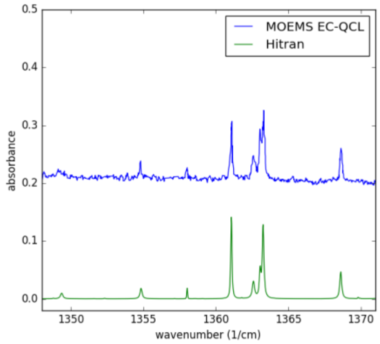

Figure 2: Part of high resolution absorption spectrum of water vapor recorded within 10 ms using an MOEMS EC-QCL

* Author for correspondence: ralf.ostendorf@iaf.fraunhofer.de

Development of GaSbBi for the fabrication of Mid-IR laser diodes

O. Delorme[1], L. Cerutti[1], R. Kudrawiec[2], E. Luna[3], J. Kopaczek[2], M. P. Polak[2], M. Gladysiewicz[2], A. Trampert[3], E. Tournié[1], and J.-B. Rodriguez[1*]

[1] IES, Univ. Montpellier, CNRS, 34000 Montpellier, France.
[2] Paul-Drude-Institut für Festkörperelektronik, Leibniz-Institut im Forschungsverbund Berlin e.V., Hausvogteiplatz 5-7, D-10117, Berlin, Germany
[3] Faculty of Fundamental Problems of Technology, Wrocław University of Science and Technology, Wybrzeże Wyspiańskiego 27, 50-370 Wrocław, Poland

Recently, dilute bismuth (Bi) III-V alloys have attracted great attention, particularly due to their properties of band-gap reduction and spin-orbit splitting. Therefore, the incorporation of Bi into antimonide based III-V semiconductor is very attractive for the development of new optoelectronic devices working in the mid-infrared range (2 – 5 µm). However, due to its large size, Bi does not readily incorporate into III-V alloys and the Bi incorporation needs very low growth temperature as compared to the values used for standard antimonide compounds. Moreover, a slight variation of the growth conditions causes the formation of Ga-Bi droplets and a degradation of the crystallographic quality. The epitaxy of III-V dilute bismide alloys is thus very challenging.

We have investigated the molecular beam epitaxy (MBE) of GaSbBi single layers on (001) GaSb substrates. Various sets of samples were grown at different V/III ratios and substrate temperatures to achieve high Bi content $GaSb_{1-x}Bi_x$ ($0 < x < 14\%$) alloys [1] with excellent crystal quality. We also report on the growth of quantum well heterostructures using an active zone composed of GaSbBi/GaSb type-I quantum wells, with different Bi contents and GaSbBi thicknesses. Addition of 3.7% In into GaSbBi single layers and QWs with Bi content up to 10.5% has also been achieved. Material quality and homogeneity were assessed by both High-Resolution X-Ray diffraction (HR-XRD) and transmission electron microscopy (TEM) measurements (Fig. 1). The electronic properties of these samples were studied using photoluminescence and photoreflectance. These experiments coupled with theoretical calculations allowed determining the band offsets of the GaSbBi/GaSb heterostructure, Bi-induced modifications of the band positions and the electron effective mass of GaSbBi. Finally, the first GaSbBi-based laser structure [2] was also realized using the same active region, exhibiting continuous-wave lasing operation at 2.5 µm at 80 K and lasing under pulsed operation at room-temperature near 2.7 µm. We will also discuss on an original way of setting the optimum growth conditions (substrate temperature and Sb flux) based on RHEED oscillations measurements (Fig. 2) [3].

[1] O. Delorme, L. Cerutti, E. Tournié and J.-B. Rodriguez, J. Cryst. Growth (2017), 477, pp. 144-148
[2] O. Delorme, L. Cerutti, E. Luna, G. Narcy, A. Trampert, E. Tournié, J.B. Rodriguez, Appl. Phys. Lett. (2017), 110 222106
[3] O. Delorme, L. Cerutti, E. Tournié and J.-B. Rodriguez, J. Cryst. Growth (2018), 495, pp. 9-13

*Corresponding author: jean-baptiste.rodriguez@umontpellier.fr

Mid-infrared 2.7-µm GaSbBi/GaSb quantum well lasers studied under high hydrostatic pressure

Igor P. Marko[1], O. Delorme[2], L. Cerutti[2], E. Tournié[2], J.-B. Rodriguez[2] and Stephen J. Sweeney[1+]

[1] *Advanced Technology Institute and Department of Physics, University of Surrey, Guildford GU2 7XH, United Kingdom*

[2] *IES, Univ. Montpellier, CNRS, 34000 Montpellier, France*

Mid-infrared semiconductor lasers operating in the wavelength range of 2-3 µm are motivated by a variety of applications including pollutant gas sensing for environmental monitoring, non-invasive medical diagnosis as well as free-space communications. Conventional type-I GaInAsSb/GaSb quantum well (QW) lasers have performance limitations due to major non-radiative Auger recombination and relatively weak hole confinement causing higher threshold currents and stronger temperature sensitivity [1]. In this work, we have studied GaSbBi/GaSb based QW lasers. These are expected to provide better hole confinement owing to increased valence band offset made possible due to valence band anti-crossing, thereby moving up the top of the valence band in GaSbBi. The details of the laser structure, growth and initial characterisation was reported earlier [2]. The lasers consisted of three GaSbBi QWs with 11.5% of Bi and were fabricated in Fabry-Perot chips with as-cleaved facets. Despite the high Bi composition and not fully optimised laser design, the lasers showed room temperature lasing operation at 2.7 µm with threshold current density (J_{th}) of 4.3 kA/cm^2. This is higher than for conventional InGaAsSb/GaSb lasers but promising for this emerging new material system. The higher J_{th} is consistent with GaAsBi/GaAs QW lasers where low temperature growth caused significant defect related recombination [2].

In this paper we will present a high hydrostatic pressure study of these devices. This allows us to identify the carrier recombination processes and, using their specific dependencies on pressure, to quantitatively determine their contribution to the total threshold current. Hydrostatic pressure reversibly changes the materials bandgap, which is approximately the same for the QW and barriers, therefore, the band offset remains relatively constant. The dependencies of J_{th} on lasing energy were obtained using high pressure for 293 K and 100 K. The pressure dependence of the Auger related current (J_{Aug}) was taken from [1], the radiative current (J_{rad}) was assumed to be proportional to squared band gap (ideal) [3] and the monomolecular current path (J_{mono}) due to defects was assumed to be pressure independent [3]. From the 100K data, which were pressure insensitive and where J_{Aug} was negligible, we estimate J_{rad} to be less than 5% of J_{th}. From that, we found that at 293 K J_{rad} was at most 2-3% of J_{th} with J_{Aug} and J_{mono} accounting for 50% and 48% of J_{th}, respectively. This suggests that at room temperature the threshold current is dominated by defect- and Auger-recombination, with strong scope for reduction of J_{th} as the material quality develops.

[1] T. D. Eales et. al, IEEE J. Select. Topics Quant. Electr., **23** (6), 1500909 (2017).
[2] O. Delorme et. al, Appl. Phys. Lett., **110**, 222106 (2017).
[3] I. P. Marko, S. J. Sweeney, IEEE J. Select. Topics Quant. Electr., **23** (6), 1501512 (2017).

+ Author for correspondence: s.sweeney@surrey.ac.uk

Growth and optical properties of III-V-bismide alloys for mid-IR device applications

Stephen T. Schaefer,[1] **Rajeev R. Kosireddy**,[2] **Arvind J. Shalindar**,[2] **Shane R. Johnson**[1]
[1] Center for Photonics Innovation & Electrical, Computer, and Energy Engineering,
[2] Center for Photonics Innovation & Engineering of Matter, Transport, and Energy,
Arizona State University, Tempe, AZ, USA

Efficient high-performance mid-infrared detection and emission is desired for numerous applications, including gas detection, thermal imaging, infrared spectroscopy, and autonomous vehicles. Mid-IR quaternary III-V-bismide alloys allow the material designer to independently specify strain and bandgap energy. In addition, bismuth reduces the host material bandgap at a greater rate per unit strain than As or Sb, while lifting the valence band edge for improved hole confinement in heterostructures. By adding a fifth atomic constituent to form a quinary alloy such as GaInAsSbBi, the conduction and valence band offsets can be adjusted independently of bandgap and strain. This additional degree of freedom enables the design of quantum wells with unity electron-hole wavefunction overlap at any wavelength and strain. The optical properties and molecular beam epitaxy growth of III-V-bismide alloys at the GaSb lattice constant are presented. As an example, 10 nm thick $InAs_{0.910}Sb_{0.081}Bi_{0.009}$ quantum wells with InAsSb barriers characterized by X-ray diffraction, Rutherford back-scattering, and photoluminescence spectroscopy, exhibit strong luminesce at 4.6 µm, demonstrating the potential of this material system for high-performance mid-IR devices.

Figure 1 (upper right). Low temperature photoluminescence from a nearly lattice-matched $InAs_{0.910}Sb_{0.081}Bi_{0.009}$ quantum well. Luminescence at 4.6 µm across a wide range of photoexcitation densities, indicates good quantum efficiency.

Figure 2 (lower right). Band offset diagram of $InAs_{0.910}Sb_{0.081}Bi_{0.009}/InAs_{0.916}Sb_{0.084}$ quantum well.

Figure 3 (lower left). Band offset diagram of a lattice-matched $Ga_{0.60}In_{0.40}As_{0.377}Sb_{0.571}Bi_{0.052}/GaSb$ quantum well designed for 4.6 µm emission. The conduction and valence band edges of the quinary alloy are adjusted independently to achieve unity electron-heavy hole wavefunction overlap.

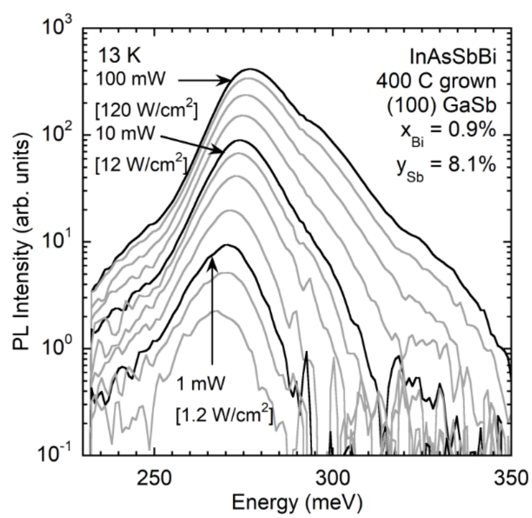

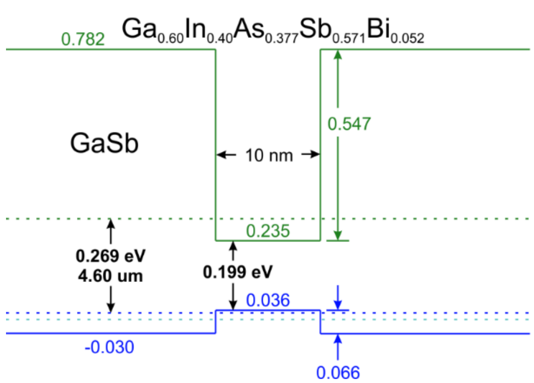

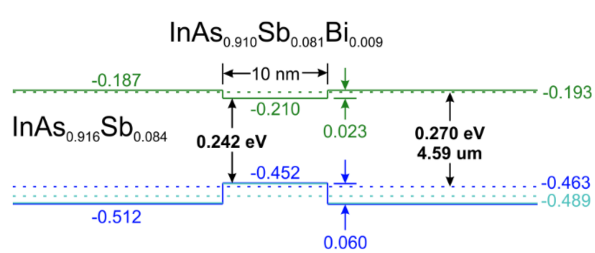

+ Author for correspondence: shane.johnson@asu.edu

Influence of substrate orientation on structural properties of InAsSbBi alloys for mid IR applications

Rajeev R. Kosireddy,[1] **Stephen T. Schaefer**,[2] **Arvind J. Shalindar**,[1] **Shane R. Johnson**[2]

[1] Center for Photonics Innovation & Engineering of Matter, Transport, and Energy,
[2] Center for Photonics Innovation & Electrical, Computer, and Energy Engineering,
Arizona State University, Tempe, AZ, USA

Advances in semiconductor growth technologies have enabled further development of III-V-Bi alloys – an emerging semiconductor material system that has several applications, including navigation, night vision, communications, imaging, and spectroscopy. In this work the properties of InAsSbBi epilayers grown by molecular beam epitaxy on (100), (100) 1° to (011), and (100) 4° to (111) offcut GaSb substrates are studied. The crystal structure is examined using X-ray diffraction and transmission electron microscopy, the surface morphology is examined using atomic force microscopy, and the bismuth mole fraction is determined using Rutherford back-scattering spectrometry. The results from structural characterization are compared with results from photoluminescence measurements to determine how substrate offcut affects the material properties and optical quality.

Results from a 210 nm thick -0.031% compressively strained $InAs_{0.92}Sb_{0.07}Bi_{0.01}$ layer grown at 400 °C on a (100) 4° to (111) offcut GaSb substrate.

Figure 1 (upper right). X-ray diffraction pattern (black curve) and simulation (red curve).

Figure 2 (lower right). Rutherford backscattering spectrum (black curve) and simulation (red curve). A breakdown of the signal from each individual element is provided.

Figure 3 (lower left). High resolution scanning transmission electron micrograph from the InAsSbBi/AlSb bottom interface showing the atomic steps at the vicinal surface.

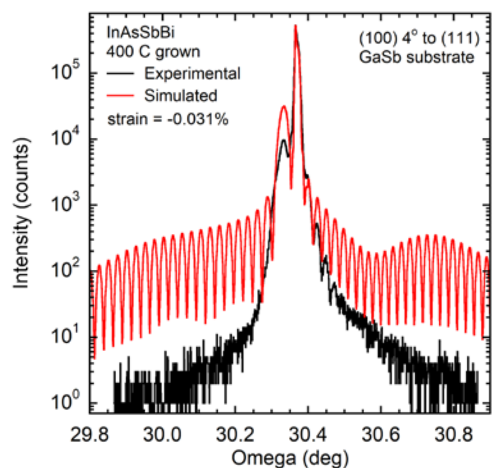

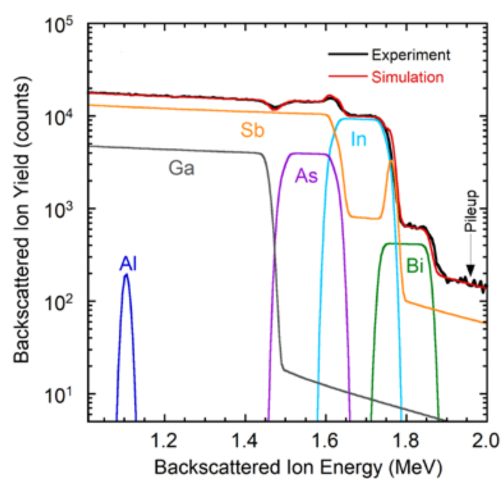

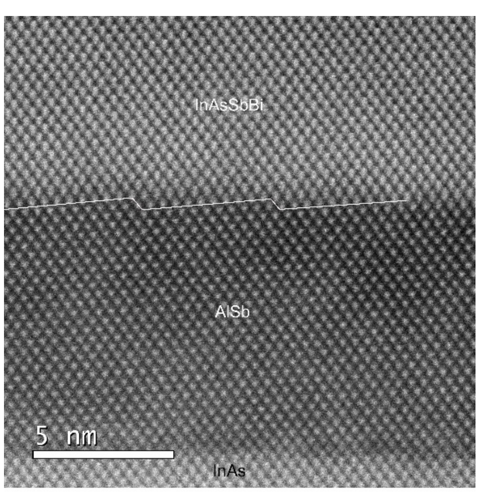

+ Author for correspondence: shane.johnson@asu.edu

Mid-IR and UV-VIS-NIR Mueller matrix ellipsometry characterization of the hyperbolic dielectric tensor of crystallized films of carbon nanotubes

S. Schoeche[1], J. A. Fan[2], J. Roberts[2], P.-S. Ho[3], and A. L. Falk[3]
[1] *J.A. Woollam Co., Inc., 645 M St., Suite 102, Lincoln, NE 68508 USA*
[2] *Electrical Engineering Department, Stanford University, 348 Via Pueblo, Spilker Building, Room 307, Stanford, CA 94305-4088 USA*
[3] *IBM T.J. Watson Research Center, 1101 Kitchawan Road, Yorktown Heights, NY 10598 USA*

Hyperbolic metamaterials (HMM) were proposed as a multi-functional platform to realize waveguiding, imaging, sensing, quantum and thermal engineering beyond conventional device performance [1]. HMMs display hyperbolic (or indefinite) dispersion, which originates from one of the principal components of their electric or magnetic effective tensor having the opposite sign to the other two principal components. Type I HMMs have one negative component of the dielectric tensor ($\varepsilon_{zz} < 0$; ε_{xx}, $\varepsilon_{yy} > 0$) while Type II HMMs have two negative components (ε_{xx}, $\varepsilon_{yy} < 0$; $\varepsilon_{zz} > 0$). Traditionally, HMMs are formed by combining a metallic and dielectric building block, either as thin sheets (Type II) or metal nanorods embedded in a dielectric matrix (Type I).

In this contribution, we demonstrate a novel approach to form Type I HMMs based on carbon nanotubes (CNT). The one-dimensional character of electrons, phonons and excitons in individual single-walled CNTs leads to extremely anisotropic electronic, thermal and optical properties. Recently, preparation of large-scale monodomain films of aligned single-walled CNTs using slow vacuum filtration was demonstrated [2]. A refinement of this technique showed that nanotubes in these films can be aligned as well as crystallized into two-dimensional ordered arrays with domain sizes of approximately 25 nm [3]. Control of the doping level leads to highly tunable optical properties.

The determination of the entire in-plane anisotropic dielectric function tensor requires advanced optical characterization techniques and measurement geometries. A multi-sample, multi-angle-of-incidence and multi-azimuth approach using Mueller matrix spectroscopic ellipsometry in the Mid-IR and the UV-VIS-NIR spectral ranges is applied here to characterize the free-electron, excitonic, interband transition and π-plasmon resonance related features perpendicular and along the CNT axis and identify regions of hyperbolic dispersion. The effects of crystallinity and doping on the dispersion are characterized.

[1] Shekhar, P., Atkinson, J., & Jacob, Z. (2014). Hyperbolic metamaterials: fundamentals and applications. *Nano convergence*, **1**(1), 14 (2014).
[2] He, X. *et al.*, Wafer-scale monodomain films of spontaneously aligned single-walled carbon nanotubes, *Nat. Nanotechnol*. **11**, 633–638 (2016).
[3] Ho, P.-S. *et al.*, Intrinsically Ultrastrong Light-Matter Interactions in Crystalline Films of Carbon Nanotubes, arXiv:1803.01087

+ Author for correspondence: alfalk@us.ibm.com

Antimonide Unipolar Barrier Infrared Detectors and Focal Plane Arrays

David Z Ting*, Alexander Soibel, Arezou Khoshakhlagh, Sam A Keo, Sir B Rafol, Anita M Fisher, Edward M Luong, Cory J Hill, Brian J Pepper, Sarath D Gunapala
NASA Jet Propulsion Laboratory, California Institute of Technology
4800 Oak Grove Dr, Pasadena, CA 91109, USA

The past decade has seen accelerated progress in the development of III-V semiconductor infrared photodetector technology. The advent of the unipolar barrier infrared detector device architecture such as the nBn, the pBp, and the CBIRD has in many instances greatly alleviated generation-recombination (G-R) and surface leakage dark current issues that had been problematic for III-V photodiodes. Advances in bulk III-V material such as lattice-matched InGaAsSb and metamorphic InAsSb, as well as in a variety type-II superlattices, including InGaAs/GaAsSb, InAs/GaSb, and InAs/InAsSb, have provided continuously adjustable cutoff wavelength coverage from the short wavelength infrared (SWIR) to the very long wavelength infrared (VLWIR). Together they have led to a new generation of versatile, cost-effective, high-performance infrared detectors and focal plane arrays (FPAs) based on robust III-V semiconductors, providing a viable alternative to HgCdTe (MCT). Images taken with antimonide semiconductor based FPAs with various cutoff wavelengths are shown in Fig. 1.

The InAs/InAsSb (Gallium-free) type-II strained-layer superlattice has emerged as an alternative adjustable band gap, broad-band III-V infrared detector material to the more established InAs/GaSb type-II superlattice. We will provide a comparison of the different aspects of the InAs/InAsSb and InAs/GaSb type-II superlattices for infrared detector applications, and show that the former can be highly effective when implemented in the mid-wavelength infrared (MWIR). We will report results on an InAs/InAsSb superlattice based MWIR high operating temperature barrier infrared detector (HOT-BIRD). In particular, an MWIR HOT-BIRD FPA exhibits a 300 K background, f/2 aperture mean noise equivalent differential temperature (NEDT) of 18.7 mK and 26.6 mK and NEDT operability of 99.7% and 99.6% at 160 K and 170 K, respectively, demonstrating significantly higher operating temperature than InSb.

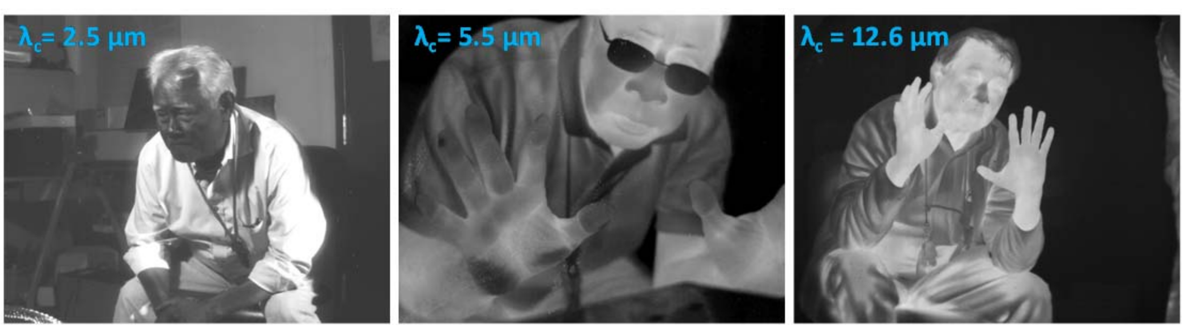

Figure 1. Short-, mid-, and long-wavelength infrared images taken with FPAs based on antimonide-semiconductor barrier infrared detectors, all grown on GaSb substrates.

* Corresponding author: David.Z.Ting@jpl.nasa.gov

Mid-Infrared Resonant Cavity Detectors

G.W. Wicks[1,2], G.R. Savich[1,2], T.D. Golding[2], K.D. Jamison[2], L. Fredin[2], M. Jain[3], A.P. Craig[4], A.R.J. Marshall[4], T.A. O'Loughlin[1], B.T. Marozas[1]
[1]The Institute of Optics, University of Rochester, Rochester, NY, USA
[2]Amethyst Research Inc., Ardmore, OK, USA
[3]Amethyst Research Ltd, Glasgow, UK
[4]Physics Dept., Lancaster University, Lancaster, UK

Mid-Infrared Resonant Cavity Detectors (RCDs) consist of a thin optical absorber layer inserted between two integrated distributed Bragg reflectors (DBRs), forming an optical cavity. Light recirculates inside the cavity, making multiple passes (up to several hundred) through the optical absorber layer, enabling the use of absorbers that are much thinner than those in conventional, single pass detectors. Thin absorbers are expected to enable large decreases in dark current and increases in speed. An intra-cavity intensity, much larger than the incident intensity, builds up in a narrow band of wavelengths that are resonant with cavity, producing a detector with a narrow spectral response.

We have constructed a variety of RCDs in III-V materials lattice-matched to either InAs or GaSb substrates, with resonant wavelengths in the range of 2.8 – 4.5 µm, and spectral linewidths of 50-100 nm. These preliminary results were obtained with DBR mirrors with 4-10 pairs of layers; narrower linewidths are anticipated from the use of higher reflectivity mirrors (work in progress). Optical reflectivity measurements on the as-grown wafers exhibit large dips at the resonant wavelength, providing early indications (before device processing) on the detector's responsivity peak and spectral width, as shown in figure 1. The small discrepancy between reflectivity dip and responsivity peak is due to wafer non-uniformity: the measurements are from different parts of the wafer. Tunability of the RCD's has been examined. Temperature tuning is shown in figure 2, and tilt tuning shown in figure 3. Tuning ranges of $\Delta\lambda$=100 nm have been demonstrated.

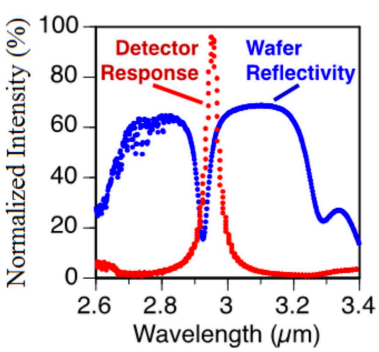

Figure 1. Reflectivity of as-grown wafer and spectral response of resonant cavity detector.

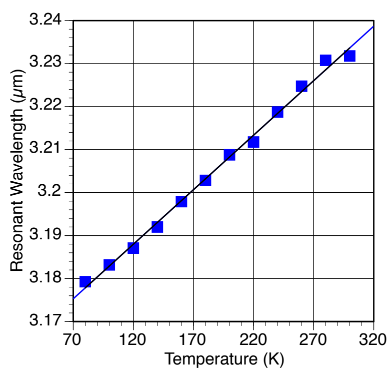

Figure 2. Temperature tuning of resonant wavelength of Mid-IR Resonant Cavity Detector.

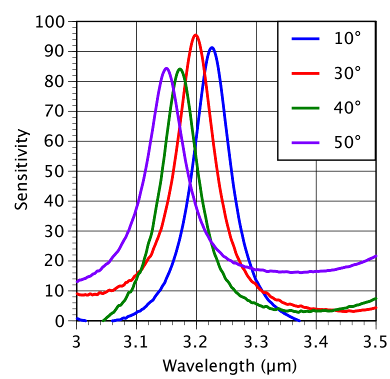

Figure 3. Tilt tuning of Mid-IR Resonant Cavity Detector photo-response.

+ Author for correspondence: wicks@optics.rochester.edu

Minority Carrier Lifetime and Recombination Dynamics in Strain-Balanced InGaAs/InAsSb Superlattices

P. T. Webster,[1] E. H. Steenbergen,[1] G. Ariyawansa,[2] C. J. Reyner,[2] J. K. Kim[3]
[1] Air Force Research Laboratory, Space Vehicles Directorate, Kirtland AFB, NM, 87117, USA
[2] Air Force Research Laboratory, Sensors Directorate, Wright-Patterson AFB, OH, 45433, USA
[3] Sandia National Laboratories, Albuquerque, NM, 87185, USA

Strain-balanced InAs/InAsSb superlattices are rapidly emerging as a contending mid-infrared sensing technology as decreasing dark currents lead to ever more sensitive detectors. Dark current can be minimized by increasing the absorption coefficient and utilizing a thinner absorber region, thereby reducing the volume over which dark current is generated. While the InAs/InAsSb superlattice design may be optimized for maximum absorption [1], there remains great room for improvement by establishing a more favorable strain-balance condition. Specifically, replacing the lightly-tensile InAs layers with more-tensile InGaAs leads to a more symmetric wavefunction overlap profile and correspondingly stronger absorption for the same energy cutoff [2]. The figure plots the wavefunction overlap square and absorption coefficient of InGaAs/InAsSb superlattices designed for maximum absorption as a function of ground state transition energy, which shows that absorption coefficient improves substantially with Ga content up to 20%.

In this work, two strain-balanced InGaAs/InAsSb superlattices (0% and 37% Ga) are designed to maximize absorption for a 5 µm wavelength ground state transition. These samples are examined using temperature- and excitation-dependent photoluminescence spectroscopy and time-resolved microwave reflectance. The superlattices are 1 µm thick and doped 4×10^{15} cm^{-3} *n*-type in order to examine the optimal doping density × lifetime product in a potential diffusion-limited detector [3]. The minority carrier lifetime determined from the microwave reflectance decay is plotted as a function of temperature in the inset, and shows that the InGaAs/InAsSb superlattice exhibits a 5× longer lifetime than its Ga-free counterpart at 80 K. The photoluminescence is evaluated using a recombination rate model to extract the Shockley-Read-Hall, radiative, and Auger rate constants as a function of temperature and to compare to the temperature-dependent minority carrier lifetime.

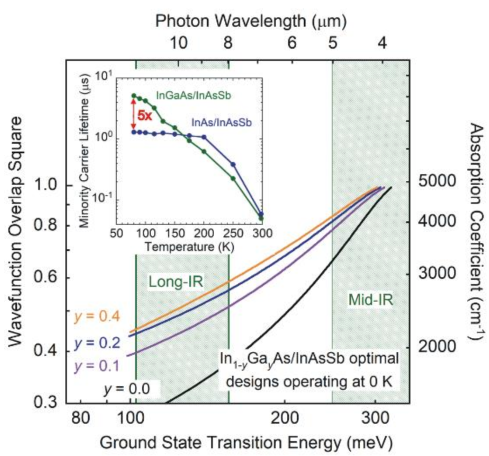

Wavefunction overlap square and absorption coefficient of InGaAs/InAsSb superlattice designs. Inset shows temperature-dependent minority carrier lifetime of 5 um wavelength designs with 0% and 37% Ga in InGaAs.

[1] P. T. Webster, et. al., J. Appl. Phys. **119**, 225701 (2016).
[2] G. Ariyawansa, et. al., Appl. Phys. Lett. **108**, 022106 (2016).
[3] E. A. Kadlec, et. al., Appl. Phys. Lett. **109**, 261105 (2016).

[+] Author for correspondence: preston.webster.2@us.af.mil

Large photocurrent amplification in n-GaSb/InAs/p-GaSb heterostructure with a single quantum well

M.P. Mikhailova[1], H.M. Salikhov[2], G.G. Konovalov[1], L.V. Danilov[1], R.V. Levin[1], B.V. Pushny[1], I.A. Andreev[1] and Yu.P. Yakovlev[1]

[1] Ioffe Institute, 26 Politekhnicheskaya, St Petersburg 194021, Russia

[2] Institute of Applied Research, Tatarstan Academy of Sciences, 36 A, Levobulachnaya str., Kazan 422111, Russia

We report on the first observation of large photocurrent/ photoconductivity amplification at very low applied bias in type II n-GaSb/InAs/p-GaSb heterostructures with a single deep quantum well (d=5 nm) grown by MOVPE. P-i-n structures were grown at AIXTRON-200 set-up at 560°C on n-GaSb:Te ($n=5\cdot10^{17}$ cm^{-3}) substrate with non-doped InAs QW and p-GaSb:Si cap layer ($p=4\cdot10^{17}$ cm^{-3}). Energy band diagram at reverse bias was estimated (Fig. 1). The structure has two broken-gap junctions on the both interfaces. The mesa-diodes were prepared by standard photolithography and wet etching with diameter about 300 μm. Exponential increasing of the photocurrent is obtained at reverse and forward bias starting from 5 mV up to 200 mV under illumination by monochromatic light with λ=1.2-1.6 μm at 77 K (Fig. 2). A gain reaches up to $G=10^2$. In addition, a linear increase of photoconductivity is observed with up to one order magnitude. The observed phenomenon can be explained by electron tunneling from InAs QW at reverse bias through n-GaSb barrier while heavy holes are accumulated into valence band offset on p-GaSb interface [1]. Theoretical calculation of photocurrent enhancement is made taking into account electron screening effect in InAs QW in the electric field and electron mass filtration through barrier on the interface. So, the effect under study has the quantum nature. It must be common both for type I and type II heterojunctions. These results can be used to create “non-threshold” photomultipliers for the spectral range 1.3-1.55 μm with low power consumption.

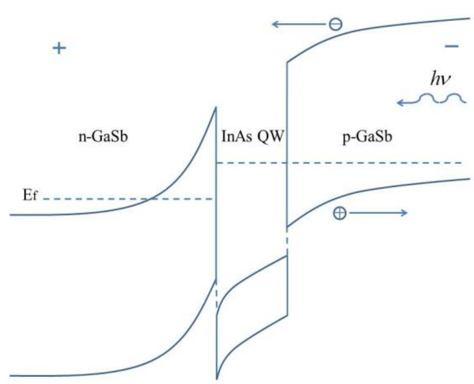

Figure 1. Energy band diagram of n-GaSb/InAs/p-GaSb structure with a single quantum well at reverse bias

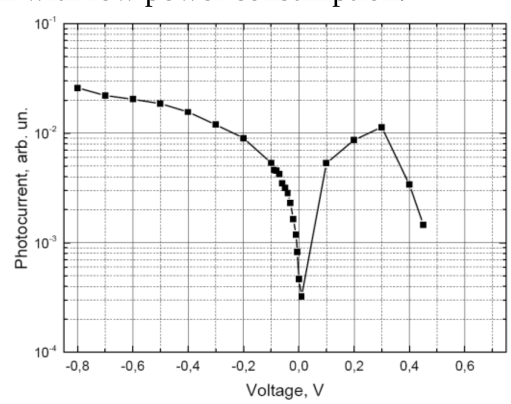

Figure 2. Experimental photocurrent vs. voltage characteristics of the structure. Illumination by monochromatic light λ=1.5 μm

[1] I.A. Andreev, A.N. Baranov, M.A. Mirsagatov, M.P. Mikhailova, A.A. Rogachev, G.M. Filaretova, Technical Letters **14** (5), 389 (1988).

[+] Author for correspondence: mayamikh@gmail.com

A unified figure of merit for interband and intersubband cascade devices

Wenxiang Huang,[1,2,+] S.M. Shazzad Rassel,[1] Lu Li,[1] Jeremy A. Massengale,[1,2] Rui Q. Yang,[1,+] Tetsuya D. Mishima,[2] Michael B. Santos[2]

[1] *School of Electrical and Computer Engineering, University of Oklahoma, Norman, Oklahoma 73019, USA*

[2] *Homer L. Dodge Department of Physics and Astronomy, University of Oklahoma, Norman, Oklahoma 73019, USA*

There are two major families of semiconductor optoelectronic devices with cascade configurations in the mid-infrared region. Quantum cascade (QC) devices are based on intersubband transitions within the same band (*e.g*. the conduction band), while interband cascade (IC) devices are based on interband transitions between the conduction and valence bands. The family of IC devices (ICDs) includes IC lasers [1-3], IC infrared photodetectors [4-5] and photovoltaic (PV) cells [6]. QC devices (QCDs) include QC lasers [7] and QC detectors [8]. Both IC and QC devices are based on quantum-engineered layer structures, and have been developed nearly in parallel with remarkable advances. However, they were frequently discussed and presented without reference to their counterparts. In particular, there is no evaluation or comparison based on a common figure of merit to fairly describe their characteristics with different device functionalities.

In this work, a semi-empirical model is employed to describe their current-voltage characteristics, and the saturation current density J_0 is proposed as a unified figure of merit. J_0 values were extracted from both QCDs reported in the literature and our ICDs and are shown in Fig.1 as a function of transition energy ΔE, which is the bandgap for ICDs and the energy difference between the two involved subbands for QCDs. It is found that J_0 increases approximately exponentially with a decrease of ΔE, and is more than one order of magnitude lower in ICDs than in QCDs. This is a reflection of the distinctive difference in carrier lifetime between them. The significance of J_0 on detector performance and open-circuit voltage for PV devices in converting light into electricity will be discussed at the conference.

Acknowledgements: We thank H. Ye and J. Gupta for the growth of some ICD wafers, D. Hofstetter, J. Liu, K. Fujita, B. Schwarz, Q. K. Yang, T. Dougakiuchi and G. Strasser for providing helps and data for QCDs. This work was supported in part by NSF (DMR-1608224) and AFOSR (FA9550-15-1-0067).

1. R. Q. Yang, at *7th Inter. Conf. on Superlattices, Microstructures and Microdevices*, Banff, Canada, August, 1994; *Superlattices and Microstructures* **17**, 77 (1995).
2. R. Q. Yang, Chap. 12 in *Semiconductor lasers: fundamentals and applications*, edited by A. Baranov and E. Tournie (Woodhead Publishing Limited, Cambridge, UK), 2013.
3. I. Vurgaftman, R. Weih, M. Kamp, J.R. Meyer, C.L. Canedy, C.S. Kim, M. Kim, W.W. Bewley, C.D. Merritt, J. Abell, and S. Höfling, *J. Phys. D. Appl. Phys.* **48**, 123001 (2015).
4. J. V. Li, R. Q. Yang, C. J. Hill, S. L. Chuang, Appl. Phys. Lett. **86**, 101102 (2005).
5. R. Q. Yang, Z. Tian, Z. Cai, J. F. Klem, M.B. Johnson, H.C. Liu, *J. Appl. Phys.* **107**, 054514 (2010).
6. R. Q. Yang, H. Lotfi, L. Li, R. T. Hinkey, H. Ye, J.F. Klem, L. Lei; T.D. Mishima, J.C. Keay, M.B. Santos, M.B. Johnson, *Proc. SPIE*. **8993**, 899310 (2014).
7. J. Faist, F. Capasso, D. L. Sivco, C. Sirtori, A. L. Hutchinson, A. Y. Cho, *Science* **264**, 553 (1994).
8. F. R. Giorgetta, *et. al*. IEEE J. Quantum Electron. **45**, 1039 (2009).

[+] Author for correspondence: wxhuang@ou.edu; rui.q.yang@ou.edu

Epitaxial Lift-Off Technology Based on Water-Soluble MgTe for Multi-Color Photodetector and Solar Cell Applications

Cheng-Ying Tsai,[1,2] Calli M. Campbell,[1,3] and Yong-Hang Zhang[1,2]
[1]*Center for Photonics Innovation, Arizona State University, Tempe, AZ 85287, USA*
[2]*School of Electrical, Computer and Energy Engineering, Arizona State University, Tempe, AZ 85287, USA*
[3]*School for Engineering of Matter, Transport and Energy, Arizona State University, Tempe, AZ 85287, USA*

An epitaxial lift-off (ELO) technology using a water-soluble sacrificial MgTe layer grown on InSb has been developed, which enables many device applications based on a new material platform with lattice constants near 6.5 Å, such as InSb, CdTe, PbTe, and HgCdTe. The nearly lattice-matched and coherently strained MgTe sacrificial layer is etched away with water and releases the film on top of it from the substrate. The optical quality of several free-standing CdTe/MgCdTe double-heterostructures obtained using this technique survives to give much enhanced photoluminescence (PL). The drastic increase in PL intensity is a result of luminescence concentration, strong evidence of photon-recycling.

Coupled with the ability to monolithically grow II-VI and IV-VI materials on III-V layers and vice versa, the potential applications of this ELO method are diverse and far-reaching. This technology enables the integration of free-standing thin films from the 6.5 Å family into devices not limited to multi-color photodetectors ranging from IR to UV, as well as ultra-high efficiency solar cells. Notably, two-terminal, two-color (visible/midwave-infrared, MWIR) photodetectors (2CPDs) consisting of monolithically-integrated CdTe nBn and InSb PN sub-detectors grown on lattice-matched InSb substrates have been demonstrated by this group. The 2CPD can be switched between MWIR (1.5–5.5 μm with a peak responsivity of 0.75 A/W at 77 K) and visible (350–780 nm with a peak responsivity of 0.3 A/W) detection bands by applying different optical and electrical biases.

*Author for correspondence: cheng-ying.tsai@asu.edu

Development of Low-Cost Uncooled/TE-cooled PbSe MWIR Detector For Sensing and Imaging Applications

Zhisheng Shi, Jijun Qiu, Lance McDowell
School of Electrical and Computer Engineering, University of Oklahoma
110 W Boyd, Devon Energy Hall 150, Norman, OK 73019
Phone: 405-325-4292, Fax: 405-325-7066, Email: shi@ou.edu

To date, uncooled/TE-cooled, low-cost polycrystalline Pb-salt PbSe photoconductive (PC) detectors remain the choice for many sensing and imaging applications in the 3-5 µm mid-IR spectral range. High peak detectivity of 4.2×10^{10} $cm\cdot Hz^{1/2}\cdot W^{-1}$ at room temperature was reported for PbSe photoconductor.[1,2] TE-cooled 240 × 320 format arrays of PbSe photoconductor FPA monolithically fabricated on Si ROIC was also reported. [3] These reports generated renewed interests of using lead salt PbSe for high temperature imaging applications in the mid-infrared region. The homogeneity of current PC PbSe detector FPA is, however, poor which requires expensive customer-designed readout integrated circuitry (ROIC) for imaging applications.

We report our recent development of ways to improve homogeneity of PbSe PC detector while maintaining the high performance. We also report our development of polycrystalline PbSe/CdS_xSe_{1-x} heterojunction detector for monolithically integrated FPA applications based on our proposed IV-VI Pb-salt/II-VI semiconductor heterojunction detectors. [4] With these development, a low-cost, large-format detector focal plane array (FPA) operating at near room temperature is envisioned.

---

[1] Jijun Qiu, Binbin Weng, Zijian Yuan, and Zhisheng Shi, "Study of sensitization process on mid-infrared uncooled PbSe photoconductive detectors leads to high detectivity", J. Appl. Phys., **113,** 103102 (2013)

[2] Binbin Weng, Jijun Qiu, Zijian Yuan, Preston Larson, Gregory W. Strout, and Zhisheng Shi, "Responsivity enhancement of mid-infrared PbSe detectors using CaF2 nano-structured antireflective coatings", Appl. Phys. Lett. 104, 021109 (2014).

[3] Kenton Green, Sung-Shik Yoo, Christopher Kauffman, "Lead Salt TE-cooled Imaging Sensor Development", Infrared Technology and Applications XL, edited by Bjørn F. Andresen, Gabor F. Fulop, Charles M. Hanson, Paul R. Norton, Proc. of SPIE Vol. 9070, 90701G · © 2014 SPIE CCC code: 0277-786X/14/$18 · doi: 10.1117/12.2053302

[4] B. Weng, J. Qiu, L. Zhao, C. Chang, and Z. Shi, "CdS/PbSe heterojunction for high temperature mid-infrared photovoltaic detector applications", Appl. Phys. Lett. 104, 121111 (2014).

MBE Growth of Monocrystalline PbTe/CdTe/InSb Heterovalent Heterostructures for MWIR Device Applications

M.B. Lassise, **T.T. McCarthy, B.D. Tracy, D.J. Smith, and Y.-H. Zhang**
Arizona State University, Tempe, AZ 85282

Lead chalcogenides are promising materials for MWIR optoelectronic device structures due to their small band gap and low Auger coefficient. Although these materials typically have a rock-salt crystal structure, they have been shown to be epitaxially compatible with common zinc blende II-VI crystals with similar lattice constants. In particular, the common Te atom between PbTe and CdTe enables high-quality interfaces between these two dissimilar materials. In this study, monocrystalline PbTe/CdTe heterostructures have been grown on both polar (211) and nonpolar (100) InSb substrates in a single-chamber MBE system, and the PbTe/CdTe interface was optimized by varying the flux and temperature conditions during an interruption between the CdTe and PbTe growth. By integrating IV-VI, II-VI, and III-V materials, we hope to alleviate many of the problems associated with each individual material alone. Wide-band gap II-VI materials can be used for electrical and optical confinement, and the III-V materials with better thermal conductivity can reduce the thermal load on the IV-VI laser active region. The integration of II-VI/III-V materials with large refractive contrasts can result DBRs with high reflectivity for optical cavities.

The optical, electronic, and structural properties of the heterovalent heterostructures were characterized to examine how the growth parameters affect the PbTe material. Optical emission from the PbTe layer was observed with a peak energy of 278 meV at low temperatures, as shown in Fig. 1, and an approximate room-temperature band gap of 335 meV was determined from reflectance measurements. TEM and RHEED were used to determine the crystal structure of the PbTe layer, preliminary results show that the crystal structure undergoes a transition from zinc blende to rock-salt during the growth on a Te-terminated CdTe buffer layer. A streaky RHEED pattern was observed throughout the growth suggesting smooth 2D layer formation, and Fig. 2 shows an XRD scan of the double heterostructure which shows prominent features around the InSb substrate peak from the PbTe layer and the CdTe interfaces. Transport measurements of the PbTe/CdTe interface will be presented at the conference.

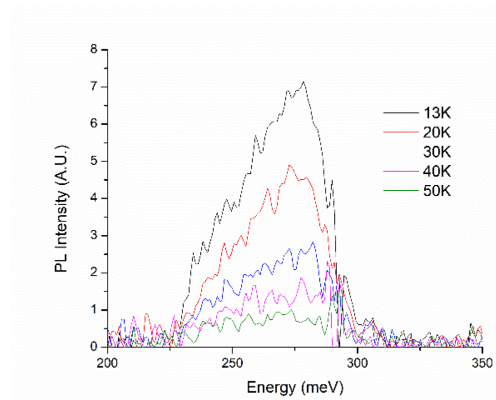

Fig. 1: PL spectrum of PbTe/CdTe double heterostructure.

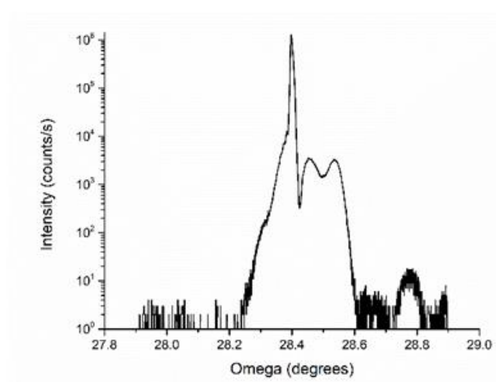

Fig. 2: XRD Omega/2Theta scan of PbTe/CdTe double heterostructure.

+ Author for correspondence: mlassise@asu.edu

Mid-wave Infrared Imaging with HgTe Colloidal Quantum Dots Photovoltaic Devices

Xin Tang[+], **Matthew Ackerman, and Philippe Guyot-Sionnest**[+]
James Franck Institute, 929 E. 57th Street, The University of Chicago, Chicago, IL 60637

In recent years, mercury telluride (HgTe) colloidal quantum dots (CQDs) have emerged as a promising low-cost nanomaterial for broadband infrared detection, which could be the key to facilitate civilian applications. Prior HgTe CQDs Schottky photovoltaic detectors achieved background limited performance with detectivity up to 3.8×10^{10} Jones at cryogenic temperature [1]. A vast improvement was demonstrated recently with Ag_2Te-doped HgTe CQDs with detectivity of 1.2×10^{11} Jones at 85 K with internal quantum efficiency (IQE) was estimated to be as high as 90% [2]. To improve the performance, the absorption of the CQD films must be increased. Here, we report the construction of HgTe CQDs MWIR photovoltaic detectors with plasmonic disk arrays, as shown in Figure 1a. COMSOL simulations have been conducted and showed that a trilayer structure of plasmonic disks/HgTe CQDs film/ metal contact creates an optical resonant cavity that increases the absorption within the CQDs film (Figure 1b). Obvious enhancement of spectral responsivity was observed in the MWIR ranges (Figure 1c). Overall, the responsivity was enhanced by two to three-fold over the wide range of operating temperature from 295 K to 85 K, as shown in Figure 1d. With the addition of an interference reflector structure, the peak detectivity was improved to 4×10^{11} Jones at 85 K and 7×10^{8} Jones at 295 K (Figure 1e). The high detectivity enables the demonstration of a scan-imaging camera with improved NETD of 25 mK at 90K operation temperature (Figure 1f).

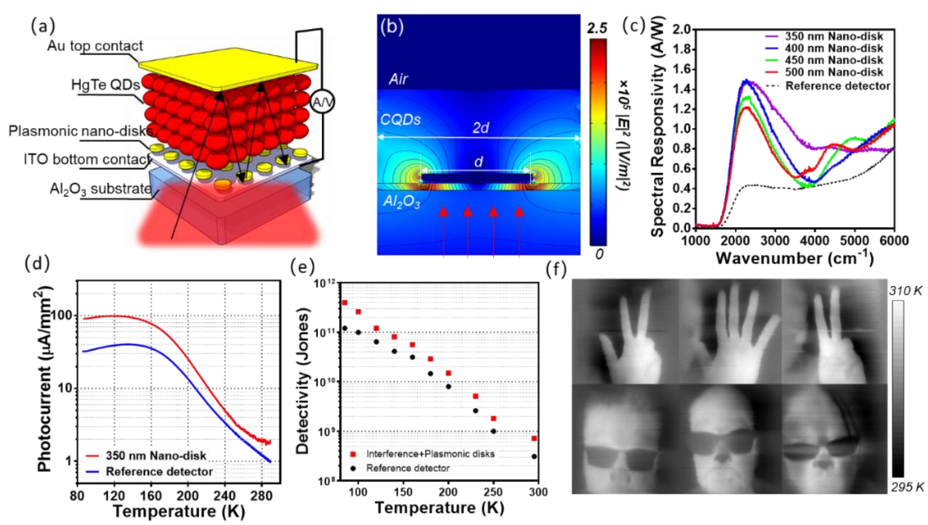

Figure 1. (a) Design of the HgTe CQDs photovoltaic detectors. (b) COMSOL simulation of electric field distribution. (c) Spectral responsivity of HgTe CQDs photovoltaic detectors with plasmonic disk. (d) Photocurrent as a function of temperature. (e) Temperature-dependent detectivity. (f) Captured thermal images.

[1] P. Guyot-Sionnest and J. A. Roberts, Appl. Phys. Lett., **107**, 253104(2015).
[2] M. Ackerman, X. Tang, and P. Guyot-Sionnest, Submitted.

[+] Author for correspondence: pgs@uchicago.edu and xintang@uchicago.edu

Scanning tunneling microscopy with atomic resolution on HgCdTe

Fangxing Zha,[1] Feng Hong,[1]
[1] *Department, Shanghai University, Shanghai 200444, China*

Mercury cadmium telluride (HgCdTe) is the most important semiconductor for IR technology. In contrast to many other semiconductors, the experimental atomic surface structure of the material has however been absent until our recent achievement with the ultrahigh vacuum scanning tunneling microscopy (STM) [1]. The sample studied is the (111)B surface of $Hg_{0.78}Cd_{0.22}Te$ grown by liquid phase epitaxy. We disclose that the surface is dominated by two types of (2×2) reconstructions, which are induced by cadmium adsorption and by single telluride vacancy formation, respectively. However, we also observed several other surface structures, including the (1×1) structure which is metastable and may transform to the more stable (2×2) reconstructions. The first-principle calculation confirms that the two reconstructions are the energetically most stable types. The calculation of surface energy also shows that the (2×2) reconstruction induced by the single Te vacancy is more stable than that of multi-vacancies in contrast to the prevailing view. The simulated (2×2) reconstructions can be well compared with the observed STM images.

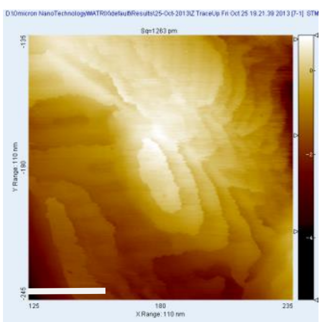

Figure 1 STM morphology of the (111) B surface of HgCdTe.

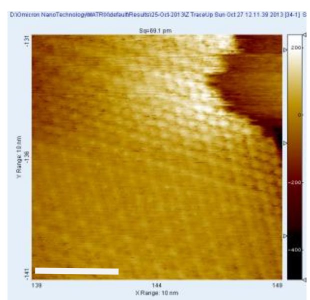

Figure 2 STM image with atomic resolution on the (111)B surface.

[1] F.-X. Zha, F. Hong, B.-C. Pan, et al., Phys. Rev. B 97, 035401 (2018).

+ Author for correspondence: fxzha@shu.edu.cn

Spectroscopic chemical sensing and hyperspectral imaging with quantum cascade laser frequency combs

Gerard Wysocki
Department of Electrical Engineering, Princeton University, NJ, USA

Laser spectroscopic detection of large molecular compounds with unresolved rotational-vibrational spectroscopic signatures in the mid-infrared and THz spectral ranges requires spectroscopic techniques that can provide broadband coverage. Ideal spectrometers should also provide fast spectral acquisition rates to resolve chemical dynamics at millisecond to microsecond timescales. In such a domain of applications broadband dual-comb spectroscopy (DCS) with semiconductor quantum (QCL) and interband cascade laser (ICL) frequency combs has the potential to meet these stringent requirements in terms of broadband coverage (with >50cm^{-1} features), high spectral resolution (<0.001cm^{-1}), and fast measurement time (<ms per spectrum) while providing these capabilities in a compact footprint and all-electrically driven semiconductor platform.

In this talk I will discuss examples of mid-IR DCS at ~7.8μm using QCLs (with coupled-waveguide dispersion-compensated devices developed by J. Faist [1]) as well as at ~3.2μm using ICLs (passively locked devices developed by M. Bagheri et al [2]) . Spectroscopic detection of gases such as isobutene, ammonia, methane and ethylene has been performed using DCS system capable of molecular absorption spectroscopy over instantaneous optical bandwidth of ~1THz, with noise-equivalent absorption detection limit at ~10^{-3}/Hz$^{1/2}$ level, and with fast spectral acquisition down to <100 μs [3, 4]. In the THz region the DCS system was developed using dispersion compensated THz-QCLs developed by Burghoff et al. [5] operating at ~3 THz. The THz DCS system is realized by combining radiation from two QCL combs on a hot electron bolometer (Scontel)[6]. Multiheterodyne spectroscopy of NO_2, NH_3 and H_2O is performed over ~150 GHz spectral window with 10 μs/spectrum time resolution and a noise-equivalent absorption detection limits down to 7×10^{-4}/Hz$^{1/2}$. This THz DCS system was also developed to address the need for multi-heterodyne hyperspectral imaging of solid samples and preliminary characterization of its performance in this operation mode will be presented.

1. B. Yves, K. Filippos, J. Pierre, B. Mattias, and F. Jérôme, "Coupled-Waveguides for Dispersion Compensation in Semiconductor Lasers (Laser Photonics Rev. 12(5)/2018)," Laser & Photonics Reviews **12**, 1870025 (2018).
2. M. Bagheri, C. Frez, L. A. Sterczewski, I. Gruidin, M. Fradet, I. Vurgaftman, C. L. Canedy, W. W. Bewley, C. D. Merritt, C. S. Kim, M. Kim, and J. R. Meyer, "Passively mode-locked interband cascade optical frequency combs," Scientific Reports **8**, 3322 (2018).
3. L. A. Sterczewski, J. Westberg, C. L. Patrick, C. S. Kim, M. Kim, C. L. Canedy, W. W. Bewley, C. D. Merritt, I. Vurgaftman, J. R. Meyer, and G. Wysocki, "Multiheterodyne spectroscopy using interband cascade lasers," Optical Engineering **57**, 12 (2017).
4. J. Westberg, L. A. Sterczewski, and G. Wysocki, "Mid-infrared multiheterodyne spectroscopy with phase-locked quantum cascade lasers," Appl Phys Lett **110**, 141108 (2017).
5. D. Burghoff, T.-Y. Kao, N. Han, C. W. I. Chan, X. Cai, Y. Yang, D. J. Hayton, J.-R. Gao, J. L. Reno, and Q. Hu, "Terahertz laser frequency combs," Nature Photonics **8**, 462 (2014).
6. J. Westberg, L. A. Sterczewski, Y. Yang, D. Burghoff, J. Reno, Q. Hu, and G. Wysocki, "Terahertz dual-comb spectroscopy using quantum cascade laser frequency combs," in *Conference on Lasers and Electro-Optics*(Optical Society of America, San Jose, California, 2018), p. STu4D.2.

[+]Author for correspondence: gwysocki@princeton.edu

GaSb-based Lasers for Trace Gas Sensing

J.A. Gupta,[+] A. Bezinger, J. Lapointe, G.C. Aers, D. Poitras, S. G. Razavipour, G. Sabiston, N. Sabourin and X. Wu
National Research Council of Canada, Ottawa ON K1A 0R6

A growing awareness of the potentially disastrous effects of climate change and the adverse health effects of poor air quality has led to rapid growth in the demand for gas sensing systems. Tunable laser absorption spectroscopy is a highly effective method for trace gas sensing because of its sensitivity, selectivity and the inherent robustness of semiconductor lasers. This presentation will describe the National Research Council of Canada's (NRC's) development of single-mode distributed feedback lasers for sensing of a number of target trace gases in the mid-infrared wavelength range around 1.8-3.3um. The quantum well diode lasers are based on GaSb and Al(In)GaAsSb heterostructures grown on GaSb substrates by solid-source molecular beam epitaxy. At NRC we have developed a comprehensive suite of modelling tools which provide accurate designs of the quantum well active regions and the ridge-waveguide DFB structures. These tools allow us to design, grow and fabricate lasers with high luminescence efficiency at the desired wavelength and to accurately calculate the required grating pitches for fabrication of single-mode DFBs. We will show examples of various lasers thus produced and their application in trace gas sensing. A particularly important example is the detection of fugitive methane emissions from natural gas pipelines, for which we have developed a lightweight sensing system suitable for drone-based airborne measurements.

[+] Author for correspondence: james.gupta@nrc.ca

Determination of the Auger Coefficient and its Wavelength Dependence in Type-I Mid-Infrared Laser Diodes

T. Eales,[1] I. P. Marko,[1] B. A. Ikyo,[1] A. R. Adams,[1] A. Andrejew,[2] K. Vizbaras,[2] M-C. Amann,[2] L. Shterengas,[3] G. Belenky,[3] I. Vurgaftman,[4] J. R. Meyer,[4] S. J. Sweeney[1,+]

[1] *Advanced Technology Institute and Department of Physics, University of Surrey, Guildford GU2 7XH, United Kingdom*

[2] *Walter Schottky Institut, Technische Universität München, Am Coulombwall 3, 85748 Garching, Germany*

[3] *Department of Electrical and Computer Engineering, State University of New York at Stony Brook, New York 11794, USA*

[4] *US Naval Research Laboratory, 4555 Overlook Avenue SW, Washington DC 20375, USA*

Type-I quantum well (QW) lasers based on the GaSb material system show attractive characteristics in the mid-infrared [1]. However, as the wavelength (λ) increases in the range of 2-4 µm their performance begins to deteriorate due to increasing Auger recombination [2]. In the Auger process, the energy released from an electron-hole recombination is transferred to a third carrier. In order to develop strategies to suppress Auger recombination, it is crucial to understand the magnitude and nature of the dominant Auger recombination pathway, and their dependencies on the operating λ and temperature (T). In QW structures two fundamentally different Auger process can occur [3]. In an *activated* Auger process, initial and final carrier states are confined to the plane of the QW. The recombination rate due to this process depends exponentially on T because it is determined by an activation energy, which is a consequence of energy and momentum conservation. In a *thresholdless* Auger process, the initial carrier states can exist near the band edge (bottom of conduction/valence band) and the third carrier is excited into the continuum of unbound states in a direction perpendicular to the plane of the well. Without an activation energy, the thresholdless Auger process exhibits only a weak T dependence. In this work, we report on the T and λ dependence of the threshold current density (J_{th}) of type-I QW devices operating in range 1.95-3.2 µm. From T-dependent measurements, we find that radiative recombination dominates from low T up to a break point temperature [4]. Beyond this break point the temperature sensitivity of J_{th} increases rapidly, indicating the onset of a strongly temperature-sensitive *activated* Auger process. Using hydrostatic pressure, we tune the operating λ of the lasers in order to probe the λ dependence of the Auger coefficient. Modelling the gain and loss characteristics of the lasers allowed the threshold carrier density (n_{th}) to be determined. Since the carrier density calculations depend sensitively on the threshold gain, we undertook segmented contact measurements to experimentally determine the optical loss. By extracting the experimentally-determined radiative component of J_{th} and assuming the remaining non-radiative current $J_{nr} = Cn_{th}^3$, C and its λ dependence were calculated, although the analysis also provides evidence that the dependence is not strictly cubic (i.e., C depends on n_{th}).

[1] S. D. Sifferman, et al, IEEE J. Sel. Top. Quantum Electron. **21**, 6(2015).
[2] T. D. Eales, et al, IEEE J. Sel. Top. Quantum Electron. **23**, 6(2017).
[3] R. I. Taylor, et al, Semicond. Sci. Technol. **5**, 1(1990).
[4] S. J. Sweeney, et al, Photonics Technol. Lett. **10**, 8(1998).

+ Author for correspondence: s.sweeney@surrey.ac.uk

Efficiency Limiting Mechanisms in Interband Type-II 'W' Lasers Operating in the Mid-IR

T. D. Eales,[1] I. P. Marko,[1] S. Sprengel,[2] A. Andrejew,[2] K. Vizbaras,[2] M-C. Amann,[2] and S. J. Sweeney[1,+]

[1] Advanced Technology Institute and Department of Physics, University of Surrey, Guildford GU2 7XH, United Kingdom

[2] Walter Schottky Institut, Technische Universität München, Am Coulombwall 3, 85748 Garching, Germany

The conventional approach for laser diodes in wavelengths range of 2-3 µm is based on type-I quantum well (QW) devices using (In,As)GaSb material system. However, these devices suffer from significant Auger recombination and poor hole confinement [1]. An alternative approach is based on the type-II structure, where spatial separation of electrons and holes permits energy transitions less than the bandgap of the constituent layers. This extends the wavelength range accessible within a given material system and offers greater flexibility in optimizing device design [2]. In this work, we report on the efficiency limiting mechanisms in type-II 'W' lasers operating between 2-3 µm and compare these to type-I operating at similar wavelengths. The 'W' lasers are grown on InP substrate with the QWs composed of ternary GaInAs/GaAsSb alloys, rather than the quaternary GaInAsSb/GaSb materials used in the type-I structures. From spontaneous emission (Fig. 1a) and high hydrostatic pressure (Fig. 1b) measurements we find that an Auger recombination process is the dominant recombination pathway in both devices. The nature of the Auger recombination mechanisms in the two devices will be discussed.

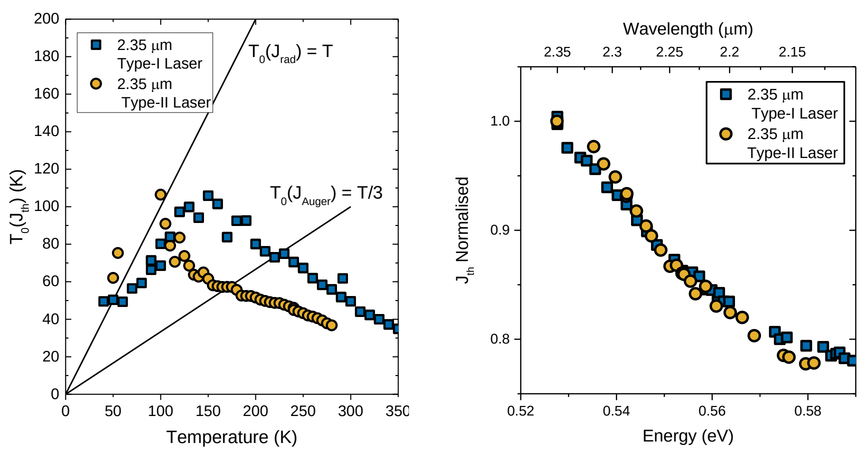

Figure 1 comparison of a) characteristic temperature vs T and b) pressure dependence of threshold current density vs lasing wavelength tuned by pressure in type-I and type-II devices operating at 2.35 µm.

[1] S. D. Sifferman, *et al*, IEEE J. Sel. Top. Quantum Electron. **21**, 6(2015).
[2] S. Sprengel, *et al*, Semicond. Sci. Technol. **31**, 11(2016).
[3] S. Sprengel, *et al*, IEEE J. Sel. Top. Quantum Electron. **19**, 4(2013).

+ Author for correspondence: s.sweeney@surrey.ac.uk

Dynamic Stabilization of Efficient Mid-Infrared III-V Semiconductor Frequency Combs Using Two-Color Pumping

R. Joseph Weiblen* **and Igor Vurgaftman**
Code 5613, Naval Research Laboratory, 4555 Overlook Ave SW, Washington, DC 20375
**ASEE Postdoctral Fellow Residing at NRL*

Integrated mid-infrared (mid-IR) frequency combs promise to revolutionize chemical sensing [1]. A novel and particularly interesting approach is to employ a III-V semiconductor in a microresonator-based nonlinear comb [2]. Since $\chi^{(3)} \propto E_g^{-4}$, the nonlinearity can be much higher than in the currently used wide-gap materials, and $Q \sim 10^5$ can be obtained by tuning the energy gap E_g so that it somewhat exceeds $2\hbar\omega_{max}$ in the comb. For example, for a comb centered on 4.5 μm the waveguide material could be InGaAs on InP. However, this approach also introduces pronounced higher-order group velocity dispersion (GVD) that can make it difficult to achieve stable broadband output.

One way to stabilize multiple solitons and the repetition rate is to pump simultaneously at two wavelengths separated by one or a few free spectral ranges of the microresonator. However, previous computational studies of bichromatic microresonator-comb pumping [3,4] have not addressed the higher-order material dispersion. Here we show theoretically that this pumping scheme can lead to stable soliton crystals and calculate the required ranges of pump powers and wavelengths. Figure 1 shows a schematic of the soliton crystal system with pulses stabilized near the intracavity pump nulls. The second pump can create a soliton crystal that remains stable throughout the duration of the second pump. Figure 2 shows two unevenly spaced solitons locked into stable positions when the second pump is turned on at 150 ns. The nonlinear conversion efficiency scales with the number of solitons, which is of great interest since single-soliton combs have low efficiencies (~1%) [5].

Figure 3 shows that this stabilization effect occurs only over a limited range of parameters. While there is a range of detunings Δ for which the pulses are stabilized when the pump ratio P_2/P_1 is greater than about 0.4, as depicted by Region I of the figure, outside this range of Δ and P_2/P_1 the pulses are either not stabilized (Region II), exhibit spatiotemporal chaos (Region III), or collapse to a low-power CW solution (Region IV).

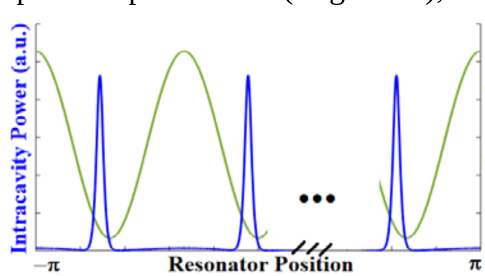

Fig. 1: Stabilized soliton crystal schematic

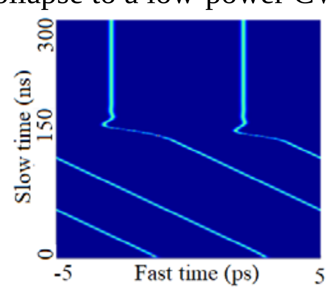

Fig. 2: Stabilization of two solitons

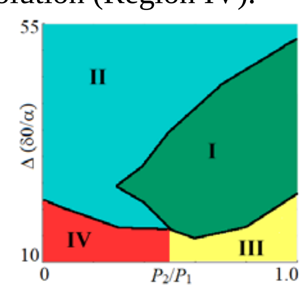

Fig. 3: Stability regions

[1] A. Schliesser et al., "Mid-infrared frequency combs," Nat. Photonics **6**, 440–449 (2012).
[2] M. Pu, et al., "Efficient frequency comb generation in AlGaAs-on-insulator," *Optica* **3**, 823 (2016).
[3] T. Hansson and S. Wabnitz, *Physical Review A* **90**, 013811 (2014).
[4] H. Taheri et al., "Optical Lattice Trap for Kerr Solitons," *Eur. Phys. J. D* **71**, 151 (2017).
[5] C. Bao, et al., *Opt. Lett.* **39**, 6126 (2014).
+ Author for correspondence: robert.weiblen.ctr@nrl.navy.mil

Quantum Dot Cascade Laser: From Concept to Practice

Feng-Qi Liu[1,2] , Ning Zhuo[1], J.-C. Zhang[1], F.-M. Cheng[1,2], Y. Zhao[1,2], S.-Q. Zhai[1], J.-Q. Liu[1,2], L.-J. Wang[1,2], S.-M. Liu[1,2], Z.-G. Wang[1,2]

[1] *Key Laboratory of Semiconductor Materials Science, Institute of Semiconductors, Chinese Academy of Sciences, Beijing 100083, China*

[2] *College of Materials Science and Opto-Electronic Technology, University of Chinese Academy of Sciences, Beijing 100049, China*

Quantum dot cascade laser (QDCL) possesses high wallplug efficiency and broad tunability. The QDCL based on three-layer QD active region design combined with two-step strain-compensation growth technique, gives continuous wave operation at room temperature at wavelength of 7.2 µm. In the coupled QD active structure, the upper laser state is quantum well (QW) dominated hybrid state of QW-QD, the lower laser state is QD dominated hybrid state of QW-QD. The QD dominated hybrid state is quasi-separate states, which sustains the "phonon bottle neck effect", consequently reduces the nonradiative decay rate of the lasing transition. In order to enhance the renovated "phonon bottle neck effect", the QD active region should be based on two-layer QD or single-layer QD.

In this talk, the QDCLs based on two-layer QD active region, and single-layer QD active region have been exploited. The QDCL based on two-layer QD active region presents room temperature lasing at wavelength of 6.85µm, while the QDCL based on single-layer QD active region shows lasing at wavelength of 6.5µm at 80K. Considering the structure of QDCLs consists of GaAs layers and the accurate energy levels are difficulty to exact match the injection and extraction levels, the materials quality and electronic design of active regions are not good enough. What is more, the detailed physics of electron scattering and tunneling should be explored in the future. This feasible method paving a route for developing QDCLs.

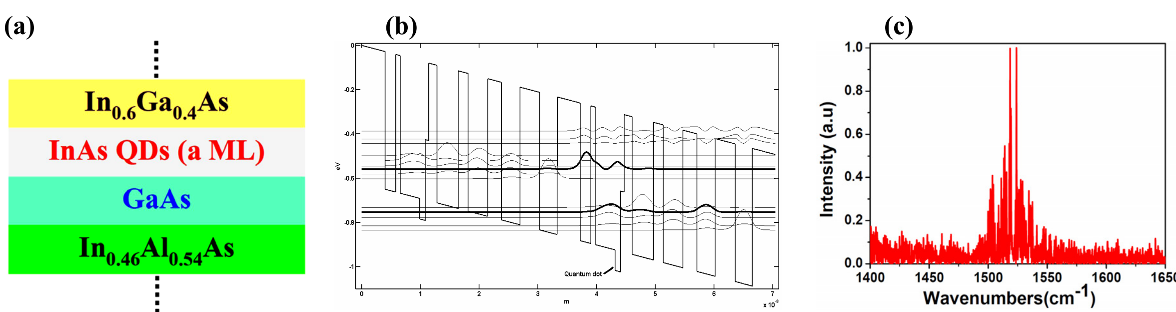

Figure 1. (a) The layer structure of QDCL based on single-layer QDs active region. (b) Calculated conduction band diagram and subband wave functions under electric bias. (c) Lasing spectrum at 80 K.

[1] N. S. Wingreen,and C. A. Stafford, **IEEE J. Quantum Electron. 33**, 1170 (1997).

[4] (a) N. Zhuo, F. Q. Liu, J. C. Zhang, L. J. Wang, J. Q. Liu, S. Q. Zhai, and Z. G. Wang, **Nanoscale Res. Lett. 9**, 144 (2014); (b) N. Zhuo, J. C. Zhang, F.J.Wang, Y.H.Liu, S. Q. Zhai, Y.Zhao, D.B.Wang, Z.W.Jia, Y.H.Zhou, L. J. Wang, J. Q. Liu, S.M.Liu, F. Q. Liu, and Z. G. Wang, J.B.Khurgin, and G. Sun, **Opt.Express 25**,13807(2017).

+ Author for correspondence: fqliu@semi.ac.cn

Glass-based MIR optoelectronic devices: State-of-the-art and future outlook of mid-infrared fiber lasers, microresonators and molecular sensors

R.K. Jain, B. Behzadi, and M. Hossein-Zadeh
Center for High Tech Materials, U. of New Mexico, Albuquerque, NM 87106

We will review the state-of-the-art and critical device optimization issues related to glass-based mid-infrared optoelectronic devices, notably mid-infrared fiber lasers and fiber amplifiers, and microresonators for sensors and mid-IR microlasers.

The development of high purity mid-IR "soft" glasses (notably fluorides, chalcogenides, and tellurites) was driven originally by the possibility of ultralow loss "reduced Rayleigh scattering" fibers [1] for optical fiber communications. The subsequent development of low-loss mid-infrared glasses containing rare earth ions -- along with deeper understanding of the energy level systems and ion-ion interactions [2] – led readily to the development of high-power mid-infrared fiber lasers and amplifiers [2, 3]. Low loss mid-IR optical fibers with high optical nonlinearities have led to the development of a wide variety of unique mid-IR fiber light sources, including Raman fiber lasers, Raman fiber amplifiers, comb generators, and "mid-IR continuum" generators. More recently, researchers have developed high-Q (high "quality factor") microresonators [6] and microlasers [7] with ultralow-loss high thermal stability fluoride (ZBLAN) glass materials.

In this talk, we will discuss the role of critical material and device parameters related to the design and fabrication of advanced mid-IR devices; the latter includes control of the refractive index and doping densities of the glasses, and design and fabrication of advanced high power and narrow linewidth mid-IR fiber lasers. The use of new fabrication techniques for fabrication of mid-IR microresonators and microlasers, including the use of specialized molds for pouring molten glass to cast such microresonators will be discussed. Specific milestone achievements, including the attainment of >20 Watts of output power in mid-IR fiber lasers [4] will be discussed, along with the prospect of achieving narrow linewidth sub-megahertz operation of mid-IR fiber lasers [8] spanning the entire mid-IR spectral range between 2 to 7 microns, and the prospects of compact spectroscopic molecular sensors based on advanced mid-IR glass optoelectronic devices.

[1] M. Saad, Proc. SPIE, vol 7316, 73160N-1 (2009)
[2] B. Srinivasan, J. Tafoya, and R.K. Jain, Opt. Express, vol. 4, pp. 490-495 (1999)
[3] X.S. Zhu and R.K. Jain, Opt. Lett., vol. 32, No. 1, pp 26-28 (2007)
[4] S.Tokita, M.Murakami, S. Shimizu, M. Hashida, and S. Sakabe, Opt. Lett, vol 34, pp. 3062-3064 (2009)
[5] S. D. Jackson, Nature Photonics, vol 6, pp. 423-431 (2012).
[6] B. Way, R. K. Jain, and M. Hossein-Zadeh, Optics Letters, Nov. 1, 2012, 37, # 21 (2012)
[7] Y. Deng, R. K. Jain, and M. Hossein-Zadeh, Optics Letters, Vol. 39, pp. 4458-4461 (2014)
[8] B. Behzadi, M. Aliannezhadi, M. Hossein-Zadeh, and R. K. Jain. *JOSA B* 34, pp. 2501-2513 (2017)

+ Author for correspondence: jain@chtm.unm,edu

Materials issues related to the fabrication of high-Q mid-infrared glass optical microresonators

M. Hossein-Zadeh and **R.K. Jain**
Center for High Tech Materials, Univ. of New Mexico, Albuquerque, NM 87131

High optical quality (high-Q) Whispering-Gallery Mode (WGM) microcavities have been a subject of intense study in recent years, in part because of their potential for several unique photonic devices, including low-threshold and narrow-linewidth lasers, ultra-high sensitivity molecular detectors, and nonlinear optical mixers (including comb generators). Nevertheless, there is still a strong need for improved microresonator devices, particularly in the mid-IR range, particularly for molecular sensing and comb generation applications.

This talk will focus on materials issues related to the fabrication of high-Q mid-IR microresonators. Fluoride glasses are not only highly amenable to be drawn into high quality single-mode fibers, but are the only glasses to date that show high transparencies in a wavelength range from the near-uv (as short as 0.25 μm) to the mid-IR (as long as 8 μm), with extremely low loss characteristics exhibited in the 0.3 μm to 4.5 μm range for practically all fluoride glasses. Numerous fluoride glasses and glass families have been developed in the last three decades, notably the fluorozirconates (ZrF_4), fluoroindates (InF_3), fluoroaluminates (AlF_3), fluorogallates (GaF_3), and fluorozincates (ZnF_2) leading to hundreds of combinations of glass alloys, a few of which – notably ZBLAN -- have emerged as the most promising and reliable combinations in terms of glass purity, glass stability, and transparency over broad spectral ranges.

As an illustrative example, the relatively large transparency window of indium fluoride glasses (from 0.3 to 7 μm) combined with their low thermal expansion coefficients, low values of *dn/dT*, low dispersion, and low phonon energies make InF_3 glasses excellent candidate materials for the fabrication of unique high-Q optical microcavities. Figure 1 illustrates an experimental demonstration of the fabrication of high-*Q* microspheres using an ultralow-loss InF_3 fiber. Other issues re: optimization of alternative materials, including fabrication of high-Q microresonators with low-loss tellurite glasses will also be discussed,

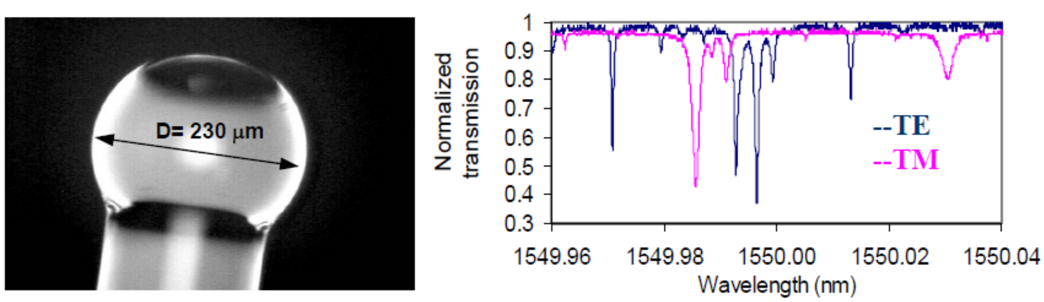

(a) (b)

Figure 1. (a) A micrograph of an InF_3 (Indium Fluoride) microsphere formed at the tip of a InF_3 fiber. (b) Spectrum of TE and TM WGMs illustrating attainment of a Q of $3x10^6$.

Recent Progress on GaSb-based Photonic Integrated Circuits

S. Arafin[1+], A. P. McFadden[1], M. Pendharkar[1], C. J. Palmstrøm[1,2] and L. A. Coldren[1,2]
[1]*Dept. of Electrical and Computer Engineering,*
University of California, Santa Barbara, CA-93106, USA
[2]*Dept. of Materials, University of California, Santa Barbara, CA-93106, USA*

Despite significant technological achievements in InP-photonic ICs with sampled-grating distributed Bragg reflector (SG-DBR) laser tuning technology near 1.55 µm over the past few decades, such platform in the short-wave infrared (SWIR) or mid-infrared (MIR) regimes has not yet reached its full potential. By employing an InGaAsSb/AlGaAsSb/GaSb gain material and necessary processing steps, we aim to develop photonic integrated circuits (PICs) technology in the GaSb material system. The proposed concept for an agile tunable PIC transmitter is shown in Fig. 1. The SG-DBR lasers are the tunable component and each is limited ~6.5% of the center wavelength in order to obtain a good side-mode suppression ratio using a simple cavity geometry; therefore, multiple SG-DBR lasers will be heterogeneously integrated together to cover the entire tuning range. Tunable light output from the SG-DBR cavity will be amplified in the semiconductor optical amplifier (SOA) to increase power to ~10 mW.

As can be seen in Fig. 1, the wavelength range from 2.2-2.8 µm can be covered with only four chips using broad bandwidth of the gain materials. Second, we integrate each chip with the desired phase modulator. Light will then be coupled from the GaSb PICs to the SOI combiner planar lightwave circuit (PLC). We suggest a simple non-dispersive 4 × 1 combiner as illustrated in Fig. 1. This combiner could be accomplished by the indicated “y-branch” structures or by 2 × 1 multi-mode interference (MMI) structures. Alternative to the non-dispersive combiner, a wavelength selective 4 × 1 MMI can also be thought of.

For the phase modulators, we propose current injection into the passive waveguide regions. The modulation depth is expected to be approximately π radians of phase modulation for a current input of 5 mA with a typical modulator length ~100 µm. The modulation is almost independent of modulator length for current densities in the 0.2-2 kA/cm^2 range. Higher bandwidths are possible by using reverse biased *p-n* junctions, also using the same passive regions of the platform.

The offset quantum-well (OQW) integration platform is chosen for processing SG-DBR lasers and compatible PICs because it requires a relatively simple process. A schematic cross-section of the layer structure of a GaSb-based offset quantum-well (OQW) integration platform is illustrated in Fig. 2(a). After growing the base structures, passive regions were formed by removing the multiple-QW active region from the base structure prior to the regrowth. Atomic steps were observed after MBE regrowth in both active and passive areas with and without MQWs, respectively. The film exhibits atomically smooth surface morphology with root-mean-square (RMS) roughness value of <0.3 nm, as shown in Fig. 2(b)-(c). The presented concepts and encouraging materials growth results pave the way for the realization of transmitter PICs covering a large SWIR wavelength range using GaSb-technology.

Chip-Integrated Plasmonic Flat Optics for Mid-Infrared Polarization Detection

Jing Bai[1,2], Chu Wang[1,2], Xiahui Chen[1,2], Ali Basiri[1,2], Chao Wang[1,2], Yu Yao[1,2]

[1] School of ECEE, Arizona State University, Tempe, AZ

[2] Center for Photonic Innovation, Arizona State University Tempe, AZ

Polarization detection is essential for various applications, including remote sensing, polarization imaging and biomedical diagnosis like cancer detection [1]. It is desirable to develop a simple, compact and economic way to measure the polarization detection. Conventional methods require bulky optical system which limits the integration and miniaturization. And polarization detection in MIR range is challenging due to material absorption. Here we present the theoretical modeling and experimental demonstration of MIR polarization detection based on monolithically chip-integrated plasmonic metasureface. Our technique enables full Stokes Parameters detection for arbitrary polarized states of light, including partially polarized light. The MIR polarization detector is composed of 6 detection units (Fig. 1a), including 4 linear polarized (LP) light detection units and 2 circular polarized (CP) light detection units. Our design is based on biomemetic bi-layer metasurface with around 500nm thickness, only 1/10 of the working wavelength. The measured Stokes Parameters agree reasonably well with the input polarization states of the light. The average error of S1, S2, S3 measured from 9 experiments is 0.035, 0.025, and 0.104, respectively (Fig. 1b). And the average error of DOLP and DOCP is 3.6% and 10%, respectively. The detector we proposed can be easily scaled to any wavelength from NIR to MIR by changing the design dimensions based on the same material platform, which is promising for multi-wavelength or broadband polarization detection.

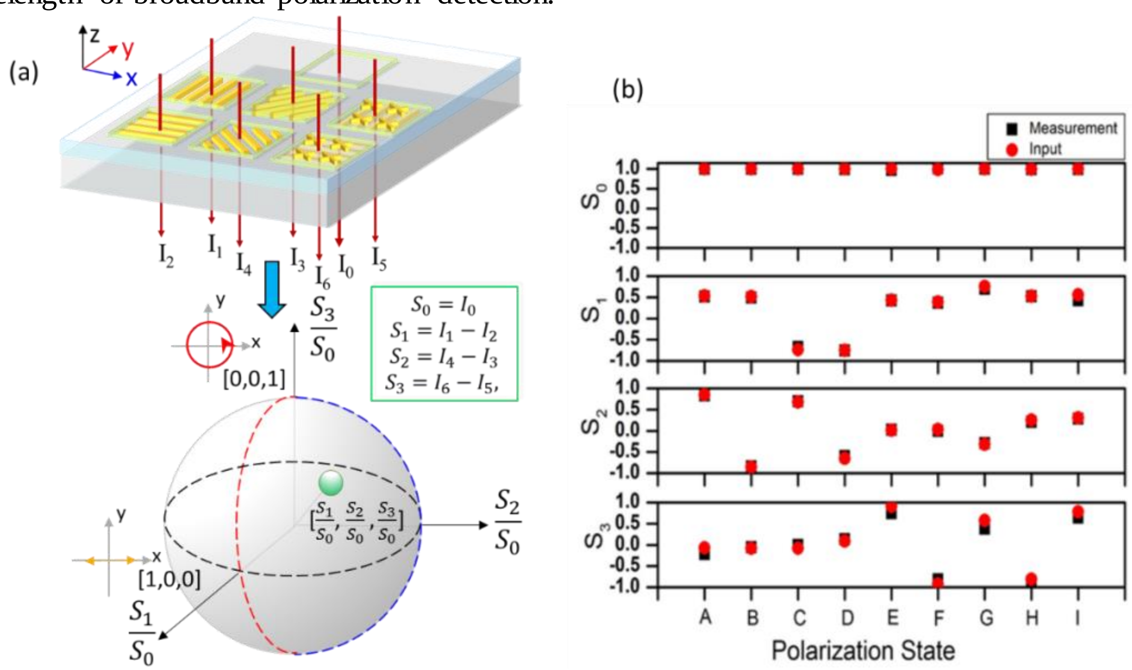

Figure 1 (a) Schematic of the device design (b) Measurement results for Stokes Parameter detection

[1] Snik, F., et.al., SPIE Proceedings 2014, 90990B.

+ Author for correspondence: yuyao@asu.edu

Mid-Infrared Modulation in Silicon

W. Cao,[1] M. Nedeljkovic,[1] D. Hagan,[2] C. G. Littlejohns,[1] Z. Qu,[1] A. Z. Khokhar,[1] F. Y. Gardes, A. P. Knights,[2] D. J. Thomson,[1] G. Z. Mashanovich[1,3+]

[1] *Optoelectronics Research Centre, University of Southampton, Southampton, Hampshire, SO17 1BJ, UK*

[2] *Department of Engineering Physics, McMaster University, Hamilton, Ontario L8S 4L7, Canada*

[3] *School of Electrical Engineering, University of Belgrade, 11120 Belgrade, Serbia*

Optical modulators are one of the most important devices in silicon photonics. A number of high performance silicon modulators have been demonstrated in the telecom wavelength range. Here we report the realization of silicon modulators in the mid-IR which can find applications in fibre and free space communications as well as in sensing.

By using the free carrier plasma dispersion effect in silicon, we have demonstrated a Mach-Zehnder interferometer (MZI) modulator and a microring modulator at a wavelength of 2 μm. For the MZI configuration we have utilized the carrier-depletion modulation to demonstrate a data rate of 20 Gbit/s with an extinction ratio of 5.8 dB and modulation efficiency ($V_\pi L_\pi$) of 2.68 Vcm at 4 V reverse bias. We have also shown a ring modulator with a 55.6 pm resonance shift under 4 V reverse bias, and when operating in carrier injection mode it achieves a data rate of 1 Gbit/s with extinction ratio of 4.71 dB. We have also quantified the electro-optic effect in Si from 1.3 to 2 μm showing that the semi-empirical equations for the free-carrier effect for Si presented in [1], which predicts that the strength of the effect would increase approximately proportionally to the square of wavelength, can be used with confidence for the modulator design.

Following the design rules presented in [1], we have designed and fabricated modulators in SOI for 3.8 μm, in which PIN diodes are integrated with waveguides (Figure 1), and carrier injection into the waveguides increases the absorption of the waveguide core. The SOI PIN diode was 2 mm long and grating couplers were used to couple light in and out of the waveguide. The transmission was measured while applying varying forward bias across the PIN diode using a DC power supply. The modulation depth achieved is > 30 dB. The SOI PIN modulator had an insertion loss of 2.9 dB.

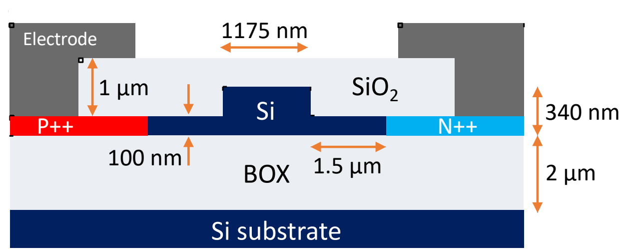

Figure 1. Schematic diagram of SOI PIN carrier injection modulator, designed for 3.8 μm

[1] M. Nedeljkovic et al., IEEE Photonics J. **3**, 1171 (2011).

+ Author for correspondence: G.Mashanovich@soton.ac.uk

Extreme nonlinearities in the compositional dependence of band gaps in the Si – Ge – Sn system

P. M. Wallace,[1] C. Xu,[1] J. Kouvetakis,[1] and J. Menéndez[2]
[1] *School of Molecular Sciences, Arizona State University, Tempe, AZ 85287-1604, USA*
[2] *Department of Physics, Arizona State University, Tempe, AZ 85287-1504, USA*

The demonstration of thermally robust GeSn and GeSiSn alloys via CVD methods have led to an explosion of research into these materials, motivated to a great extent by the possibility of achieving direct gap conditions. A significant finding from early optical studies is the observation of strong nonlinearities in the compositional dependence of optical transitions [1]. For example, the crossover concentration from indirect to direct band gap in GeSn alloys is predicted to be close to 20%Sn by linear interpolation, but is found experimentally to be close to 9%Sn [2]. This is in strong contrast with observations from the well-known GeSi alloys, in which all important band gaps display an almost perfectly linear compositional dependence.

The simplest phenomenological description of band gap nonlinearities incorporates a quadratic term with a coefficient known as the bowing parameter b. The much larger values of b in GeSn relative to GeSi are associated with the increased atomic size mismatch in the former system. This implies that even larger bowing parameters might be expected in systems containing both Si and Sn, such as the ternary GeSiSn alloys. Furthermore, it is expected on theoretical grounds that such giant bowing parameters will be compositional dependent (in other words, large deviations from linearity are not simply quadratic) [3]. We present here experimental evidence for a compositional dependence of bowing parameters in GeSn as well as GeSiSn alloys using photoluminescence and absorption spectroscopy. The experiments require very accurate measurement of compositions and must be carried out on large sets of samples to obtain meaningful statistics.

The results have important implications for the prediction of the alloy band structure over the entire compositional ranges. In particular, the regions of compositional space corresponding to direct gap conditions can vary very drastically depending on the precise functional form of the assumed nonlinearities, and the possibility of designing Type-I GeSn/GeSiSn quantum well systems, as desired for optimized laser structures, is strongly affected by the magnitude of the nonlinearities.

[1] V. R. D'Costa *et al*., Phys. Rev. B **73** (12), 125207 (2006).
[2] J. D. Gallagher *et al*., Appl. Phys. Lett. **105** (14), 142102 (2014).
[3] S. H. Wei and A. Zunger, Phys. Rev. Lett. **76** (4), 664 (1996).

[+] Supported by the US AFOSR under grant FA9550-17-1-0314 (Gernot Pomrenke).

The rise of the GeSn/SiGeSn multiple quantum well laser

D. Grützmacher[1+], **D. Buca**[1], **Nils von den Driesch**[1], **Daniela Stange**[1], **Dennis Rainko,**[1] **Z. Ikonic**[2], **J.M. Hartmann**[3], **H. Sigg**[4]

[1] *Inst. Semicond. Nanoelectron., PGI-9, Forschungszentrum Jülich, 52425 Jülich, Germany*
[2] *Pollard Institute, School of Electronics and Electrical Engineering, University of Leeds, Leeds LS2 9JT, United Kingdom*
[3] *Univ. Grenoble Alpes, CEA, LETI, F-38000 Grenoble, France*
[4] *Laboratory for Micro- and Nanotechnology (LMN), Paul Scherrer Institute, CH-5232 Villigen, Switzerland*

Alloying of group IV elements germanium (Ge) and tin (Sn) has a large potential to be a solution for Si-photonics, since a direct bandgap, as well as optical pumped lasing has been evidenced for Sn incorporations above ~9 at.% [1]. The value of the bandgap can further be controlled by adding Si into the mix, which can be exploited for the formation of heterostructures for carrier confinement [2].

Here, we will present a comprehensive characterization of direct bandgap heterostructures (DHS) and multiple quantum well (MQW) structures, formed from active GeSn layers and SiGeSn ternary claddings. Fig. 1 shows spectra of an optically pumped μ-disc MQW laser taken at various optical pump power. The data reveal a lasing threshold at 20 K from light in/light out curves of 39 kW/cm2, which is an order of magnitude smaller than the threshold observed for devices fabricated from bulk GeSn layers, clearly evidencing the superiority of M structures over bulk layers. The performance of the optically pumped laser were investigated in dependence of temperature, pump power and excitation wavelength. The gained insight reveals that carrier dynamics are crucial and that the "directness" of the bandgap $\Delta E=E_\Gamma-E_L$ is a decisive parameter on the path towards an electrically pumped laser operating at room temperature. Fig. 2 compares the modeled carrier distribution in MQW and heterostructures. The population in the Γ-valley reflects the maximum operation temperature of the laser. The impact of design, composition and strain of the SiGeSn/GeSn MQW structures on ΔE will be discussed.

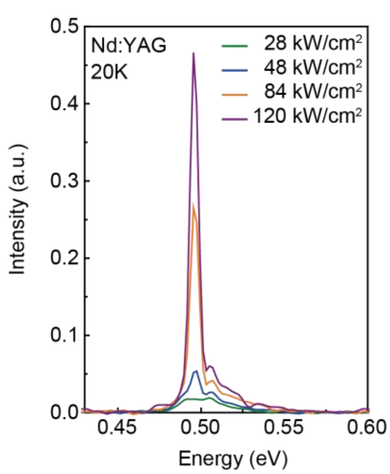

Fig 1: Power dependence of lasing spectra taken at 20K of a optically pumped GeSn/SiGeSn μ-disc laser. Threshold at 20 K from LL: 39 kW/cm²

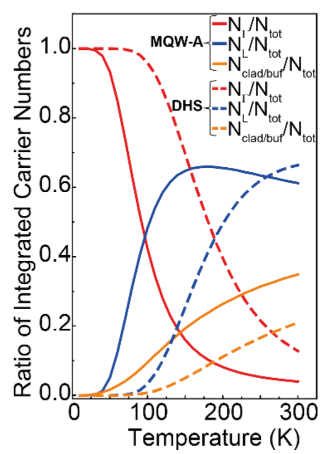

Fig 2: Modeled electron numbers in the Γ- (red) and, L-valleys (blue) of the active material, and in the barriers/buffer layer (orange) as a fraction of total electron concentration, MQW (solid line) and DHS (dashed line).

[1] Wirths, S. et al. Lasing in direct-bandgap GeSn alloy grown on Si. Nat. Photonics 9, 88–92 (2015)
[2] von den Driesch, N. et al. SiGeSn Ternaries for Efficient Group IV Heterostructure Light Emitters. Small 1603321 (2017).

+ Author for correspondence: D.Gruetzmacher@fz-juelich.de

GeSn lasers and Photodetectors: Key Components for Mid-IR Integrated Microwave Photonics on the SOI Platform

Wei Du,[1] Seyed A. Ghetmiri,[2] Yang Zhang,[3] Samir M. El-Ghazaly,[3] Joe Margetis,[4] John Tolle,[4] Greg Sun,[5] Richard A. Soref,[5] Baohua Li,[6] Greg Salamo,[7] Mansour Mortazavi,[2] and Shui-Qing Yu,[3]

[1] *Department of Electrical Engineering, Wilkes University, Wilkes-Barre, PA 18766*
[2] *Department of Chemistry and Physics, University of Arkansas at Pine Bluff, Pine Bluff, AR 71601*
[3] *Department of Electrical Engineering, University of Arkansas, Fayetteville, AR 72701 USA*
[4] *ASM, 3440 East University Drive, Phoenix, AZ 85034*
[5] *Department of Engineering, University of Massachusetts Boston, Boston, MA 02125 USA*
[6] *Arktonics, LLC, 1339 South Pinnacle Drive, Fayetteville, AR 72701*
[7] *Institute for Nanoscience and Engineering, University of Arkansas, Fayetteville, AR 72701*

Integrated microwave-photonic (IMWP) circuits on a chip offer the promise of reduced size-weight-and-power (SWAP) at very low cost when manufactured in a foundry [1]. Currently, IMWP is mainly implemented in three material platforms: InP, TriPleX™ technology (Si_3N_4/SiO_2), and Silicon on Insulator (SOI). A recent publication pointed out that the limitations and challenges in the IMWP field are strongly correlated with a monolithic integrated solution combining the high-performance light sources and detectors, low loss passive devices, and complementary metal-oxide-semiconductor (CMOS) and radio frequency (RF) circuits on a single platform [2]. Since the current IMWP is built upon the great success of modern fiber-based telecom techniques with the working wavelength of 1.55 µm, where two photon absorption limits the use of Si, the major components have reliance on InP based optoelectronic devices, whose propagation losses can be an order of magnitude higher compared to waveguides based on silica or silicon [3]. Here we propose a high performance self-consistent technology on the SOI platform operating at **2-2.2 µm**, which is enabled by the emergence of a monolithic Si-based factory compatible SiGeSn technology. The platform interfaces easily with new low-loss HCPBG fibers. SiGeSn is a newly developed all-group-IV alloy with outstanding material properties including: i) independent tuning of the lattice constant and bandgap [4]; ii) the all group-IV- based true direct-bandgap material [5]; iii) the potential to cover near/mid IR wavelengths up to 12 µm through band-to-band transitions; and iv) a low material growth temperature fully compatible with CMOS processes. The advantages of SiGeSn approach are: i) immediate partnering with the proven high-performance SOI passive and EO components that are scaled up in size by 30%; ii) enhanced dynamic range as two-photon absorption at 1.55 µm in Si under high laser power operation is effectively suppressed by shifting the operating wavelength to 2 µm.

Reference

[1] J. Capmany and D. Novak, Nat. Photon. **1**, 319-330 (2007).
[2] J. Capmany, et al. Opt. Express **21**, 22862-22867 (2013).
[3] J. Fandiño, et al., Nat. Photon. **11**, 124-129 (2017).
[4] W. Du, et al., ECS Trans. **75**, 231-239 (2016).
[5] S. Ghetmiri, et al., Appl. Phys. Lett. **105**, 151109 (2014).

+ Author for correspondence: syu@uark.edu

Growth and characterization of GeSn using UHV-CVD system

Perry C. Grant,[1,2,3] **Joshua M. Grant**,[2,3] **Wei Dou**,[3] **Bader Alharthi**,[3] **Huong Tran**,[1,3] **Aboozar Mosleh**[4], **Wei Du**,[5] **Baohua Li**,[1] **Mansour Mortizavi**,[4] **Hameed Naseem**,[3] **Shui-Qing Yu**,[3]

[1] *Arktonics LLC, 1339 South Pinnacle Drive, Fayetteville, AR, 72701, USA*
[2] *Microelectronics-Photonics Program (µEP), University of Arkansas, Fayetteville, AR, 72701, USA*
[3] *Department of Electrical Engineering, University of Arkansas, Fayetteville, AR,72701, USA*
[4] *Department of Chemistry & Physics, University of Arkansas at Pine Bluff, Pine Bluff, AR, 71601, USA*
[5] *Department of Electrical Engineering, Wilkes University, 84 West South Street, Wilkes-Barre, PA, 18766, USA*

Progress in group IV photonics over recent years has elevated the GeSn material system to the forefront of photonic integration on Si substrates [1]. Demonstrations of true direct bandgap GeSn, LED, and lasers show the budding potential of the GeSn material system [2], [3]. Growth of GeSn has been discussed in literature, however no result has yet to demonstrate the entire development from poor quality to high quality GeSn material. The goal of this work was to detail the development of high-quality GeSn on Ge buffers. The effect of growth temperature and $SnCl_4$ over-pressure were examined. Sn reduction produced high-quality GeSn film shown in Figure 1. Control of the growth of GeSn was achieved and the dominate mechanisms to produce high-quality films of prescribed thickness and composition identified. After growth condition optimization, continued reduction of growth temperature continued to show increasing peak wavelength, shown in Figure 2. While conditions will change between different growth chambers, the method used to develop high-quality GeSn is applicable across growth systems.

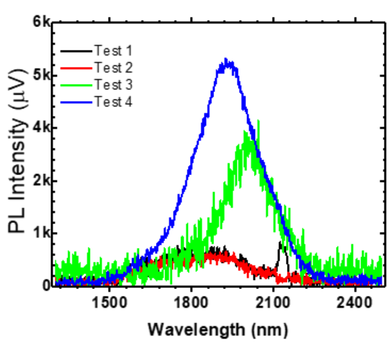

Figure 1: PL of Sn reduction testing showing pathway to high quality.

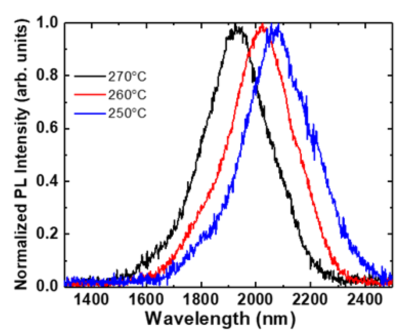

Figure 2: PL of high quality GeSn thin films with increasing Sn incorporation.

[1] R. Soref, *Opt. Photonics News*, vol. 27, no. 1, pp. 32–39, 2016.
[2] Y. Zhou, *J. Appl. Phys.*, vol. 120, no. 2, pp. 1–8, 2016.
[3] J. Margetis, *ACS Photonics*, vol. 5, no. 3, pp. 827–833, 2017.

+ Author for correspondence: syu@uark.edu

Buffer-free GeSn on Si Substrate by Plasma Enhanced Chemical Vapor Deposition

Wei Dou,[1] Bader Alharthi,[1] Perry C. Grant,[1,2,3] Joshua M. Grant,[1,3] Huong Tran,[1] Wei Du,[4] Mansour Mortazavi,[5] Baohua Li,[2] Hameed Naseem,[1] and Shui-Qing Yu,[1,+]

[1]*Department of Electrical Engineering, University of Arkansas, Fayetteville, AR, USA*
[2]*Arktonics, LLC, 1339 South Pinnacle Drive, Fayetteville, AR, USA*
[3]*Microelectronics-Photonics Program, University of Arkansas, Fayetteville, AR, USA*
[4]*Department of Electrical Engineering, Wilkes University, Wilkes-Barre, PA, USA*
[5]*Department of Chemistry and Physics, University of Arkansas at Pine Bluff, AR, USA*

Group IV GeSn alloy is a promising candidate as a tunable direct bandgap material for optoelectronic devices. GeSn on Si substrate has been grown by various research groups using the conventional chemical vapor deposition (CVD) technique [1][2]. In this paper, we reported at the first time the single crystalline GeSn growth directly on Si by plasma enhanced CVD (PE-CVD) with GeH_4 and $SnCl_4$ as precursors. The growth rate of 58 nm /min and Sn content of 6% were achieved. The 1µm-thick GeSn film on Si exhibits the good optical and structural properties.

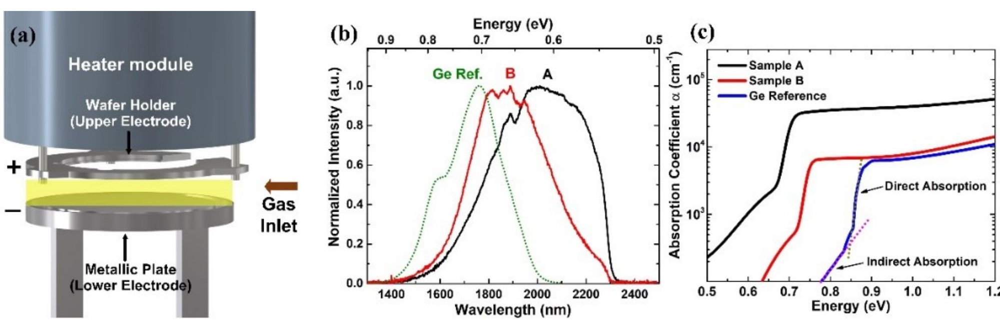

Figure 1 (a) The schematic diagram of PE-CVD system. (b) PL spectra of samples A and B. (c) Absorption coefficients of samples A and B measured by Ellipsometry.

The Capacitively Coupled Plasma (CCP) was employed to generate the plasma, as shown in Figure 1 (a). The power supply of plasma was fixed at 50 W. Two samples of A and B were grown at the temperature of 350 ºC and 400 ºC, respectively. After the PE-CVD epitaxy, the room-temperature PL was measured, as shown in Figure 1 (b). The PL spectra of both samples A and B exhibit the clear red shift compared with the PL spectrum of bulk Ge, suggesting that Sn was efficiently incorporated into Ge. Compared to sample B, sample A has the longer peak wavelength, which is due to more Sn incorporation at lower growth temperature. The absorption coefficients of samples A and B were measured by Ellipsometry. Both direct and indirect absorption edges for samples A and B shift to a smaller energy value compared with absorption edges of bulk Ge.

[1] J. Tolle, Appl. Phys. Lett. 88, 252112 (2006).
[2] A. Mosleh, Front. Mater. **2**, 30 (2015).
[+] Author for correspondence: syu@uark.edu

GePb alloys for Mid-IR Optoelectronics applications

Aboozar Mosleh,[1,*] Hakimah Alahmad[2], Murtadha Alher,[2,3] Seyedeh Fahimeh Banihashemian,[2] Seyed Amir Ghetmiri,[1] Sattar Al-Kabi,[2] Wei Du,[4] Bauhoa Li,[5] Shui-Qing Yu,[2] Hameed A. Naseem[2]

[1]*Department of Physics & Chemistry, University of Arkansas at Pine Bluff, Pine Bluff, AR*
[2]*Department of Electrical Engineering, University of Arkansas, Fayetteville, AR*
[3]*Mechanical Engineering Department, University of Kerbala, Kerbala, Iraq*
[4]*Department of Electrical Engineering, Wilkes University, Wilkes-Barre, PA, 18766 USA*
[5]*Arktonics, LLC, 1339 S. Pinnacle Dr., Fayetteville, AR 72701, USA*

Group IV alloys have been largely studied for different electronic and optoelectronic device applications. However, Si and Ge are not suitable for many optoelectronic applications due to their indirect bandgap. Recent development of Si-Ge-Sn group IV alloys has shown the possibility of achieving a tunable direct bandgap group IV alloy to enhance the absorption and emission efficiency in the infrared range. Nevertheless, achieving the direct bandgap using Sn requires incorporation of 8-10% Sn [1]. The major technical challenge with Sn incorporation into the Ge lattice is the large (15%) lattice mismatch, instability of α-Sn, and low solubility of Sn and Ge (<0.5%). Therefore, developing a new group IV alloy that requires less structural changes would be able to minimize these challenges and facilitate achieving high efficiency optoelectronic devices. Recent theoretical results show that Ge bandgap could be tuned to direct bandgap by only 1-3% incorporation of Pb [2]. However, Pb solubility in Ge is less than 1% and the two lattices are incompatible. These challenges suggest a far from equilibrium growth conditions for the development of the material.

In this paper we report on the growth and characterization of the novel group IV alloy of GePb to be used for infrared optoelectronic applications. Material characterization shows crystalline GePb has achieved with 13.5% Pb incorporation in the Ge lattice. Figure 1 shows the X-ray diffraction (XRD) of the GePb grown on Si after etching the sample in the HCl to remove residual Pb. Figure 2. shows the photoluminescence (PL) study of the GePb grown on Si and on glass. The PL spectra shows a redshift towards longer wavelength of 2240 nm which indicates that incorporation of Pb in Ge has resulted in lower energy bandgap. Further material characterization (Raman, SEM, TEM) along with the post growth annealing results that has resulted in enhancement of material quality will be presented at the conference.

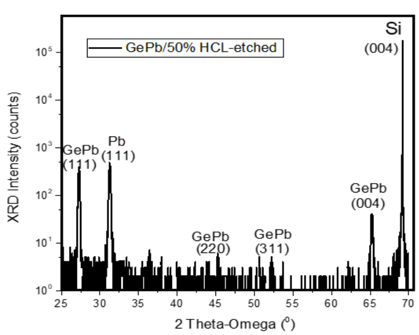

Figure 1 2θ-ω XRD scan of GePb sample.

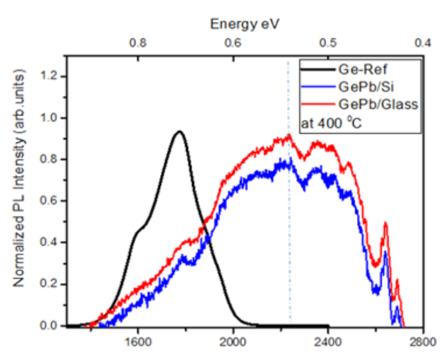

Figure 2. PL spectra of GePb films on Si , Glass

[1] Ghetmiri et al., Appl. Phys. Lett. **105**, 151109 (2014).
[2] W. Huang, B. Cheng, C. Xue, H. Yang, J. Alloys Compounds 701, 816 (2017).
* Author for correspondence: mosleha@uapb.edu

Reduction of Twin formation in GaAs/Sapphire grown by MBE

R. Kumar,[1] S. K. Saha,[1,2] Andrian Kuchuk,[1] T. Al. Morgan[1,3], P.K. Ghosh,[1,4] M. Zamani-Alavijeh,[1,2] Shui-Qing Yu,[4] G.J. Salamo[1,2]

[1] *University of Arkansas, Institute for Nanoscience and Engineering, Fayetteville, AR, United States*

[2] *University of Arkansas, Physics Department, Fayetteville, AR, United States*

[3] *University of Arkansas, Microelectronics-photonics, Fayetteville, AR, United States*

[4] *University of Arkansas, Electrical Engineering, Fayetteville, AR, United States*

Heteroepitaxy of III-V semiconductors is a well-established field. Generally, the heteroepitaxy term is used to denote the growth of dissimilar materials having similar crystal structure but a different lattice constant. Very few examples exist in the literature regarding single-crystal epitaxy of two semiconductors with dissimilar crystal structures such as cubic on wurtzite or cubic on trigonal. There have been few investigations regarding cubic SiGe growth on a trigonal sapphire substrate. Here, we are reporting on the growth of crystalline GaAs semiconductor on c-plane sapphire. Our motivation to grow GaAs on sapphire is based on its potential use in III-V microwave photonics, optoelectronics and electronics owing to their properties, such as, the large refractive index contrast between GaAs and sapphire, high resistivity of sapphire substrate, and transparency of sapphire substrate near the III-As band gap. When grown on c-plane sapphire, III-As will grow along the [111] direction. In our research, a weak in-plane correlation has been observed for direct growth of GaAs on sapphire. In fact, twin formation is a major challenge for obtaining a single crystalline GaAs orientation on sapphire. These twin crystals are rotated by 60° to the original phase. In case of direct growth of GaAs on sapphire, there is a weak in-plane correlation or in-plane orientation relationship with sapphire substrate. We have improved the quality of material, suppressed the twin formation in growth of material and strengthen the in-plane orientation relationship with the sapphire substrate by introducing a thin layer of AlAs between GaAs and sapphire. Further in-situ annealing has been found to decrease the twin volume drastically. Twin volume has been reduced to less than 2% of the total grown material.

III-As Growth on c-plane Sapphire by MBE

S. K. Saha,[1,2] R. Kumar,[2] Andrian Kuchuk,[2] T. Al. Morgan[2,3], P.K. Ghosh[2,4], M. Zamani-Alavijeh[1,2], Shui-Qing Yu,[4] G.J. Salamo[1,2]

[1] *University of Arkansas, Physics Department, Fayetteville, AR, USA*
[2] *University of Arkansas, Institute for Nanoscience and Engineering, Fayetteville, AR, USA*
[3] *University of Arkansas, Microelectronics-photonics, Fayetteville, AR, USA*
[4] *University of Arkansas, Electrical Engineering, Fayetteville, AR, USA*

To study the interface between the dissimilar (lattice parameters, crystal structure, thermal expansion) materials like III-As are grown on Al_2O_3 (0001) substrate. Previous studies for arsenides on sapphire have focused on thick layered growth as opposed to investigating the initial nucleation. The III-V growth on Al_2O_3(0001) can create the opportunity to realize monolithic integrated combining high performance III-V semiconductor light sources, modulators and detectors, low loss waveguides and passive devices, and CMOS and RF silicon circuits on a sapphire platform. The potential integration of microwave photonic (MWP) functionality on a photonic chip can dramatically increase speed, bandwidth, processing capability and dynamic range. In our research, molecular beam epitaxy (MBE) is used to grow ternary (InGaAs) and binary (GaAs, AlAs and InAs) arsenide materials on well define step and terrace surface of the substrate. At the initial stage of the growth we observed the 3D growth mode for the InGaAs, GaAs and InAs from 1ML to 50 nm (Fig.1). For the 50 nm GaAs the faceted crystal structure is observed and from rocking curve measurements of X-ray diffraction (XRD) only one out-of-plane orientation [111] has been detected. Rocking curve of 50 nm GaAs shows small linewidth (242 arcsec) indicating high quality of the grown crystals. Asymmetric (113) phi-scan shows a weak correlation with the sapphire substrate. The In incorporation is very low for very small amount of InGaAs deposition on the sapphire substrate and the amount of In incorporation increased with increasing the thickness of InGaAs. The [111] crystal plane of InGaAs is the major out-of-plane orientation.

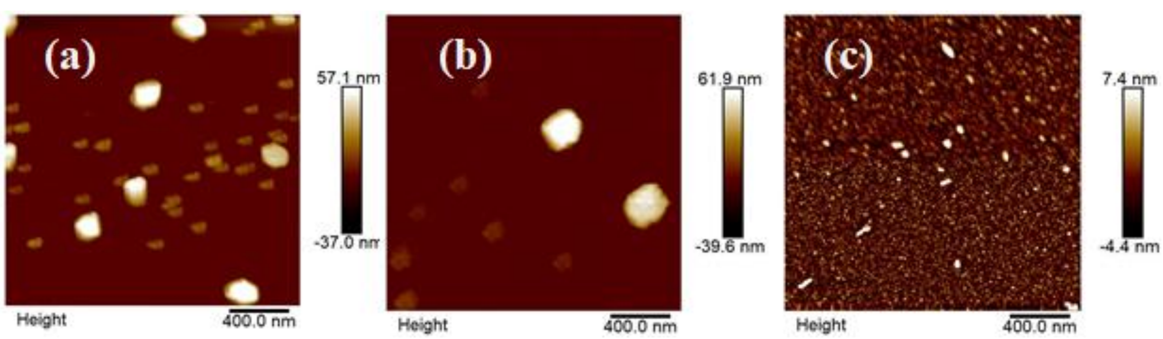

Fig.1: AFM images of (a) 1 nm GaAs (b) 2 ML InGaAs (c) 2 ML AlAs

InGaAs photodetector grown on InP substrate with $InAs_xP_{1-x}$ metamorphic buffer layers

Hao-Kai Hsieh[1], Chieh Chou[1], Jiunn-Jye Luo[2], Shao-Yi Li[2], and Hao-Hsiung Lin[1,3,*]

[1] *Graduate Institute of Electronics Engineering, National Taiwan University, Taipei 10617, Taiwan*

[2] *National Chung-Shan Institute of Science & Technology, Taoyuan 32546, Taiwan*

[3] *Department of Electrical Engineering, National Taiwan University, Taipei 10617, Taiwan*

**Corresponding author: +886-2-33663670 (tel.), +886-2-23632442 (fax), hhlin@ntu.edu.tw (email)*

Metamorphic InGaAs is an active medium used for commercial SWIR detectors. Traditional metamorphic buffer is composed of step or graded InAlAs layers. In this work, instead of InAlAs, we used step-graded $InAs_xP_{1-x}$ layers as the metamorphic buffer. InAsP is a mixed group 5 alloy and has the advantages of constant grown rate and low interaction parameter. An $In_{0.69}Ga_{0.31}As$ photodetectors was grown strain-freely on top of the InAsP step-graded layers by MOVPE. Figure 1 show the RSMs for (004) and (115) reflections obtained from the sample, the $In_{0.69}Ga_{0.31}As$ is almost fully relaxed through the using of $InAs_xP_{1-x}$ step-graded buffer layers. Figure 2 is a cross-sectional TEM image of the buffer layers showing that misfit dislocations are confined in the buffers. No threading dislocation is observed in the $In_{0.69}Ga_{0.31}As$ absorption layer. Figure 3 shows that the detector is with a dark current of 4.5×10^{-4} A/cm^2 at -0.5 V, indicating the good quality of the epilayers. Figure 4 shows the spectral response at zero bias. The spectrum shows a cutoff wavelength of 2.14 μm. This work was financially supported by the Ministry of Science and Technology, ROC, under contract MOST 107-2623-E-002-005-D.

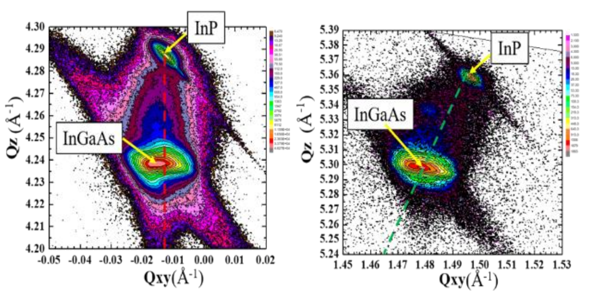

Figure 1 (004) and (115)RSM of InAsP/InGaAs/InAsP/InP structure.

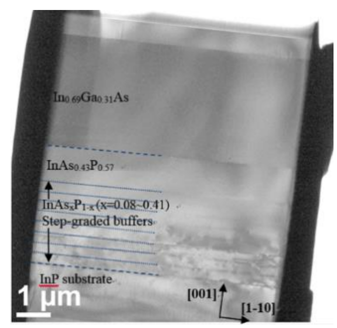

Figure 2 Cross-sectional TEM image of InAsP/InGaAs/InAsP/InP structure.

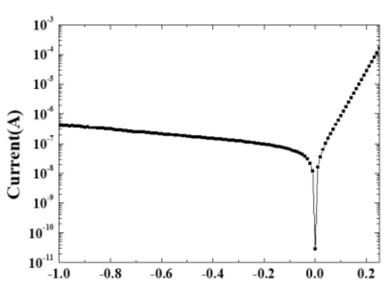

Figure 3 I-V curve of InGaAs/InAsP detector. Device area is 4×10^{-4} cm^2.

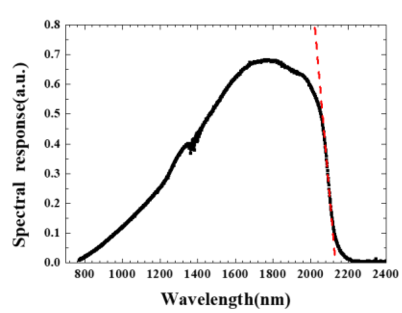

Figure 4 Spectral response of InGaAs/ InAsP detector.

Supplemental Document Author Index

Bold page numbers indicate presenter

Supplemental Document Author Index